AD_____

Award Number: DAMD17-00-1-0393

TITLE: Optical Transillumination Spectroscopy of Breast Tissue to Determine the Cancer Risk in Pre and Post-Menopausal Women

PRINCIPAL INVESTIGATOR: Lothar D. Lilge, Ph.D.

CONTRACTING ORGANIZATION: Ontario Cancer Institute
Toronto, Ontario
Canada M5G 2L7

REPORT DATE: August 2003

TYPE OF REPORT: Final

PREPARED FOR: U.S. Army Medical Research and Materiel Command
Fort Detrick, Maryland 21702-5012

REPORT DOCUMENTATION PAGE

Form Approved
OMB No. 074-0188

1. AGENCY USE ONLY (Leave blank)	2. REPORT DATE	3. REPORT TYPE AND DATES COVERED
	August 2003	Final (1 Jul 2000 - 1 Jul 2003)

4. TITLE AND SUBTITLE
Optical Transillumination Spectroscopy of Breast Tissue to Determine the Cancer Risk in Pre and Post-Menopausal Women

5. FUNDING NUMBERS
DAMD17-00-1-0393

6. AUTHOR(S)
Lothar D. Lilge, Ph.D.

7. PERFORMING ORGANIZATION NAME(S) AND ADDRESS(ES)
Ontario Cancer Institute
Toronto, Ontario
Canada M5G 2L7

E-Mail: llilge@uhnres.utoronto.ca

8. PERFORMING ORGANIZATION REPORT NUMBER

9. SPONSORING / MONITORING AGENCY NAME(S) AND ADDRESS(ES)
U.S. Army Medical Research and Materiel Command
Fort Detrick, Maryland 21702-5012

10. SPONSORING / MONITORING AGENCY REPORT NUMBER

11. SUPPLEMENTARY NOTES

12a. DISTRIBUTION / AVAILABILITY STATEMENT
Approved for Public Release; Distribution Unlimited

12b. DISTRIBUTION CODE

13. ABSTRACT (Maximum 200 Words)

Cancer risk assessment is becoming an important tool in determining an individual's screening and surveillance needs in order to maximize the probability of early cancer detection, or to initiate interventions. We investigated the use of optical transillumination spectroscopy as a physical measurement to quantify breast cancer risk, using breast tissue density resulting form standard mammography as comparator. By using only non-ionizing radiation, optical transillumination spectroscopy can be applied to women of all ages and frequently. Here, we established the sensitivity and specificity of identifying the parenchymal tissue density in women without radiological lesions, as an indirect measure of breast cancer risk. Parenchymal density pattern and optical transillumination spectroscopy quntifies physical parameters of the breast. Using visible/near infrared light the tissue chromophore compositions and morphology is interrogated. We measured spectra for 4 quadrants in each breast and using principle component analysis were able to achieve a sensitivity and specificity of > 0.97 each, demonstrating that optical transillumination will provide at least the same odds ratio for breast cancer risk as mammographic densities. Future work will focus on establishing a direct link with risk, so as to determine the true odds ration towards breast cancer, and on the feasibility to monitor risk changes in individuals undergoing intervention strategies.

14. SUBJECT TERMS
Cancer risk diagnosis, cancer prevention, radiology, risk assessment

15. NUMBER OF PAGES
120

16. PRICE CODE

17. SECURITY CLASSIFICATION OF REPORT	18. SECURITY CLASSIFICATION OF THIS PAGE	19. SECURITY CLASSIFICATION OF ABSTRACT	20. LIMITATION OF ABSTRACT
Unclassified	Unclassified	Unclassified	Unlimited

Table of Contents

Introduction

Two previously published observations were combined to suggest a new physical method to assess breast cancer risk. The first published observation demonstrated that optical transillumination spectroscopy can provide information about the molecular contributions in breast tissue, and the second showed that parenchymal density patterns, which are caused by differences in molecular composition of breast tissue, have the highest odds ratio towards breast cancer as a physical examination method. Thus, this study intended to establish a correlation and the strength thereof, between optical transillumination spectroscopy (OTS) and parenchymal density patterns, as an intermediary towards breast cancer risk in a case-control cross sectional study on 300 women. The study was based on two hypotheses: 1) transillumination spectroscopy of the female breast correlates with the parenchymal tissue density patterns as demonstrated by x-ray mammography, and 2) transillumination spectra can be understood quantitatively in terms of constituent tissue chromophores and morphology through analytical modelling of the spectra. To date 282 women were recruited into the study (SARS related shortfall of the complete intended recruitment).
We established that OTS can predict high versus low tissue density with a sensitivity and specificity of > 0.97 each, thus effectively providing the same odds ratio towards breast cancer as parenchymal density patterns, without the use of ionizing radiation and the need for a trained radiologist in evaluating the mammograms.

Body

The previous approved statement of work for this project is listed below, as are the outcomes throughout this study period to date. It is important to note that the project yielded a large body of results, the analysis of which will most likely continue for the next few months.

Task 1. Instrument improvements (1-4)

- *A spectrophotometer with extended wavelength range will be constructed using a Si and an InGaAs based CCD arrays with a bifurcated fiber bundle directing the light from the skin to the two detectors. Note funds are requested only for the InGaAs detector and the associated spectrophotometer. Additionally an excitation light source delivering ~ 500 mW in the 550 nm to 1.3 um range will be designed. (1-4 month)*
- *The system will be tested initially on 6-8 volunteers to demonstrate comfort and safe operation (e.g. no heating of the skin) and to optimise the signal integration parameters. (3-4 month)*

The spectrophotometer and light source were constructed and tested on a limited number of volunteers. The light source could deliver up to 400 mW to the tissue in the intended optical window from 550 nm to 1.3 μm. Testing initially executed exclusively on Caucasian volunteers (n=6) with instructions to the volunteers to report any sensation of warmth or heat, resulted in a report of warmth from a fair (>50 %) number of volunteers. Reducing the total delivered power to approximately 250 mW spread over the entire wavelength band resulted in poor signal to noise ratio. At this time we decided to limit the wavelength band to 550 nm to 1.1 μm at 250 mW total power on a larger group of volunteers (n=28) to determine the achievable signal to noise ratio and the predictive power of OTS using only the restricted wavelength band. As the analysis of the 2nd subset was encouraging in terms of predictive power (using PCA, see below) and signal to noise ratio without any further report of warmth in the irradiated tissue, we

continued with this restricted wavelength bandwidth. Additionally, our initial exclusion of women with highly pigmented skin, as in Latin American and African American women, was no longer required and hence dropped. Table 1 shows the ethnic makeup of the study population in relation to the general population of the Greater Toronto Area. Figure 1 shows a volunteer undergoing OTS. For a more detailed description of the instrument hardware and the execution of the measurements please see Simick et. al.[1] also provided in Appendix 1. The publication also describes how the attenuation spectra were derived from the raw spectra using a daily transillumination standard to correct for variations in the wavelength dependent transfer function of the system.

Table 1. Study ethnic contributions of volunteers (May 2003)

Ethnic Group	% Study population	% General Population in the Greater Toronto Area
Caucasian	88.8	63.2
South Asian	3.8	10.2
South east Asian	0.0	1.2
Black	5.1	6.7
Indigenous	0.3	0.4
Others/ including Hispanics	2.0	18.4

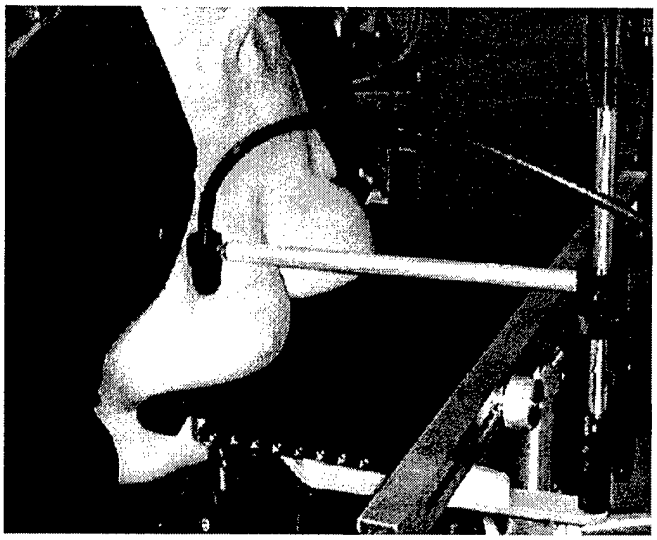

Figure 1. Setup for transillumination of breast for cancer risk assessment. Light delivery via a liquid light guide with the detector fiber visible at the bottom of the image. Minimal pressure is applied only to provide good coupling between the optodes and the tissue.

Task 2. Correlation of optical transillumination spectroscopy and parenchymal tissue density pattern (4-30 months). Related to specific aim 1.

- *Total of 300 subjects will contribute to the spectroscopy database, stratified into 6 groups (low, medium and high parenchymal density pattern for pre- and post-menopausal women respectively) (5 -30 months).*
- *A subgroup of the subjects (60) will be asked to participate in the low resolution sector scans to analyse the variability of transillumination patterns with local changes in the parenchymal density pattern (6-24 months).*

- *Initial set-up of PCA model for extracting spectral contributions and ranges of interest (4- 8 months).*
- *Establishing initial model identifying wavelength ranges which show possible correlation with tissue density (12 months and 24 months).*

Just prior to the outbreak of SARS in various Toronto Hospitals (March 2003) and the associated restrictions of allowing volunteers into any hospital, including the institute where this study was conducted, recruitment stood at 282 volunteers. (We are currently completing the recruiting with all 13 volunteers scheduled by August 15th). Global analysis, based on PCA is available based on all 282 volunteers; however, some specific tests are completed only on a subset of 156 volunteers, with some analysis methods still pending. Table 2 shows the recruitment breakdown based on tissue density for those volunteers whose classification is available, along with a comparison to the population proportions based on the Canadian National Breast Cancer Screening Survey [2]. As the study and the population proportions are similar, all analyses are presented with the assumption that the results are actually those expected for the general population. This is a deviation from the initial statement of work, but we feel that the conclusions to be drawn from this study are now stronger. Table 2 also gives the total number of spectra available for the most recent PCA analysis. As a first approach we did not introduce stratifications either based on menopausal status, week during the monthly cycle (if applicable), ethnic background, age, body mass index (BMI), parity, or measurement position.

Table 2. Breakdown of study volunteers included in most analyses to date: including study and population proportions (numbers in parentheses refer to the total number of optical spectra available to date).

Density Category	Training Set	Validation Set	Total	Study Proportion (%)	Population Proportion (%)
Low	*80 (640)*	*26 (208)*	*106 (848)*	*37.6*	*37*
Medium	*103 (824)*	*34 (272)*	*137 (1096)*	*48.6*	*49*
High	*30 (240)*	*9 (72)*	*39 (312)*	*13.8*	*14*
Totals	*213 (1704)*	*69 (552)*	*282 (2256)*		

Performance of a low resolution sector scan of the breast was limited to only 4 volunteers. This subtask was not further pursued since, firstly, the actual volume optically interrogated can comprise up to 25 cc for a 5 cm interoptode distance, thus small variations in the tissue density between sectors are hardly noticeable. Secondly, as boundary losses of photons at the edge of the breast can introduce variability comparable to that seen due to density changes in these rather large volumes, changes in the spectra are difficult to attribute to either changes in the boundary losses or density changes. Figure 2 illustrates the changes in the transmission spectra of a volunteer undergoing a 1D sector scan from the center of the breast to the medial edge.

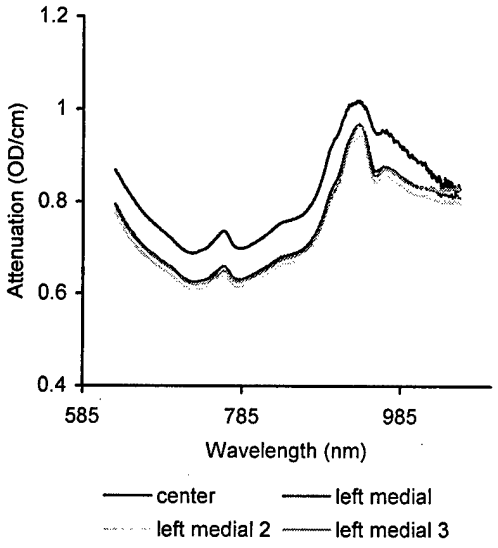

Figure 2. Changes in transillumination spectra during a 1D sector scan in a Caucasian volunteer, starting at the centre and moving towards the medial edge of the breast. 'Left medial' is about 2 cm from the edge and represents the normal measurement position, 'left medial 2' is 1.5 cm and

'left medial 3' is 1 cm from the edge. No significant spectral changes are seen for the 1 cm motion of the optode pair.

Figure 3 shows examples of thickness and transfer function corrected transillumination spectra for a) women with low and b) women with high tissue density according to the radiologist. PCA training on the entire data set resulted in the 4 principle components depicted in figure 4. Table 3, column titled 'All positions', gives the variance of the entire data set captured by these 4 principle components. As components 2 to 4 capture only a small amount of the variance, their order sometimes changes when analysing various subgroups, as shown below.

Table 3. Variance [%] accounted for by each principle component for all positions and for each measurement position.

Principle Component	*All positions*	*Center*	*Medial*	*Distal*	*Lateral*
p_1	99.86	99.85	99.89	99.87	99.88
p_2	0.07	0.09	0.06	0.07	0.06
p_3	0.05	0.04	0.03	0.04	0.04
p_4	0.01	0.01	0.01	0.01	0.01

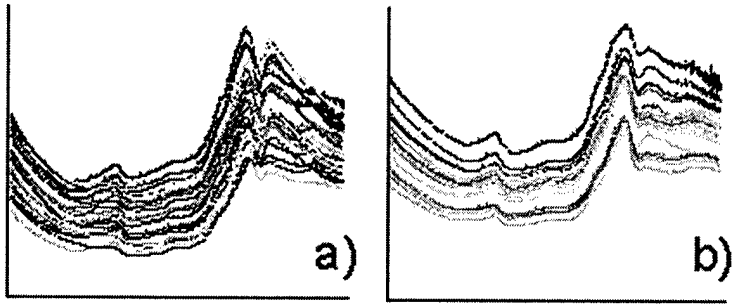

Figure 3. Representative examples of thickness and transfer function corrected transillumination spectra from women with either a) low or b) high tissue density.

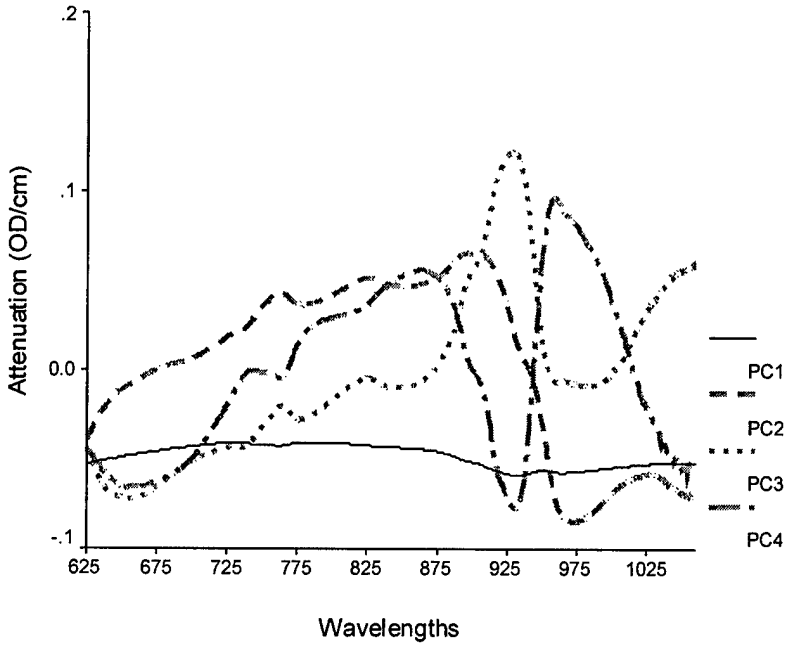

Figure 4. Resulting principle component spectra from training of non-stratified data (n=1704).

As described in Appendix 1 and 2 the principle component spectra carry information about tissue chromophores such as lipids

(925 nm), water (970nm) oxy haemoglobin (~750 nm) as well as deoxy haemoglobin, melanin and the overall light scattering.

Principle component analysis thus decomposes any given transillumination spectrum into component scores denoted t_i. Plotting these component scores, t_i, against one another in either a 2D or a 3D space, permits identification of related spectra exhibiting similar traits.
Figure 5 shows a 2D plot of the data where clusters are defined by ellipsoids giving iso-probability lines of finding members of a certain class (either high or low tissue density) within them. To calculate the sensitivity and specificity of OTS to predict high tissue density, two analytical means of cluster separation were investigated. First, clusters are analytically described by a line or plane of best fit and the resulting median plane between them is calculated. Second, based on the iso-propability ellipsoids a tangent line or plane is determined which identifies the iso-propability ellipsoids of the two clusters that are just touching. It is worth noting that the lengths of the half axes of the ellipsoids are calculated using the frequency histograms of the data points in these cluster plots along each ellipsoid axis.

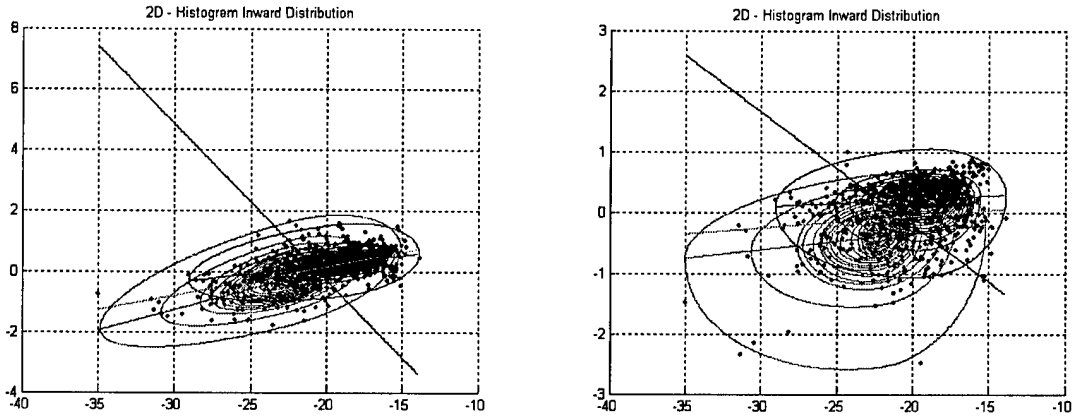

Figure 5.Two-dimensional cluster plots of a) t_1 versus t_2 and b) t_1 versus t_3 resulting from thickness and transfer corrected spectra of high and low tissue density. Only training data set shown (n = 1704). Blue circles, spectra from tissue classified as low density; red circles, spectra from tissue classified as high density. Median axis (green) and new tangent axis (black) are shown.

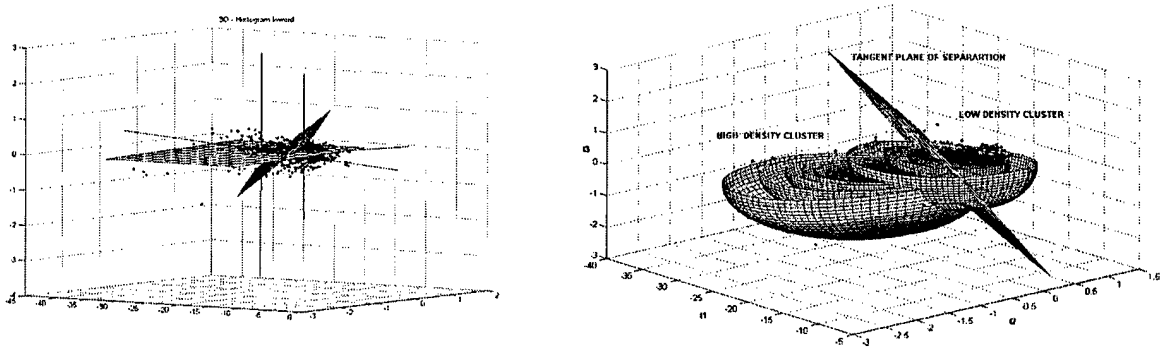

Figure 6left). Three-dimensional cluster plot of t_1, versus t_3 and t_4 resulting from thickness and transfer corrected spectra of high and low tissue density. Only training data set shown (n = 1706). Dark points, data from low density tissue; light points, spectra from high density tissue . New tangent plane (vertical) and median plane (horizontal) are shown. Figure 6 right) shows the resulting ellipsoids indicating isopropability lines and only the tangent plane of separation .

Furthermore, it should be noted that the density cluster of the low tissue density group is significantly larger than that of the high tissue density group. Figure 6 shows an example of a 3D plot with the respective median plane and the tangent plane indicated.

We calculated a high density measure (HDM) and a low density measure (LDM), defined as the number of tissue volumes correctly identified as either high or low tissue density, respectively by OTS divided by the total number of tissue volumes identified as either high or low tissue density, respectively by the radiologist. Hence, HDM represents sensitivity and LDM specificity for the detection of breast tissue with high tissue density. Table 4 presents the HDM and the LDM based on the two cluster separation schemes for PCA trained on measurements from 'All Positions'. The fact that LDM is lower than the HDM can be attributed to the fact that low tissue density is defined as 'less than 25% of the mammographic area is covered by densities', thus an individual spectrum from one quadrant can also be representative of high tissue density at this position.

Table 4. HDM and LDM for training and validation sets using all component scores or scores for individual positions as derived from 3D cluster plots. HDM and LDM results using either the median plane or the tangent plane are presented.

		Tangent Plane				***Median Plane***			
	Component	*Training set*		*Validation Set*		*Training set*		*Validation Set*	
	Scores(x,y,z)	*HDM*	*LDM*	*HDM*	*LDM*	*HDM*	*LDM*	*HDM*	*LDM*
All Positions	t_1,t_3, t_4	**88.3**	**85.8**	**98.6**	**88.9**	**68.3**	**63.0**	**76.4**	**78.9**
Center	t_1,t_3, t_4	96.7	84.4	94.4	92.3	71.7	55.6	83.3	36.5
Medial	t_1,t_3, t_4	90.0	85.0	94.4	92.3	20.0	56.3	88.9	53.9
Distal	t_1,t_2, t_3	96.7	85.0	100.0	94.2	85.0	88.1	77.8	90.4
Lateral	t_1,t_2, t_4	96.7	94.4	100.0	92.3	91.7	73.8	100.0	90.4

It should be stressed that by using the tangent plane very high HDM and LDM can be achieved without any stratification. Additionally, while the spectroscopic technique is sensitive only to average volumetric properties, the volumes sampled per spectra are less than 25% of the breast tissue, whereas the parenchymal density is a global measure. Hence, averaging the scores from all 8 spectra collected per volunteer was tested for possible improvement of the HDM and LDM. Results based on the median plane of separation for 2 different representations of the 3D data are presented in table 5, indicating an improvement in each case. Figure 7 shows the improvement in graphical form.

Table 5. HDM and LDM for test and validation sets using either scores from all 8 spectra per volunteer or the mean score per individual.

	Equation Used	Training Set		Validation Set	
		HDM	LDM	HDM	LDM
All scores	$t_2 f(t_1,t_3)$	76.9%	88.3%	75.0%	96.7%
	$t_2 f(t_1,t_4)$	69.4%	87.5%	64.3%	92.5%
Mean scores	$\overline{t}_2 f(\overline{t}_1,\overline{t}_3)$	85.0%	89.1%	85.7%	100.0%
	$\overline{t}_2 f(\overline{t}_1,\overline{t}_4)$	85.0%	82.6%	71.4%	93.3%

Thus, we have established that OTS is a valid physical assessment technique for tissue densities. As the HDM and the LDM are close to 0.9 OTS will provide a similar odds ratio toward breast

cancer risk as parenchymal density pattern. This is achieved without stratification of the volunteer population based on the above mentioned demographic risk factors, which are often employed in risk models such as the Gail Risk Model [3]. Additionally, the effects of hormonal variations resulting from the menstrual cycle on the transillumination spectra were not considered. For a more detailed statistical analysis based on n=156 volunteers please see Appendix 3, a paper submitted to Cancer Research for peer review July 21st 2003.

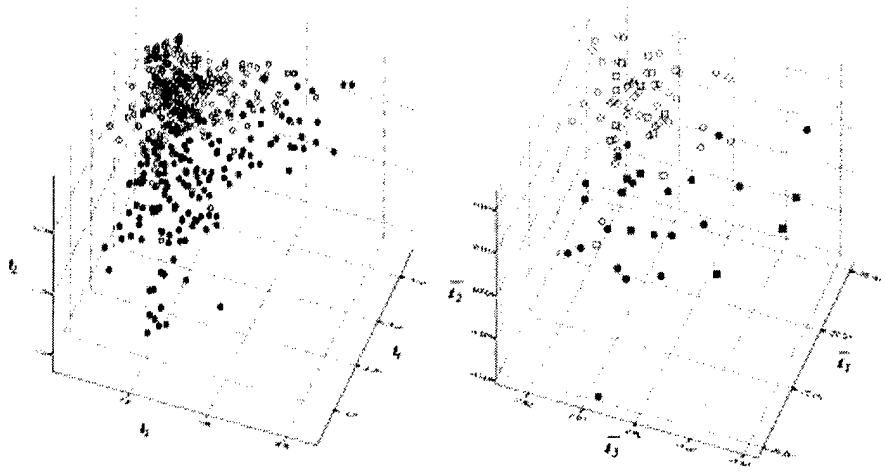

Figure 7. Three-dimensional cluster plots of a) t_2, versus $t_1$and t_3 (n = 528) and b) $\overline{t_2}$ versus $\overline{t_1}$ and $\overline{t_3}$ (n = 88). Shown are scores from spectra of high (solid symbols) and low (open symbols) dense tissues after thickness and transfer function correction.

Effects of menstrual cycle

Changes in the PCA scores measured in 20 women resulting from transillumination spectra collected 4 times during a menstrual cycle are displayed for the left centre position in figure 8. Plots of the other measurement positions showed similar results. From this we concluded that timing of OTS in pre-menopausal women and women on HRT to a certain period during the menstrual cycle is not required.

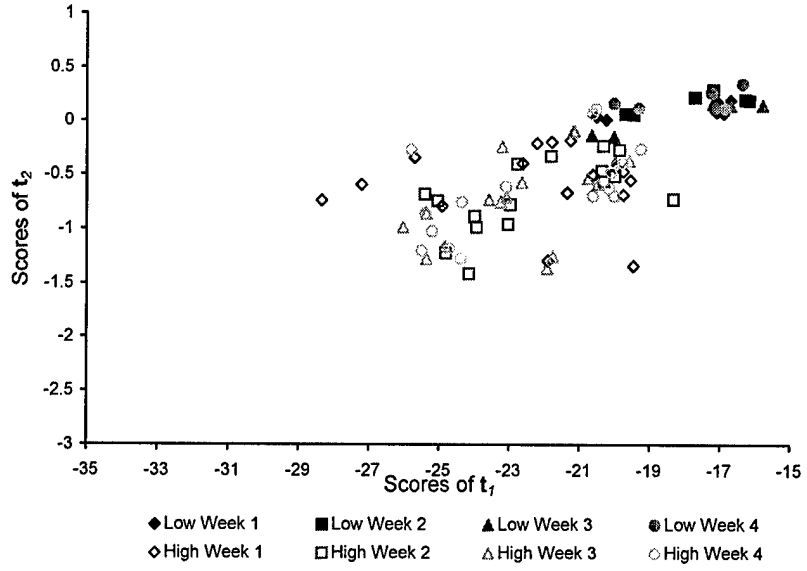

Figure 8. Scores for t_2 versus t_1 for n=20 women presenting 4 times during a menstrual cycle. Shown are results for the left center measurement position only. Low and high refer to low and high tissue density, respectively. Using a PCA model trained on n=88 volunteers.

Effects of age

It was previously shown [5] that transillumination spectra collected from breast tissue will change as a function of age due to the atrophy of glandular tissue prior, during and post menopause. On a subgroup of n=88 volunteers we analysed the PCA scores as function of age following age independent training of the PCA components. Figure 9 shows the results for the individual means of the first 2 component scores for high and low tissue densities. While component score 1 shows a slight increase with age for low and high tissue densities, component score 2 appears to be independent of age. The first result is anticipated, the 2nd somewhat surprising.
As shown below under work performed related to Task 3, component score 1 is thought to be inversely related to the overall light scattering in breast tissue, and atrophy during menopause will replace highly light scattering glandular tissue with less scattering adipose tissue. The fact that the slope for high tissue density is steeper than that for low tissue density is also anticipated as more glandular tissue can undergo atrophy. Principle component 2 shows an inverse lipid (positive) and water absorption (negative) peak (see figure 4), and thus it is anticipated that replacement of glandular by adipose tissue should result in a positive slope specifically around age 50 when atrophy is fastest. It should be noted that specifically for high tissue densities the regression analysis for the age dependence of the component scores resulted in low correlation coefficients and thus the dependency results should not be over interpreted.

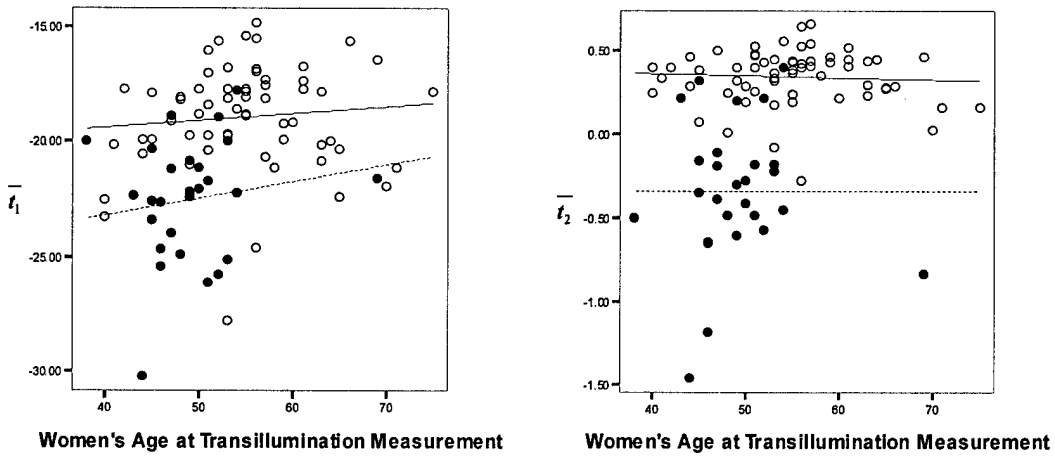

Figure 9. Scatter plots of averaged component scores; left $\overline{t_1}$ and right $\overline{t_2}$ per individual as a function of age for high and low density categories (n = 88). Open circles and solid regression line represent low tissue density, closed circles and dashed line represent high tissue density.

To further investigate if stratification of the volunteers based on age is warranted, we trained PCA models independently for volunteers younger than 50 years of age and older than 55. The results showed that the derived principle components are comparable between the two age ranges in shape and magnitude, with the exception that the water contribution in principle component 2 and the lipid contribution in principle component 3 are lower for the less than 50 year old women. A Kruscal-Wallis analysis of the component scores between the two groups revealed no statistically significant differences with the exception of effects of Body Mass Index (BMI)

Similarly we investigated if the PCA derived component scores showed a correlation with BMI and the results are displayed in figure 10 below. Here, as anticipated, correlations for the first 2 principle components are identified for both density classes, with apparently reduced light scattering for women with higher body mass index by t_1, and increased lipid content in the breast tissue by t_2. These results can be seen as additional evidence towards the interpretation of the principle component spectra.

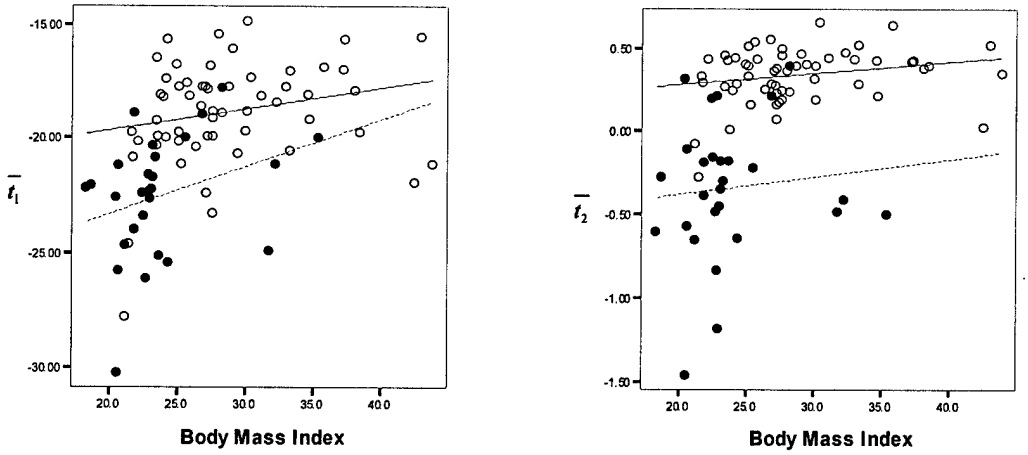

Figure 10. Scatter plots of averaged component scores a) $\bar{t}_1$ and b) $\bar{t}_2$ per individual as a function of BMI for high and low density categories (n = 88). Open circles and solid regression line represent low tissue density; closed circles and dashed line represent high tissue density.

Effects of measurement position

A multivariate analysis of the PCA results showed significant differences in the component scores between the 4 interrogated quadrants. Figure 11 shows the mean and standard deviation of the first three component scores t_i as a function of the measurement position for high and low tissue density. Subsequently, the PCA analysis was executed for each individual position. While the resulting component vectors were similar, see appendix 3 for more details, the HDM and LDM significantly improved (see Table 4). The HDM and LDM in the validation sets are all >0.92 further improving the density prediction value of OTS. From figure xxx it also becomes apparent that the scores for the low tissue densities cluster tighter than those for the high tissue densities, possibly indicating that different anatomical structures contribute to the appearance of parenchymal density pattern.

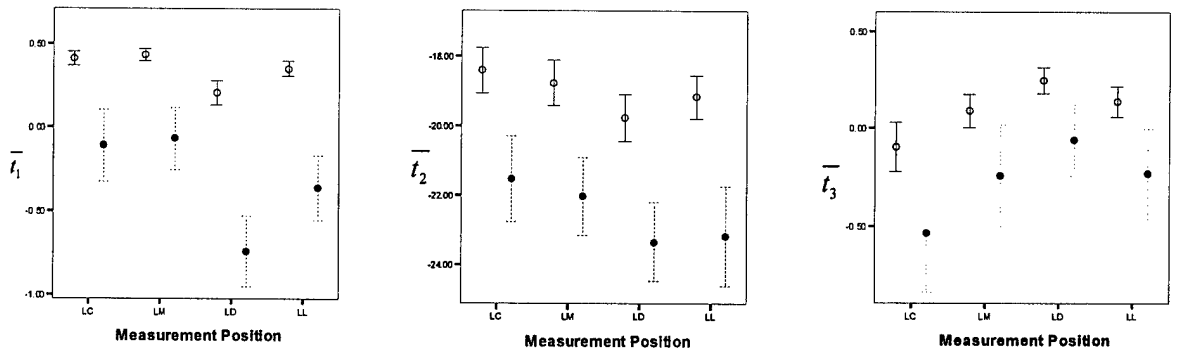

Figure 11. Mean component scores, left) $\overline{t_1}$, middle) $\overline{t_2}$ and right) $\overline{t_3}$ for the four left measurement positions (centre = LC, medial = LM, distal = LD, lateral = LL) for low (open circles) and high (closed circles) density tissue. Error bars represent 95% confidence intervals of the mean. Based on n = 88 volunteers

Pooling of results by quadrants.

As previously indicated, OTS samples the optical behaviour of the breast tissue volumetrically. Hence each OTS spectrum by itself, under samples the breast, thus possibly providing a wrong assessment relative to the density classification, which is inherently a global tissue attribute. Figure 12 shows a frequency histogram indicating the number of spectra per individual predicting a density, here high or low. If the requirement is that 3 of the 4 spectra collected in the center and distal positions on the bilateral organ must predict high density to assign high density globally, the HDM and LDM is > 0.97. The predictive values achieved for a similar condition using the lateral and medial positions are lower. The fact that the combination comprised of the center and distal positions carries a higher predictive value is not surprising since both quadrants exhibit densities less likely seen in the other two quadrants, previously also shown by Wolfe et al. [5, 6].

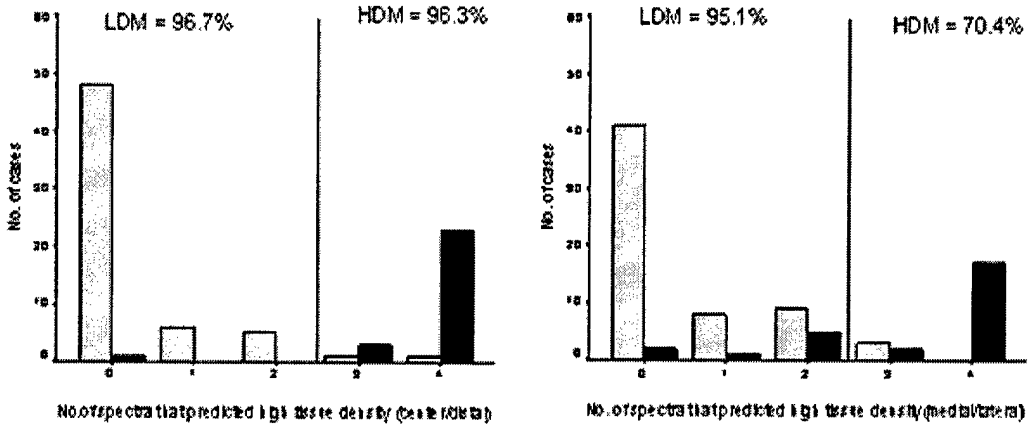

Figure 12. Frequency histogram of the number of spectra from left) the center and distal positions and right) the medial and lateral positions, that correctly predicted high tissue density. High tissue density is shown in black and low tissue density is shown in grey. Results are based on n=88 volunteers.

Task 3. Derivation of tissue chromophore concentrations and light scattering properties of the breast tissue. (4-34 months). Related to specific aim 2.

- *Setting up of PLS analysis to extract tissue chromophores from transillumination spectra by creating a look up table for light transmission as a function of tissue optical properties (4-6 months).*
- *Total of 60 subjects will contribute to the frequency domain spectroscopy database to derive the light scattering properties as a function of the hormonal status (6-18 months).*
- *Determination of chromophore concentrations for all collected spectra of the subjects (12-36 months).*
- *Establishing initial model identifying chromophore concentration ranges/ratios, which show possible correlation with tissue density (20 months and 28 months).*

To execute the correlation between the mammographic based tissue density on an interval scale and OTS, training of the research staff in a computer assisted analysis program (Cumulus), developed by the group of Dr. Yaffe [7], was required. Only recently have we achieved a 'Cumulus' training level deemed sufficient for implementation of the PLS analysis. The training level required includes that persons executing the % density assessment from mammograms achieve a >0.85 correlation for repeat assessments of the same mammograms. An additional complication that occurred was that the breast imaging center used for patient recruitment switched last year to exclusive use of digital mammograms and the computer assisted program does not have the data file filters for the .dicom file format used in digital mammography. We are currently waiting on our collaborator Dr. Yaffe to complete these filters (ETA August 2003). Some results are shown below to demonstrate the ability of OTS to predict tissue density also on a nominal scale. To date the data correlation is not entirely satisfying as the repeat correlation for the staff extracting the % density from mammograms was only ~ 0.8, thus limiting the accuracy of the PLS training. Figure 13 shows an example of a PLS derived prediction of the tissue densities for a person achieving a correlation coefficient ~0.8 versus one achieving only a correlation coefficient of 0.72, indicating the need for accurate and repeatable use of the 'Cumulus' program.

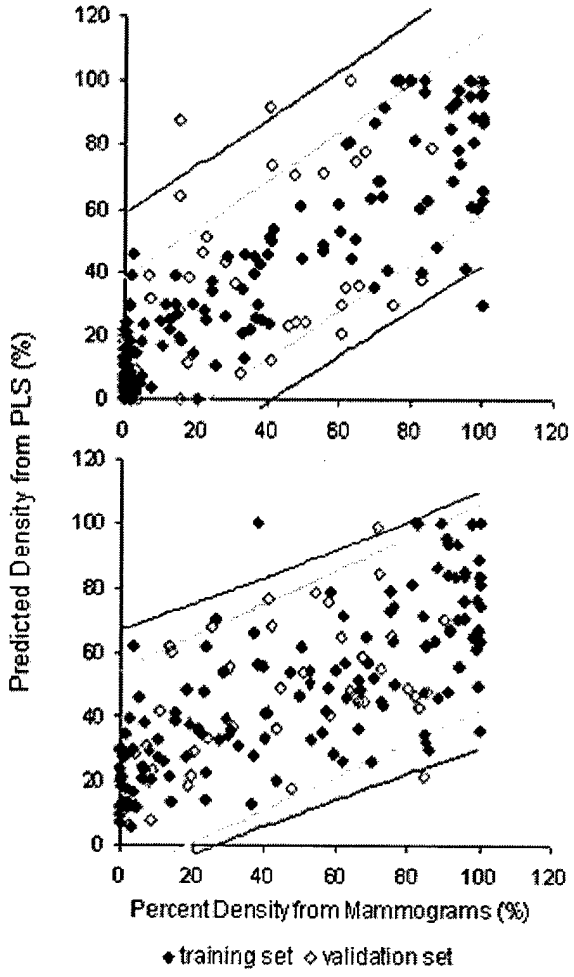

Figure 13. Partial Least Squares Regression Actual vs. Predicted Plots for top) fair trained reader and bottom) poorly trained reader. Solid symbols are for data points from the training set and open symbols for those from the validation set. Confidence intervals for training set - light, validation set - dark

From figure 13 it becomes evident that the correlation for density predicted based on OTS versus that measured by mammography is mostly limited by the accuracy of the latter. Principle component regression was investigated as an alternative to PLS but did not result in an improvement of the correlation between densities by OTS versus mammography. New PLS results will become available only in mid August. We will also attempt to use the Gail Score, a demographics based risk predictor, as the standard for OTS analysis. Comparing the component vector between a physical property based standard and a demographics based standard may provide interesting information about common elements between the two.

The frequency domain system assembled comprised three emission wavelengths (785, 808 and 905 nm) operated at 150MHz and a heterodyne detection at 150.0002 MHz. The basic setup is described by Patterson etal. [8, 9]. A total of 15 women were recruited for the frequency domain measurements. (Recruitment fell short due to the outbreak of SARS in Toronto, and as some of the equipment components were only on loan, it is difficult to reactivate these experiments now as the SARS situation has improved). The phase shift was shown to be associated with the differential pathlength factor [10], which in turn represents the scattering power of the tissue. To determine the phase shift due to the tissue versus the phase shift due to the optical path and the electronic components, measurements in distilled water were collected with the same interoptode distance and that phase shift subtracted from the one measured within the tissue.
Our hypothesis was that the principle component 1 from the PCA analysis above represents light losses due to increased pathlength and losses at the tissue boundary. Figure 14 shows a plot of the phase shift at three wavelengths (785, 808 and 905 nm) versus component scores t_1 and t_2 for this subgroup of women. As can be seen there is a correlation between the phase shift versus PC1 but only little as function of PC2. Additionally, high phase shift and low t_1 are indicative of an increased optical pathlength thus the correlation is as expected. It is surprising that the density groups do not cluster separately in the top row of graphs, that is that the optical pathlength does not depend on the radiologically derived density groups. This indicates that photon scattering by itself does not differentiate between density groups using visible and NIR radiation, whereas Compton scattering of x-rays contributes to the majority of the contrast for risk assessment based on parenchymal density pattern. This in turn indicates that OTS holds also complimentary information to ionizing radiation based risk assessment.
A different way of looking at these results is through the calculation of the differential pathlength factor (DPF) against propagation of the photon density waves as a function of tissue density and wavelength. It is noteworthy that the DPF is a function of the scattering and attenuation coefficient and both are changing as a function of wavelength and tissue density classification. Figure 15 shows similar results to figure 14 using DPF as a function of component scores t_1 and t_2. For the measured population the averages as a function of wavelength are shown. Considering that at 908 nm the influence of the density determining chromophore lipid is low, with possibly a minor effect of oxyhemoglobin, see figure 4, the noted difference in DPF for the medium and high parechnymal tissue density groups must be attributed to an increase in scattering. Accepting this line of reasoning, the fact that at 808nm no difference in DPF is noted, indicates that a strong increase in total hemoglobin absorption (805 nm is the isobestic point for oxy and de-oxy hemoglobin) is present for the medium and high tissue density classes. Similar reasoning leads to a preferential increase in oxyhemoglobin and thus higher oxygen saturation as the scattering increase is less offset at 785 nm where deoxyhemoglobin is the stronger heme based absorber. Figure 17 shows the change in DPF as a function of wavelength in a group of representative individuals of the three tissue density classes. It is unclear at this time if the individual DPF

measurements can be exploited for risk assessment similar to OTS opening a 2nd technological avenue for optical breast cancer risk assessment.

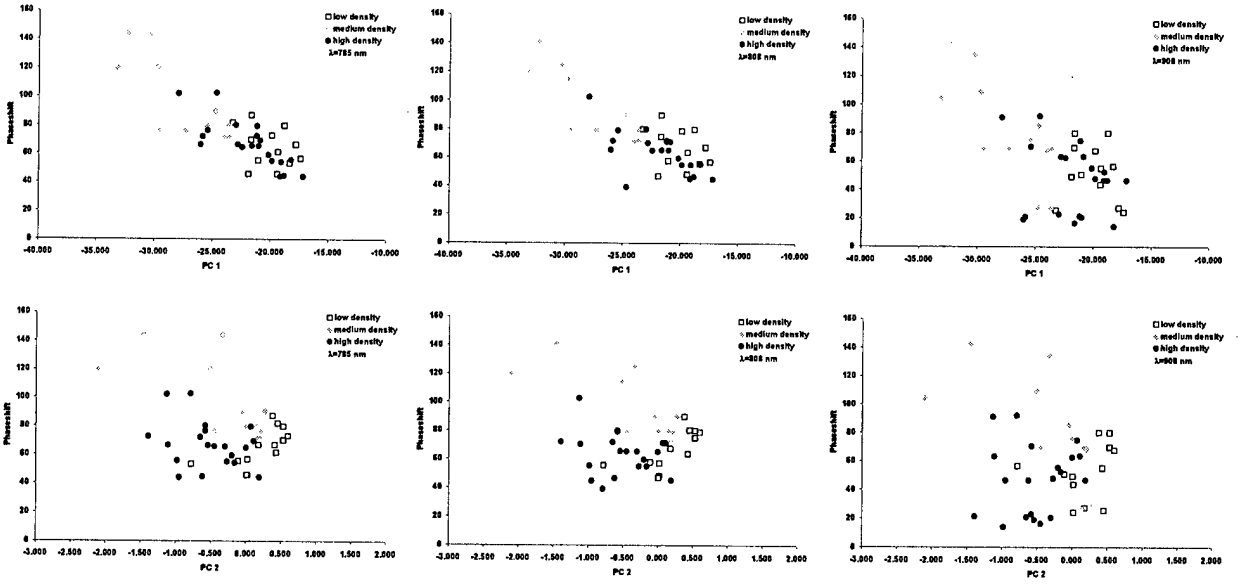

Figure 14. Phase shift as a function of component scores top) t_1 and bottom) t_2 at three wavelengths (left to right 785, 808 and 905 nm). Correlation is strong for component scores t_1 but weak for component t_2 .

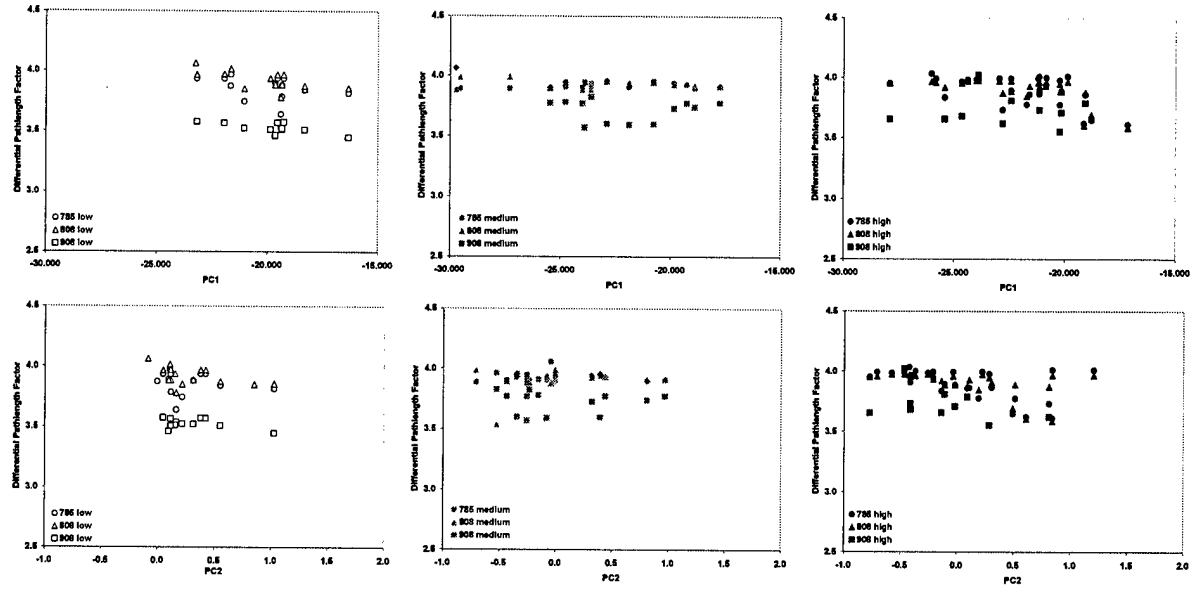

Figure 15. Differential pathlength factor versus component scores top) t_1 and bottom) t_2 for the three tissue densities (left to right low, medium and high) at the three investigated wavelength

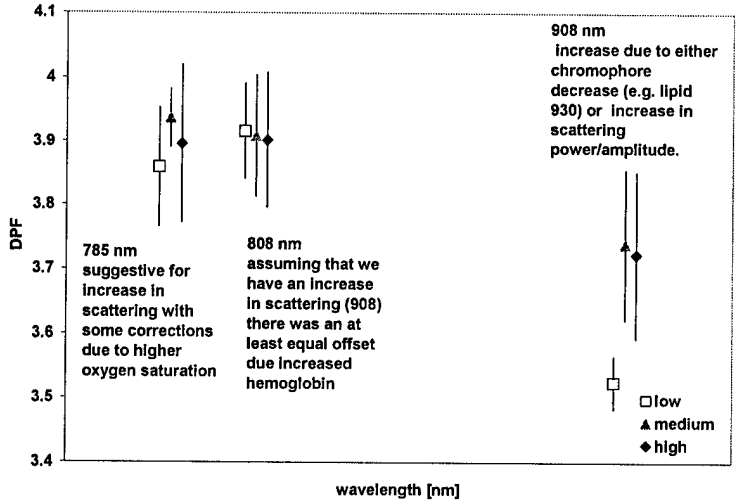

Figure 16. DPF as a function of wavelength for the three tissue classes with a qualitative explanation for the possible causes.

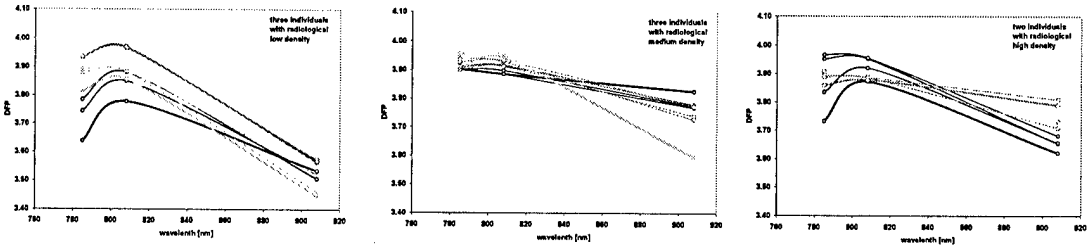

Figure 17. DPF as a function of wavelength in different individuals representing the three tissue classes (low, medium and high, left to right)

- *Determination of chromophore concentrations for all collected spectra of the subjects (12-36 months)*

The program used to determine the tissue chromophore concentrations is based on the diffusion theory as an approximate solution to the transport equation with mismatched boundary conditions (e.g. change in refractive index) to correlate the fluence $\phi(d) = \int_{4\pi} L(r,\hat{s})d\omega$ as a function of distance, d, from the light source, Beer's Law for attenuation of light $I/I_0 = e^{-\mu_a d}$ where I can be determined based on diffusion theory, and the fact that several known chromophores contribute to the attenuation coefficient μ_a according to $\mu_A = \sum_{i=1}^{n} C_i \mu_{A_i}$ and all are a function of wavelength. In order to model the wavelength dependent light scattering the function $\mu_S = a\lambda^{-b}$ according to Pogue et. al. [11] is employed. To simplify the entire equation set we elected to set the fluence beyond the boundary to zero, which was experimentally realized by black absorbing surfaces around the source and detectors. Ultimately, one derives an equation system containing $\phi(d) = \frac{4e^{-\mu_{eff}\cdot d}}{1+2\mu_A/\mu_S}$ with $\mu_{eff} = \sqrt{3\mu_A \cdot (\mu_A + \mu_S)}$ and the radiance into two

hemispheres given by $F_+(d) = e^{-\mu_{eff}d}$ and $F_-(d) = q' e^{-\mu_{eff}d}$ where $q' = \frac{\mu_{eff} - 2\mu_A}{\mu_{eff} + 2\mu_A}$. To solve this equation system the Nelder-Mead *Simplex Method* a multidimensional minimization procedure is used within MatLab, considering oxyhaemoglobin, de-oxyhaemoglobin, lipid, water and melanin to date. Figure 18 provides 3 examples of fitting between the experimental and the theoretical spectrum, including the concentrations of the detected chromophores. It is noteworthy that the haemoglobin absorption peak at ~750 nm in only poorly captured and the overall haemoglobin content of the tissue is estimated too low. We are currently re-examining the code we wrote in order to identify a possible bug.

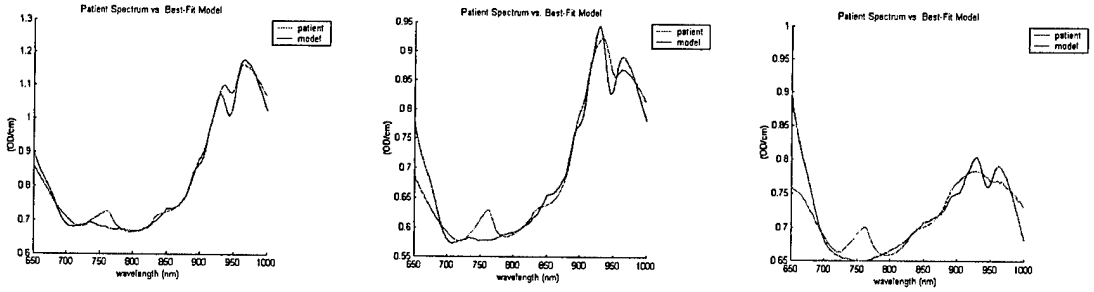

Figure 18. Examples of the decomposition of the optical transillumination spectra into chromophore concentrations. The corresponding chromophore concentrations are given respectively in Table 6 below.

Table 6. Chromophore concentrations and scattering power of preliminary spectral deconvolution.

Patient Position		**449025865 LC**	**224903682 LC**	**802723643 LC**
Water	**%**	**67.6**	**46.1**	**48.7**
Lipids	**%**	**32.37**	**38.08**	**26.9**
Hemoglobin	**mol/L**	**1.89 e-10**	**1.017 e-12**	**1.351 e-12**
Oxy-Hemoglobin	**mol/L**	**2.78 e-5**	**3.75 e-5**	**8.634 e-5**
Melanin	**mol/L**	**0.000159**	**0. 000178**	**0.00047**
Scattering amplitude	**cm-1**	**8900**	**8760**	**4790**
Scattering Power		**1.081**	**1.047**	**1.0193**
error value		**2.4956**	**3.1444**	**3.046**

- *Establishing initial model identifying chromophore concentration ranges/ratios which show possible correlation with tissue density (20 months and 28 months).*

As discussed above we are still in a debugging mode related to the program to be used and this task is still pending.

Pending data analysis (anticipated completion 1-6 Q4 2003, 7, 8 Q1 2005)

The following is a list of planned analyses of the present data set, including some of the pending tasks proposed during the initial funding period and some extending beyond those proposed.

1. PCA of OTS versus tissue density based on the classification of each quadrant.
2. PLS of OTS versus % tissue density based on each quadrant.
3. PLS of OTS versus risk score based on Gail Model (n=162).
4. Tissue chromophore extractions from OTS.
5. PLS of tissue chromophore extraction versus tissue density based on the classification of each quadrant.
6. PLS for same data as point 5 but versus % tissue density based on each quadrant.
7. Detailed analysis of outliers from analyses 1 to 6.
8. Analysis if wavelength dependent DFP provides diagnostic risk assessment.

Key Research Accomplishments

- Demonstrated the feasibility of OTS as a method to determine breast cancer risk.
- Establishment of analysis methods resulting in a sensitivity and specificity to identify women with high versus low tissue density, larger than 0.97 each.
- Through the establishment of defacto equivalence between OTS and mammographic density pattern, OTS will provide at least the same odds ratio or relative risk as tissue density in identifying women with high breast cancer risk.
- Demonstration that OTS can provide anatomical and physiological information about the breast at risk, by providing tissue density and tissue chromophore information.

Reportable Outcomes

Manuscripts submitted for peer review (two attached)

Non Ionizing Near Infrared Radiation Transillumination Spectroscopy for Breast Tissue Density and Breast Cancer Risk Assessment, by Michelle K. Simick, Roberta Jong, Brian C. Wilson and Lothar Lilge, submitted to Journal of Biomedical Optics, May 2003.

Classification of breast tissue density by Optical Transillumination Spectroscopy: optical and physiological effects governing predictive value, by Kristina Blyschak, Michelle Simick, Roberta Jong and Lothar Lilge, submitted to Cancer Research, July 2003.

Manuscripts in preparation for peer review

1. Manuscript detailing the analysis based on density given on an interval scale.

2. Manuscript detailing the extraction of the chromophore concentrations.
3. Manuscript comparing analysis on an interval scale for a physical risk standard (density) versus a demographics based standard (Gail Score).

M.Sc. Thesis

Near Infrared Transillumination Spectroscopy of Breast Tissue for Correlation with Mammographic Density, by Michelle K. Simick. A thesis submitted in conformity with the requirements for the degree of the Masters of Science, Graduate Department of Medical Biophysics, University of Toronto, September 2002.

Presentations invited

Optical Transillumination Spectroscopy of Breast Tissue: Correlation to Parenchymal Density Patterns and Cancer Risk, Lothar Lilge, Wellman Laboratories of Photomedicine, MGH, Boston, USA, November 2001.

Optical Transillumination Spectroscopy of Breast Tissue: Non-Imaging pre-screening for women of all ages, Lothar Lilge, Institute for Laser Medicine, Ulm, Germany, December 2002.

Optical Transillumination Spectroscopy, better prescreening of women? Lothar Lilge, Kristina Blyschak, Breast Club, Princess Margaret Hospital, February 2003.

Colours tell thy risk! Can spectroscopy be used in preventive oncology? Lothar Lilge, Kristina Blyschak, Michelle Simick, Roberta Jong, Brian C. Wilson, Engineering Conferences International, Banff, Canada, 3-7 August 2003.

Presentations contributions

Transillumination Spectroscopy for Breast Cancer Risk Assessment, Michelle Simick, Roberta Jong, Brian C. Wilson, Lothar Lilge, Photonics North, Rochester NY 2001. (This presentation won the best student presentation price).

Classification of breast tissue density by Optical Transillumination Spectroscopy (OTS): optical and physiological effects governing predictive value, Kristina Blyschak, Michelle Simick, Roberta Jong, Lothar Lilge, Optical Society of America, Photonics North, Montreal, Canada, May 2003.

Optical Transillumination Spectroscopy of Breast Tissue for Cancer Risk Assessment, Lothar Lilge, Kristina Blyschak, Michelle Simick, Roberta Jong, Proceedings of the Society of Opto-electronic Systems Engineers, San Jose, USA, January 2003.

Optical Transillumination Spectroscopy a possible technique to assess Breast Cancer Risk? Michelle Simick, Kristina Blyschak, Roberta Jong , Norman Boyd, Brian C. Wilson and Lothar Lilge, Proceedings of the Society of Opto-electronic Systems Engineers, Volume 5141, Munich, Germany, June 2003.

Patent

- US provisional patent submitted November 20, 2001. Title Optical Transillumination Spectroscopy to quantify disease risk. Inventors Lothar Lilge, Brian C. Wilson, Michelle Simick and Norman Boyd.
- Full US application submitted November 2002.
- PCT international Patent Application No. PCT/CA02/01771 files November 20, 2002, with a publication data May 30, 2003.

Programs and databases

A MatLab based program for PCA, PLS and chromophore analysis based on the transillumination spectra was established, the key points are:

- Online sorting of subgroups from volunteer population
- Calculation of 3D iso-probability ellipsoids for clusters under investigation
- Optimized quantification of HDM and LDM by establishing the tangent plane between ellipsoids.

The figures below show some screen prints of the GUI with the main analysis selections and the screen for the subgroups selection using the PCA interface as an example.

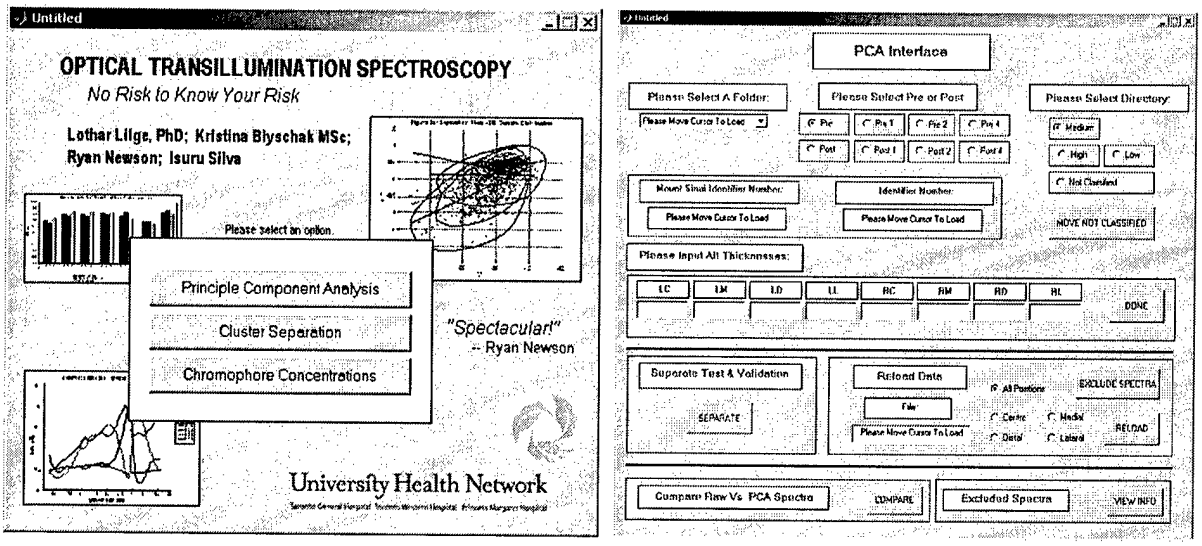

The current data base of the volunteers in our study comprises 8 spectra (or more for repeat measures), the complete information according to the original questionnaire and additionally, for about 160 volunteers, we conducted a phone back to obtain additional demographic information.

Conclusions

This study demonstrates for the first time that tissue modifications preceding the development of cancer can be detected and possibly quantified. While some of these modifications do not need to have a causal relationship with the cancer, the ability to quantify tissue constituents, such as the chromophores mentioned above, may provide additional information for oncologists interested in oncogenesis and prevention.

Optical spectroscopy shows at least the same predictive value as ionizing radiation, but is applicable to women at a younger age and more frequently. Hence, when employed in preventive oncology it offers women two distinct advantages. First, by permitting its use at an earlier age than currently available through mammography, any prevention strategy has more time to exert its influence and thus strategies with fewer negative effects on the quality of life can be explored. Secondly, by permitting frequent use, the efficacy of the intervention strategy can be monitored.

In either case women are empowered to make more educated decisions regarding the risks and benefits of the intervention strategy.

Planned studies.

The current work was very successful in identifying possible new factors or traits for risk assessment using tissue density as an intermediate outcome.

The programs future work is aimed at establishing OTS' odds ratio or relative risk directly versus breast cancer and to demonstrate its ability to monitor risk changes in individual women undergoing a risk reduction intervention. Applications to these two points have been submitted to the NIH (June 2003) and the CDMRP (March 2003), respectively. Another application to the Susan Komen Foundation is planned for September 2003.

Once the three different groups of risk factors or traits are obtained (for risk, density and possibly protection) the risk factors themselves can be compared and insight can be gained as to the physical contributions of density to risk, or density to protection etc.

In future work expanding OTS for non-oncological risk assessment is also considered.

References

1. MK. Simick, R Jong , BC. Wilson, L Lilge Non Ionizing Near Infrared Radiation Transillumination Spectroscopy for Breast Tissue Density and Breast Cancer Risk Assessment. Submitted to Journal of Biomedical Optics.
2. N.F. Boyd, J.W. Byng, R.A. Jong, E.K. Fishell, L.E. Little, A.B. Miller, G.A. Lockwood, D.L. Tritchler, M.J. Yaffe, "Quantitative Classification of Mammographic Densities and Breast Cancer Risk: Results from the Canadian National Breast Screening Study." *J Natl Cancer Inst* 87, 670-5, 1995.
3. Costantino JP, Gail MH, Pee D, Anderson S, Redmond CK, Benichou J and Wieand S. Validation studies for models projecting the risk of invasive and total breast cancer incidence. J Natl Cancer Inst. 91:1541-1548, 1999
4. R.L. Egan and P.D. Dolan, "Optical spectroscopy. Pre-mammography marker," Acta Radiologica, 29: 497-503, 1988
5. Wolfe J., Risk for Breast Cancer Development Determined by Mammographic Parenchymal Pattern. *Cancer*. 37: 2486-2492, 1976
6. Wolfe JN, Breast Patterns as an Index of Risk for Developing Breast Cancer. *Am J Roentgenol*, 126:1130-37, 1976
7. Byng JY., Boyd NF., Fishell E., Jong Ra., Yaffe MJ. Automated Analysis of Mammographic Densities. *Phys. Med. Biol.* 41: 909-923, 1996
8. Pogue BW, Patterson MS Frequency-Domain Optical-Absorption Spectroscopy Of Finite Tissue Volumes Using Diffusion-Theory Phys Med Biol 39 1157-1180, 1994

9. Patterson MS, Pogue BW Mathematical-Model For Time-Resolved And Frequency-Domain Fluorescence Spectroscopy In Biological Tissue. Appl Optics 33 1963-1974 1991
10. Troy T, Page DL, Sevick-Muraca EM., Optical Properties of Normal and Diseased Breast Tissues: Prognosis for Optical Mammography. *Biomedical Optical Spectroscopy and Diagnostics* J Opt Soc Am, 3: 59-66, 1996
11. Testorf M, Osterberg U, **Pogue B**, et al..Sampling of time- and frequency-domain signals in Monte Carlo simulations of photon migration. Appl Optics 38: 236-245, 1999

Appendices

Attach all appendices that contain information that supplements, clarifies or supports the text. Examples include original copies of journal articles, reprints of manuscripts and abstracts, a curriculum vitae, patent applications, study questionnaires, and surveys, etc.

Appendix 1

Non Ionizing Near Infrared Radiation Transillumination Spectroscopy for Breast Tissue Density and Breast Cancer Risk Assessment

Michelle K. Simick[1], Roberta Jong [2], Brian C. Wilson [1,3], Lothar Lilge[1,3] *

[1]Department of Medical Biophysics, University of Toronto, [3]Mount Sinai Hospital,
[4]University Health Network,
610 University Avenue, Toronto, Ontario, M5G2M9 416 946 4501 x 5743,
llilge@uhnres.utoronto.ca

MKS is currently with the Toronto Sunnybrook Regional Cancer Centre and RJ is currently with The Sunnybrook and Women's College Health Sciences Center

Keywords:
Cancer Risk, Transillumination Spectroscopy, Breast Cancer, Cancer Prevention

Abstract

There is increasing attention on cancer prevention as a mean to reduce cancer incidence rates. The prevention interventions or therapies in turn rely on risk assessment programs to identify those women most likely to benefit from education and lifestyle changes. These programs are usually based either on interviews to identify ethnic, genetic and lifestyle factors contributing to risk or on physical examination of the breast. For the latter it has been shown that the parenchymal density pattern observed on x-ray mammography can be used to assess an individual's risk. Extensive areas of dense, glandular tissue that are relatively radio-opaque are associated with higher breast cancer risk, with an odds ratio of 4 - 6 when compared to women in whom the breast density is low due to an abundance of adipose tissue

Near-infrared optical transillumination spectroscopy has been used previously to investigate physiological properties of the breast tissue. In this study, women were recruited who recently had X-ray mammography. The tissue density was assessed by a radiologist. They then underwent optical transillumination spectroscopy, for which an instrument was developed that delivered visible and near-infrared light to the breast. After being transmitted through the breast craniocaudally in one of 4 quadrants the light spectrum from 625 to 1050 nm was measured. The spectra were used as input to Principal Component Analysis (PCA) that used the corresponding mammographic density as the reference standard. The study group comprised 92 women age 39 to 72 years. Without further stratification for age, menopausal status or measurement position the PCA numerical model predicted the radiological assessment of tissue density in the mid 80% to low 90%.

Introduction

Breast cancer is the most commonly occurring cancer in women. In Canada, the lifetime risk of being diagnosed with breast cancer is approximately 1 in 10,[1] the highest out of all cancers for women. The probability of dying of breast cancer is 1 in 25, which is second only to lung cancer amongst all cancer-related deaths.[1] Most other developed countries are reporting similar probabilities for diagnosis and death. Breast cancer screening programs have been shown to decrease the mortality rates of women between ages 50-69, [2] since cancers are detected at an earlier, easier curable stage. Conversely, the overall incidence rate of breast cancer is still rising, possibly due to the increasing age of the population.[3] Currently, imaging by x-ray mammography, ultrasound and or magnetic resonance imaging are the primary modalities [4] used for breast imaging. These modalities use physical or chemical differences in tissue such as the radiation attenuation coefficient, water content or physical density to display differences in the tissue morphology, which may suggest aberrant growth associated with cancer.

While the understanding of the mechanisms leading to breast cancer is increasing, they are not fully understood, though it is apparent that the development of breast cancer is a slow process following initial transformation of the breast tissue.[5] There is currently an effort within the research community to understand risk factors for the disease that are exhibited before or during this slow transformation process, but definitely prior to the any clinical manifestation of breast Cancer. This would enable members of the highest risk population to form educated decisions towards increased screening and or risk reduction interventions. Risk factors are defined as those characteristics that are more common in people with the disease when compared to the population at large.[6] Risk factors related

to breast cancer include age, country of residence, first degree relatives or personal breast disease history, genetic factors, anthropometric factors, menstrual and physiological factors.

Screening and risk reduction intervention will not provide benefit to the individual member of the high risk population but are rather of benefit of the entire population at risk. This benefit is maximized when the relative risk quantifier employed is very large, so that the majority of high risk group members are identified while minimizing the inclusion and hence exposure of low or medium risk subjects to potential side effects of the risk reduction interventions. Risk reduction interventions can be as benign as modifications to a subject's lifestyle, exercise and diet, which has been shown to reduce the relative area of mammographic densities after two years,[7] or invasive such as chemoprevention, including the use of Tamoxifen [8], aromatases [9] and prophylactic mastectomy [10].

Increased fibroglandular tissue in the breast which has a high x-ray attenuation coefficient , thus appearing bright in standard mammograms, is a known physiological risk factor. Areas appearing radiologically lucent represent fatty tissue of the breast that are rarely the source of aberrant growth in the breast. Radiological opaque tissue is a common source of carcinomas and consequently the relative area of dense tissue is a strong risk factor, see Figure 1 for examples of high and low x-ray dense breast. Commonly breast tissue density is quantified following breast cancer screening program visits and it has been suggested that it can be affected by hormonal and dietary changes [11]. Parenchymal density is used as the standard risk assessment tool [12] in the study

presented here, as it provides the best available standard for risk in a cross sectional study.

Breast tissue is a highly light scattering medium and has relatively low absorption in the red and near infrared wavelength range, resulting in an adequate penetration depth of light. This allows a sufficient number of photons to be detected through up to 7 cm of breast tissue in a few seconds, while maintaining the incidence irradiance below government guidelines for exposure of skin.[13]

In previous diagnostic studies of breast tissue it has been shown that quantification of water, lipids, hemoglobin and other tissue chromophores is feasible by near-infrared spectroscopy,[14] Fibroglandular tissue is expected to result in increased water and simultaneous decreased lipid-associated absorption, identifiable through absorption peaks at 978 and 930 nm, respectively,[15] (Figure 2). It is also expected to have a higher scattering efficiency than adipose tissue as seen in Figure 3. Finally, Haemoglobin (Hb) can be identified by an absorption peak at 760 nm while oxygenated haemoglobin (HbO_2) has only a low and broad absorption with a local maximum close to 920 nm.[15] Transillumination spectroscopy have been shown to be associated with the probability for the presence of breast cancer.[16]

Light remitted from the opposite side of the breast passes at least twice through the skin with varying melanin content (depending on ethnicity and sun exposure) which can affect the transmission spectrum, and hence may limit the predictive value of transillumination spectra as the melanin content does not affect breast cancer risk. While quantification of skin color is feasible based on diffuse reflectance spectroscopy [17] and

can permit subtraction of melanin associated absorption, it is not included in this study, and participants where not stratified for skin color or ethnic background.

Optical transillumination spectroscopy is not an imaging technique and thus only bulk tissue properties are obtainable and are characterized through spectral shape and intensity analysis. Hence, for comparison with mammographic determined risk, the x-ray images were classified only as low, medium or high tissue density, omitting spatial information about the density pattern.

This investigation is set up as a cross-sectional study to evaluate the feasibility of detecting and quantifying breast tissue density as intermediate to risk prediction *in vivo* using visible and near infrared transillumination spectroscopy. The hypothesis is that optical transillumination spectroscopy provides consistent information to conventional mammography in quantifying breast tissue density and hence, indirectly to breast cancer risk with an odds ration compatible to mammography .

Methods

Instrumentation. The clinical spectrographic system, designed and built in-house, is shown in as schematic in Figure 4. A 12 Watt halogen lamp (Welch Allyn, Buffalo, NY), with a stabilized power supply was used as the broadband light source. The ultraviolet, short-visible and mid-infrared regions of the spectrum were blocked by a cut-off filter (<550 nm) and a heat rejection filter (KG4, Melles Griot, Carlsbad, CA), respectively. The remaining light in the 550-1300nm range was coupled by a 20mm focal length lens into a 5 mm diameter liquid light guide (Kaiser Electronics, San Jose, CA), placed in contact with the top of the breast. The total radiant power delivered to the skin surface was >250 mW. The transmitted light was collected by a custom-made 7 mm diameter

optical fiber bundle (P&P Optical Kitchener, ON, Canada) that was positioned coaxially with the source guide. The light guides were mounted in a caliper, the separation of which could be adjusted by hand so that both were in contact with the breast. Contact of the source guide was firm, with the breast compressed locally by not more than 5 mm to ensure good coupling to the tissue. The holder for the source guide and the plate in which the detector guide was embedded were made of black plastic to model matched boundary conditions. During spectral measurements, the subject was seated and each breast in turn resting comfortably on a support plate, the height of which could be manually adjusted. No pretreatment of the skin surface was required.

The collected light was spectrally dispersed using a high-throughput holographic grating (15.7 lines/mm:, Kaiser, Carlsbad, CA, USA) with a 0.5 mm entrance slit and detected with a 2D, liquid nitrogen-cooled back thin silicon CCD array (F-125, Photometrics, NJ, USA). The spectral resolution was <3 nm (FWHM) over the 625-1060 nm bandwidth. The peak quantum efficiency of the detector was >0.8 at 780 nm, falling to 0.2 at 1100 nm. The entrance slit of the spectrometer was imaged onto 50 rows of the CCD thus increasing the dynamic range by over 25. The dark count was ~0.06 electrons per hour. Further noise reduction was achieved using exposure times of 2-3 seconds and averaging up to 5 scans. The system dynamic range was >5 OD (optical densities) with a signal-to-noise ratio of $>10\text{-}10^4$ across the spectral range.

This study was approved under the Institutional Review Boards of the University of Toronto and the University Health Network, with informed consent. Women were recruited through the Marvelle Koffler Breast Centre at Mount Sinai Hospital, Toronto. All had prior mammograms within 12 months of the spectral measurement, classified by

a radiologist (RJ) as either low (< 25%), medium (25-75%), or high (>75%) tissue density. Women showing large variations between both sides of the bilateral organ were not included in this analysis.

Measurement procedure and Spectral Preprocessing.

The total data acquisition time was approximately 15 minutes and was completed in complete darkness. A total of 8 spectra were collected per subject, representing medial, distal, lateral and central quadrants of each breast. To date a total of 92 women have been entered in the study, of whom 58 are post-menopausal. The wavelength dependence of the sensitivity was corrected daily by normalizing the transillumination spectra made through a standard comprising of 1 cm thickness, ultra-high density polyurethane (Gigahertz Optics, Munich, Germany) which has a very flat attenuation spectrum. All tissue spectra are given as Optical Density (OD) relative to this standard. Further pre-processing of spectra included correction for the tissue thickness, by calculating the OD/cm at each wavelength. Auto-scaling of the spectra, i.e. normalizing the spectrum to average spectrum off all spectra contained in the training set data for PCA model development (see below), whereas spectra in the validation set were scaled using the same mean spectra. Table 1 lists the different pre-processing techniques employed to establish a correlation between the spectral data set and the breast tissue density.

Data analysis.

The radiological classification produces a scalar quantity, namely the mammographic density, and the optical spectra is a vector. Hence, only multivariate analysis techniques that are able to accept such parameters and that have been used extensively for different applications requiring the analysis of complex spectra where

considered .[18, 19] Typically, these methods involve first a 'training' step to identify the variance within a set of spectra and subsequently, a 'prediction' or 'validation' step to determine the accuracy of a separate set of spectra in predicting the outcome, which in this case is the tissue density classification. The specific analytic technique used here is Principal Component Analysis (PCA)

Mathematically, the PCA procedure is as follows. First, the spectral data is reduced in extent, while preserving the maximum amount of variance.[20] This is accomplished by solving for the covariance or correlation matrix of the data matrix $\mathbf{X}(m \times n)$ comprising all measured spectra (n = 544; training set only) and the spectral range (m = 436 wavelengths), such that:

$$\mathrm{cov}(\mathbf{X}) = \frac{\mathbf{X}^T \mathbf{X}}{n-1} \qquad (1)$$

PCA decomposes the data matrix $\mathbf{X}$ as the sum of the outer products of the scalars of $\mathbf{t}_i$ and vectors $\mathbf{p}_i$ and a residual matrix $\mathbf{E}$:

$$\mathbf{X} = \mathbf{t}_1 \mathbf{p}^T_1 + \mathbf{t}_2 \mathbf{p}^T_2 + \mathbf{t}_3 \mathbf{p}^T_3 + \ldots + \mathbf{t}_i \mathbf{p}^T_i + \mathbf{E}$$

$$\text{or} \quad \mathbf{X} = \mathbf{T}\mathbf{P}^T + \mathbf{E} \qquad (2)$$

,where the elements of the $\mathbf{t}_i$ $(n \times 1)$ vectors are the scores that contain information on how the spectra relate to each other, and the $\mathbf{p}_i$ vectors $(m \times 1)$ or components are the eigenvectors of the covariance matrix that relate the selected variances to each other.

The scores (elements of $\mathbf{t}_i$) can be graphically plotted against one another to show clustering of related spectra. The PCA algorithm was trained on a test set (n= 544) and

the same mathematical model, i.e. retaining the $\mathbf{p}_i$, was used to determine the scores $\mathbf{t}_i$ on the validation set comprising the remaining n_V=192 spectra.

The statistical significance for the PCA prediction was established using the high density measure (HDM), which is defined as the ratio of spectra predicting a woman as having high mammographic density by the PCA algorithm compared to those categorized as having high tissue density by the radiologist. Conversely, the low density measure (LDM) represents the ability to correctly identify those spectra that represent low tissue density. Hence, the HDM and LDM are similar to sensitivity and specificity, respectively.

Results

The data set includes mammograms and spectral results from 92 subjects (age 36 to 72 years). Fifty-eight women were post menopausal, of whom 33 were classified as having low, 18 medium and 7 high mammographic density. Of the 34 pre-menopausal 5, 18 and 11 were classified as having low, medium and high density, respectively. As seen in Table 2. At present, this classification prevalence does not reflect the general population distribution observed during the Canadian National Breast Screening Study [21] but recruitment is ongoing.

Figure 5 shows a typical set of measurements, comprising 8 spectra from a single subject. Spectra from corresponding quadrants on each breast are very similar, a fact used by Egan and Doyle [16] as a negative predictor for the presence of breast cancer.

While transillumination is a local measurement, nevertheless a large tissue volume is interrogated at each position (estimated as 25 cm^3 for 5 cm breast thickness). For positions close to the circumference of the breast boundary losses will affect the

overall intensity of the transmitted spectra and could influence the spectral shape thus could limit the predictive value of the transillumination technique. Hence, repeat measurements were made in one subject, starting at the center position and moving towards the medial position and beyond towards the circumference of the breast. The resulting transillumination spectra are shown in Figure 6, indicating that while the overall intensity is reduced and hence the OD/cm, up to a distance of 1 cm from the circumference of the breast the losses are wavelength independent and so do not effect the analysis.

The reproducibility of the optical transillumination measurements was analyzed by repeat procedures on one subject during repeat visits over a stretch of 18 month. Figure 7 shows the correlation of the $\mathbf{t}_1$ and $\mathbf{t}_2$ scores from these repeat spectra. Component scores ($\mathbf{t}_1$ and $\mathbf{t}_2$) vary between quadrants but cluster tightly for a given position indicating that the spectroscopy data are reproducible.

Figure 8 shows the principal components ($\mathbf{p}_i$) resulting from the PCA using n = 544 corrected spectra. The $\mathbf{p}_1$-$\mathbf{p}_4$ represents, respectively, 97.6, 1.2, 0.6 and 0.3 % of the variance in the total data set, for a combined 99.8% of the variance. The cluster plot of the scores for $\mathbf{t}_1$ and $\mathbf{t}_2$ are shown in Figure 9, illustrating discrimination of the breast tissue density across a diagonal line in the $\mathbf{t}_1$ vs. $\mathbf{t}_2$ space. Figure 10 shows the reconstruction of a randomly selected transillumination spectrum from according to the variance captured only by $\mathbf{p}_1$ and $\mathbf{p}_2$, as well as that captured by the first four components in thickness corrected spectra. The reconstruction from all four components shows a good representation.

Spectra that had not been corrected for thickness were used to determine the effect of thickness on the shape of the component vectors $\mathbf{p}_1$-$\mathbf{p}_4$ (Figure 11) and the resulting cluster plots of $\mathbf{t}_1$ vs. $\mathbf{t}_2$, see Figure 12. The component spectra are very similar to the thickness-corrected components, but the cluster plots of $\mathbf{t}_1$ vs. $\mathbf{t}_2$ shows discrimination as a function of $\mathbf{t}_2$ only. Similarly, component spectra and cluster plot were obtained also for autoscaled and transfer function corrected spectra (data not shown). The resulting HDM and LDM values for the different spectral pre-processing methods are shown in Table 2.

Symmetry across the same bilateral quadrants for each individual is shown in Figure 13 for all scores of $\mathbf{t}_1$ and $\mathbf{t}_2$ derived from thickness corrected spectra, reflecting a pool of women with homogenous densities across both breast.

Discussion

Bilateral symmetry in the spectra at corresponding quadrants (Figure 12) is expected in our study population as it is a criterion to indicate absence of breast cancer according to the previous studies by Egan and Dolan [16].

Autoscaling of the spectra prior to PCA modeling removes some spectral information since the subtracted mean spectrum is wavelength dependent. As the spectral features contributing to the discrimination between high and low breast density or risk are unknown, losing spectral information is not advisable, even though no significant loss in HDM and LDM was noted. Additionally, calculating component spectra after auto scaling will not enable use of principal component filters in future work as suggested elsewhere. [22]

Cluster plots (Figures 9) based on the scores $\mathbf{t}_1$ and $\mathbf{t}_2$ resulting from thickness corrected spectra demonstrated that it is possible to differentiate between subjects having low or high breast tissue densities.

While PCA models for both native and thickness corrected spectra enable differentiation between high and low breast tissue densities, their $\mathbf{t}_1$ vs. $\mathbf{t}_2$ cluster plots differ. One obvious explanation is the effect of the physical tissue thickness on the overall variance within the spectral data set. In the model based on thickness corrected data, $\mathbf{p}_1$ can not differentiate between high and low density tissue. Additionally, the range of $\mathbf{t}_1$ values is smaller in the thickness corrected data as seen in Figure 9 when compared to the non-thickness corrected data seen in Figure 12. This indicates that the thickness values contribute to the magnitude of $\mathbf{p}_1$ masking other contributions that could differentiate between tissue densities, such as light scattering, and thus leaving only $\mathbf{t}_2$ to preserve information distinguishing between the two breast tissue density groups. Principle component spectra one, ($\mathbf{p}_1$) based on the thickness corrected spectra is de facto wavelength independent but includes losses due to optical path length (and therefore light scattering) and losses at the circumference of the breast.

Pre-processing of the spectra, including thickness correction, is clinically relevant since it is controllable and it has been shown that thickness will contribute non-uniformly to the spectra due to the correlation between lower density and larger breasts.[12]

When comparing the autoscaled versus non-autoscaled data, there were minimal changes in the principal component spectra and minor differences in HDM and LDM values, see and Table 2. Autoscaling as part of the pre-processing can degrade regions with flat or extreme spectral variation.[19] Here, degraded spectral features could include

regions of the spectrum with minimal wavelength dependence and hence, a first derivative close to zero. For example, the hemoglobin inflection points are more pronounced in the non-autoscaled data than in the autoscaled components. Conversely, the spectral features of water and lipids are large compared to other structures in the spectra, but are less pronounced after auto scaling. In this study, the only differences in the model performance is in the training set using non-autoscaled spectra having about 2% higher scores for both HDM and LDM.

Principal components can reveal particular regions of the spectrum that represent important physical properties or entities within the tissue that contribute to differentiation. Component spectra $\mathbf{p}_1$ and $\mathbf{p}_2$ are the most important and cover the highest amount of variance in the data set. While components 3 and 4 have similar or inverse shape as component 2 they take less variance into account.

The derivation of OD used here, which is based on the wavelength dependent transfer function calibration by a polyurethane block with high Mie scattering resulted in the surprisingly flat spectral shape of the principle component spectra $\mathbf{p}_1$, as thus the wavelength dependent Mie-scattering cancels when the ratio of the two spectra is taken. Hence, $\mathbf{p}_1$ carries optical scattering information despite not showing the typical λ^{-1} dependency, [23] and thus the inverse of $\mathbf{t}_1$ represents the overall scattering power. Low density tissue spectra have a reduced amount of scattering compared to high density tissue, and, therefore, higher values of $\mathbf{t}_1$ as seen in Figure 9. This relationship in scattering properties is also seen in the scattering coefficient data by Peters *et al.* [24] and Troy *et al.*, [11].

Component vector $\mathbf{p}_2$, enables differentiation between low and high tissue densities through its most important spectral features related to the lipid with inverse water peaks present at 930 nm and 980 nm, respectively. Thus, when $\mathbf{t}_2$ is positive, the lipid associated attenuation is the dominant feature as anticipated for fatty or low density tissue. Spectra from the high density tissue have negative $\mathbf{t}_2$ and water absorption becomes the dominant structure in the component spectrum. Graham *et al.* (1996) [25] also observed this relationship between water and density values when using MRI to quantify percent density. In their study the water content of the tissue was measured directly and showed adequate correlation to percent tissue density ($r = 0.79$).

Contributions by hemoglobin to the spectral features of $\mathbf{p}_2$ are observed between 625 and 850 nm where the negative slope and inflection points of the hemoglobin curve are apparent. Dense breast tissue has lower $\mathbf{t}_2$ scores compared to the low density tissue, indicating higher hemoglobin and water contributions. Conversely, $\mathbf{p}_3$ shows a lipid absorption peak, but water and hemoglobin absorption are absent hence, if used as a third discriminator the overall content of fatty tissue is represented. The simultaneous appearance of water and hemoglobin absorption in $\mathbf{p}_2$ can be explained physiologically, as tissues with higher water content and hence cellular content, require improved vascular supply and, thereby, increased blood volume. [26] Since positive $\mathbf{t}_2$ scores are related to low tissue density and positive $\mathbf{t}_1$ scores are related to low tissue scatter, the cluster plot of $\mathbf{t}_1$ and $\mathbf{t}_2$ can be divided into quadrants as shown in Figure 14, highlighting the relationship between the spectral features and the known physical attributes of breast tissue.

While a cluster plots based on $\mathbf{t}_3$ and $\mathbf{t}_4$ does not allow good differentiation between high and low density tissue, regions of the corresponding component spectra $\mathbf{p}_3$

and $\mathbf{p}_4$ show interesting effects such as for $\mathbf{p}_3$ a red shifted lipid peak and a small blue shifted water peak and $\mathbf{p}_4$ shows influence from both forms of hemoglobin, with the same slope but inverse inflection points to $\mathbf{p}_2$. The underlying physical or physiological effects for these observations are unclear at this time. While the amplitudes and general shape of the spectra are similar to $\mathbf{p}_2$ the magnitude of the scores $\mathbf{t}_3$ and $\mathbf{t}_4$ are much smaller than those of the first two components, and may represent only relative corrections for $\mathbf{p}_2$

Conclusions

In vivo optical transillumination spectroscopy is technically feasible and capable of predicting breast tissue densities with good correlation to mammographic densities and hence, has good potential to be developed into a preferred method of cancer risk assessment, so the strength of a direct correlation with cancer risk needs to be proven in a case-control study and possibly a longitudinal study to estimate the validity of the correlation and hence predictive value for a longer period of time.

According to the results of the current study, it is anticipated that the odds ratio of the transillumination measurements should be close to those of the parenchymal densities seen on mammograms (i.e. between 4 and 6), since the PCA results show HDM and LDM values close to or above 0.90.

Transillumination spectroscopy may offer a novel "first step" in the risk assessment of healthy women regardless of age, menstrual cycle, ethnic background or menopausal status as the data and analysis presented here was not subject to stratification by either event.

Spectral features associated with tissue density prediction include water and lipids, as well as spectral features related to hemoglobin absorption. The effect of light scattering on measured spectra holds importance in the differentiation of breast tissue density after correction of the data for physical breast tissue thickness.

HDM and LDM values close to or above 90 % are very promising at this stage to distinguish between low and high density tissues as they are higher than other physical examinations, such as ultrasound [27] and magnetic resonance imaging,[25] reported to be between 70-80 %.

Optical transillumination spectroscopy offers the potential of a real-time and cost-effective method with the ability to classify tissue densities for breasts that are up to 7 cm in thickness in the current instrument. Improvements in CCD technology, such as deep depletion wells can increase the opto-electronic detection and thus will increase the detection ability. An added advantage of transillumination spectroscopy over ultrasound and MRI is the fact that results are derived from preset mathematical models and hence, no additional trained personnel are required for image interpretation or assessment. This reduces the overall cost to the healthcare system for this risk-assessment technique. The compactness of the devices makes it highly mobile and ideal to serve remote areas or developing countries. A painless procedure and the inherent safety of this method will likely contribute to a higher compliance rate, thus possibly assisting in affecting overall survival rates.

One notable limitation in this preliminary study was the number of study subjects, which may have resulted in sub-optimal predicted values for HDM and LDM. Also, by using cluster analysis in 3D or higher dimensions, other components such as $\mathbf{p}_4$ can be included to improve classification of tissue density.

X-ray mammography uses ionizing radiation and is considered unacceptable as a tool to assess breast density for women less than forty years of age and for frequent measurement, whereas transillumination spectroscopy is safe for women of all ages. This allows risk assessment to commence at a much younger age when the life style and diet are perhaps easier to influence and this mild risk reduction interventions have one to two decades more to effectively reduce the cancer risk, thus ultimately leading to reduced incidence rates.

While optical transillumination spectroscopy may be a promising tool to monitor the effectiveness of risk reduction interventions such as chemopreventive, dietary or lifestyle changes aimed at the reduction of breast cancer risk, its ability to detect physical changes over a period of time in the breast tissue of a given individual needs to be demonstrated in a prospective longitudinal study.

Acknowledgement

The authors wish to thank Dr. Robert Weersink for assistance in developing the specific PCA models. This work was funded under contract DAMD17-00-1-0393 from the US Army Medical Research and Material Command.

References

[1] National Cancer Institute of Canada. Canadian Cancer Statistics 2001, Toronto Canada, (2001).

[2] National Cancer Institute of Canada: Canadian Cancer Statistics 2000, Toronto, Canada, (2000).

[3] National Cancer Institute of Canada: Canadian Cancer Statistics 1997, Toronto, Canada, (1997).

[4] E. Paci, S. Duffy, M. Rosseli di Truco, "11.3 Mammographic screening: from the scientific evidence to practice" *The Oxford Textbook of Oncology*, Oxford University Press, New York, (2000).

[5] L.E. Janocko, K.A. Brown, C.A. Smith, L.P. Gu, A.A. Pollice, S.G. Singh, T. Julian, N. Wolmark, L. Sweeney, J.F. Silverman, S.S. Shackney. "Distinctive patterns of Her-2/Neu, c-myc and Cyclin D1 gene amplification by fluorescence in situ hybridization in primary human breast cancers." *Cytometry (Communications in Clinical Cytometry)* 46, 136-149 (2001).

[6] J. Byng, *Mammographic Densiites and Risk of Breast Cancer. PhD Thesis*, University of Toronto Press, Canada, (2000).

[7] N.F. Boyd, C. Greenburg, G. Lockwood, L. Little, L. Martin, J. Byng, M. Yaffe, D. Tritchler, "Effects at Two Years of a Low-Fat, High Carbohydrate Diet on Radiologic Features of the Breast: Results from a Randomized Trial." *Journal of the National Cancer Institute*" 89, 488-496 (1997).

[8] Konez O, Goyal M, Reaven RE., Can Tamoxifen cause a significant mammographic density change in breast parenchyma? *Journal of Clinical Imaging* 25 303-308, 2001.

[9] JN Ingle. "Aromatoase inhibition and anit estrogen Therapy in early breast cancer treatment and chemoprevention". Oncology 15:28-39 (2001)

[10] S Taucher, M Gnant, R Jakesz " Preventive mastectomy in patients at breast cancer risk due to genetic alterations in the BRCA1 and BRCA2 gene" Current Concepts in Clinical Surgery 388:3-8 (2003)

[11] T. Troy, D.L. Page, E.M. Sevick-Muraca, "Optical Properties of Normal and Diseased Breast Tissues: Prognosis for Optical Mammography." *Biomedical Optical Spectroscopy and Diagnostics J Opt Soc Am*, 3, 59-66 (1996).

[12] N.F. Boyd, G.A. Lockwood, J. Byng, D.L. Tritchler, M. Yaffe. "Mammographic Densities and Breast Cancer Risk". *Cancer Epidemiology, Biomarkers and Prevention* 7, 1133-1144 (1998).

[13] International Electrotechnical Commission, *Group Safety of Laser Products Part 1: Equipment classification, requirements and user's guide.* IEC, Geneva Switzerland, (1993).

[14] V. Quaresima *et al.*, "Identification and quantification of intrinsic optical contrast for near-infrared mammography" *Photochem Photobiol.* 67, 4-14 (1998).

[15] A.J. Welch and van M.J.C. Gemert (Editors) *Optical-Thermal Response of Laser-Irradiated Tissue.* Plenum Press New York, USA. (1995).

[16] R.L. Egan and P.D. Dolan. "Optical spectroscopy. Pre-mammography marker." *Acta Radiologica* 29, 497-503 (1988).

[17] Weersink RA, Marret LD, Lilge L. Validation of self-reported skin colour via Principal Component Analysis of Diffuse Reflectance Spectra of the Skin. *Proc. Soc. Photo-Opt. Instr. Eng.* 3917: 232-237, 2000. [

[18] D.M. Haaland and E.V. Thomas, "Partial Least-Squares Methods for Spectral Analysis. 1. Relation to Other Quantitative Calibration Methods and the Extraction of Qualitative Information" *Anal. Chem.* 60, 1193-1202 (1988).

[19] D.M. Haaland and E.V. Thomas, "Partial Least-Squares Methods for Spectral Analysis. 2. Application to Simulated and Glass Spectral Data" *Anal. Chem.* 60, 1202-1208 (1988).

[20] B.M. Wise., *PLS Toolbox Tutorial: Matlab Version 6*. Eigenvector Research Inc. Seattle (2000).

[21] N.F. Boyd, J.W. Byng, R.A. Jong, E.K. Fishell, L.E. Little, A.B. Miller, G.A. Lockwood, D.L. Tritchler, M.J. Yaffe, "Quantitative Classification of Mammographic Densities and Breast Cancer Risk: Results from the Canadian National Breast Screening Study." *J Natl Cancer Inst* 87, 670-5 (1995).

[22] J.N.Y. Qu, H.P. Chang, S.M. Xiong SM "Fluorescence spectral imaging for characterization of tissue based on multivariate statistical analysis" J Opt Soc Am A 19: 1823-1831 (2002)

[23] R. Cubeddu *et al.*, "Effects of the Menstrual cycle on the Red and Near-infrared Optical Properties of the Human Breast." *Photochem. PhotoBiol.* 72, 383-391 (2000).

[24] V.G. Peters, D.R. Wyman, M.S. Patterson, G.L. Frank , "Optical properties of normal and diseased human breast tissues in the visible and near infrared." *Phys Med Biol* , 35,1317-1334 (1990).

[25] S.J. Graham, M.J. Bronskill, J.W. Byng, M.J. Yaffe, N.F. Boyd, "Quantitative correlation of breast tissue parameters using magnetic resonance and X-ray mammography." *Br J Cancer* 73,162-8 (1996).

[26] J.W. Byng, J.P. Critten, M.J. Yaffe. "Thickness-equalization processing for mammographic images." *Radiology* 203, 564-8 (1997).

[27] L. Kaizer, E.K. Fishell, J.W. Hunt, F.S. Foster, N.F. Boyd, "Ultrasonographically defined parenchymal patterns of the breast: relationship to mammographic patterns and other risk factors for breast cancer." *Br J Radiol.* 61, 118-24 (1988).

Figure Captions

Figure 1: Examples of x-ray based mammograms showing breasts with either a) high and b) low tissue density. Note: different x-ray exposures were used for the two examples.

Figure 2: Absorption spectra of some major chromophores constituents in breast tissue, including, on the left side water (grey) and lipid (black) and on the right side hemoglobin (black) and oxygenated hemoglobin (grey) [15]

Figure 3: Graph of the scattering coefficient (μ_s') of adipose (black) and fibrous (grey) breast tissue in the wavelength range of interest. Adapted according to Troy *et al.* [11]

Figure 4: Set-up schematic of transmission measurement system, comprising of cw white light source, optodes (liquid light guide and fiber bundle in the caliber mount, breast support, spectrophotometer and CPU .

Figure 5: Typical spectra from a volunteer after correction for the spectral system transfer function and tissue thickness. Note the good reproducibility between corresponding sides of the bilateral organ.

Figure 6: Effect of boundary losses at the breast circumference. Attenuation spectra A: form a volunteer at various distances from breast circumference (center position black, medial position dark gray, 2 cm from circumference grey and 1 cm from circumference light grey. B: Ratio of the same spectra over the average of all four spectra to exaggerate spectral variance due to boundary losses.

Figure 7: Repeatability of $\mathbf{t}_1$ and $\mathbf{t}_2$ in one volunteer at all 8 positions. The slope of the regression line is 1.03 and 0.87, and the Pearson correlation coefficient is 0.72 amd 0.84 for $\mathbf{t}_1$ and $\mathbf{t}_2$, respectively.

Figure 8: Plot of component $\mathbf{p}_1$ to $\mathbf{p}_4$ (black to light grey, respectively) from PCA using tissue thickness and spectral transfer function corrected spectra.

Figure 9: Cluster plot of $\mathbf{t}_1$ vs. $\mathbf{t}_2$ resulting of PCA using thickness and system spectral transfer function corrected spectra from volunteers with high (square) or low (rhombus) breast tissue density. Shown are only scores for the center measurements, with the training spectra shown as closed and the validation spectra as open symbols.

Figure 10: Raw data spectrum (black) and reconstruction using either only the first two components (light grey) or the first four components (grey) based on the principle components shown in Figure 8.

Figure 11: Component spectra of $\mathbf{p}_1$ to $\mathbf{p}_4$ resulting from spectra only corrected for but the system transfer function.

Figure 12: Cluster plot of $\mathbf{t}_1$ vs. $\mathbf{t}_2$ resulting of PCA using only system spectral transfer function corrected spectra from volunteers with high (square) or low (rhombus) breast

tissue density. Shown are only scores for the center measurements, with the training spectra shown as closed and the validation spectra as open symbols

Figure 13: Comparison of the a) $\mathbf{t}_1$ and b) $\mathbf{t}_2$ scores for the left and right breasts in volunteers with either high or low tissue density. Black diamonds represent volunteers from the training set; grey squares represent those from the validation set. Slope and Pearson correlation coefficient are 0.94 and 0.76 for $\mathbf{t}_1$, and 1 and 0.83 for $\mathbf{t}_2$, respectively. .

Figure 16: Cluster plot of thickness and spectral system transfer function corrected data of high (square) and low (rhombus) tissue density volunteers. The 4 quadrant indicate common optical and anatomical tissue properties.

Table 1: Distribution of recruited volunteers and population proportions, from the National Breast Screening Study (ages 40-59).[21]

Density Category	Pre menopausal			Post menopausal			Total	Study Proportion (%)	Population Proportion (%)
	Training Set	Validation Set	Total	Training Set	Validation Set	Total			
Low	4	1	5	25	8	33	38	41	37
Medium	13	5	18	13	5	18	36	39	49
High	8	3	11	5	2	7	18	20	14

Table 2: HDM and LDM of Principal Component Analysis results for test and validation set measurements.

Data pre-processing	Test set		Validation Set	
	HDM	LDM	HDM	LDM
Transfer function corrected (Figure 12)	84.6 %	97.0 %	87.5 %	90.3 %
Thickness and transfer function corrected (Figure 9)	88.4 %	93.1 %	92.5 %	88.8 %
Autoscaled – transfer function corrected (data not shown)	85.6 %	94.4 %	90.0 %	86.1 %
Autoscaled – thickness and transfer function corrected (data not shown)	86.5 %	91.8 %	92.5 %	90.3 %

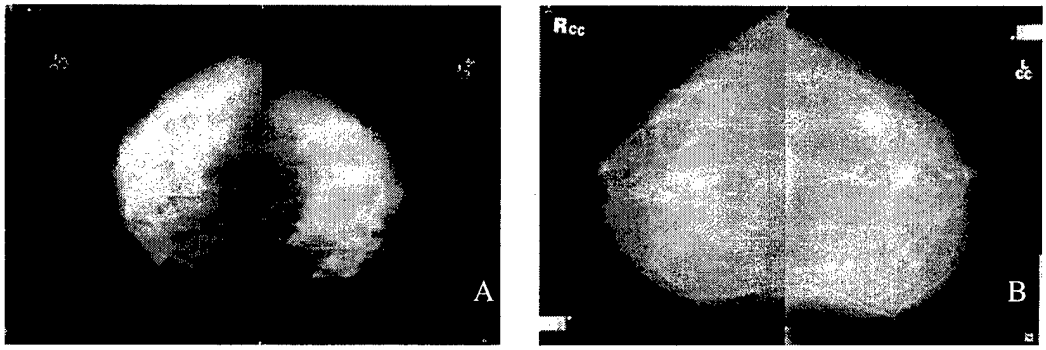

Figure 1

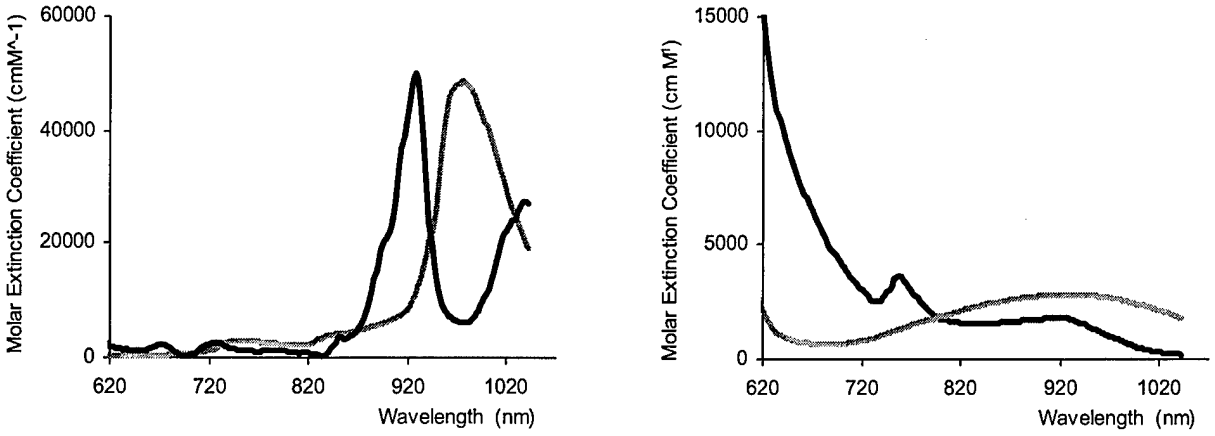
Molar Extinction Coefficient (cmM^-1)
60000
40000
20000
0
620
720
820
920
1020
Wavelength (nm)
Molar Extinction Coefficient (cm M')
15000
10000
5000
0
620
720
820
920
1020
Wavelength (nm)

Figure 2

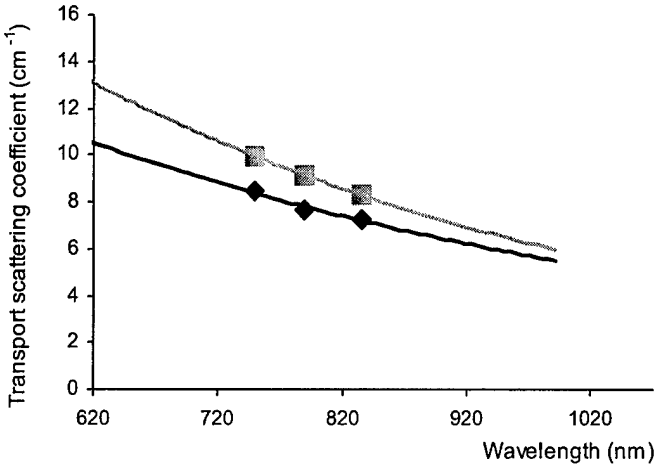
Transport scattering coefficient (cm -1)
16
14
12
10
8
6
4
2
0
620
720
820
920
1020
Wavelength (nm)

Figure 3

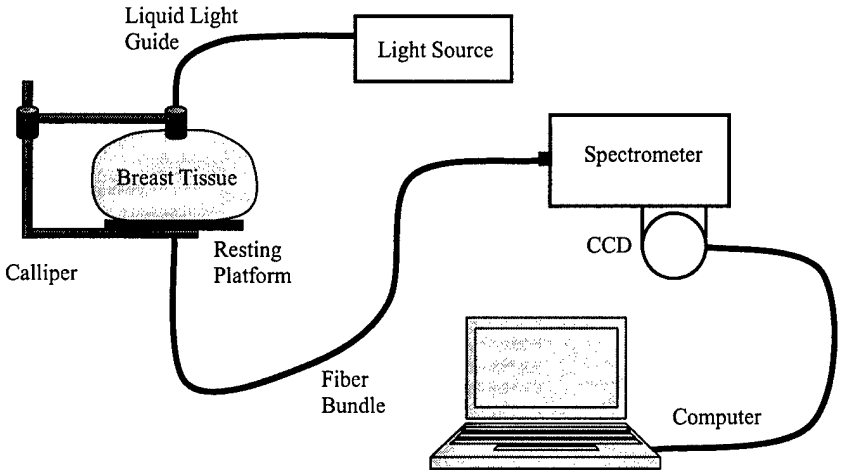
Liquid Light
Guide
Light Source
Spectrometer
Breast Tissue
CCD
Resting
Platform
Calliper
Fiber
Bundle
Computer

Figure 4

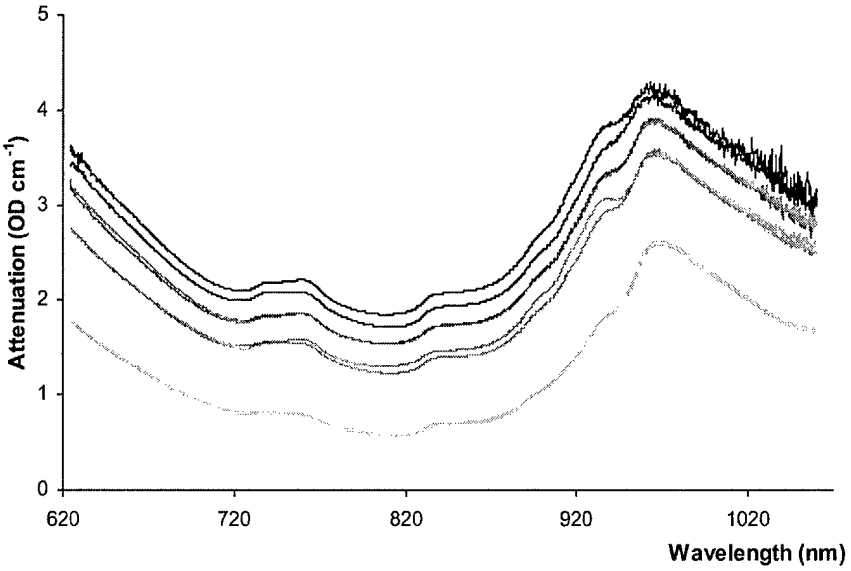
5
4
3
2
1
0
Attenuation (OD cm-1)
620
720
820
920
1020
Wavelength (nm)

Figure 5

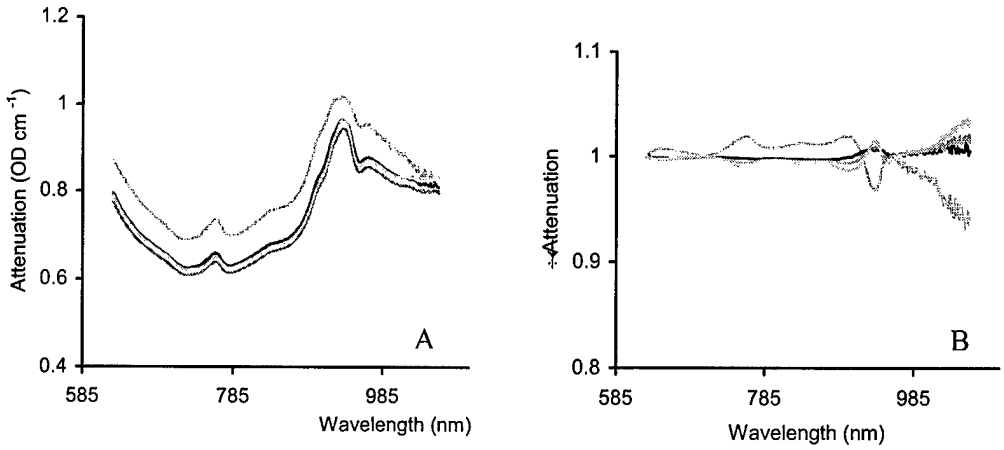
1.2
1
0.8
0.6
0.4
Attenuation (OD cm -1)
585
785
985
Wavelength (nm)
A
1.1
1
0.9
0.8
Attenuation
585
785
985
Wavelength (nm)
B

Figure 6.

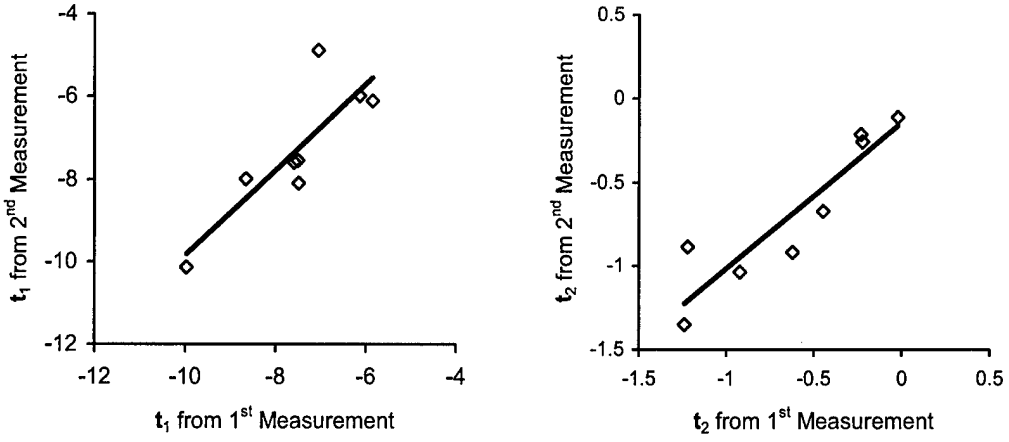
-4
-6
-8
-10
-12
-12
-10
-8
-6
-4
t1 from 2nd Measurement
t1 from 1st Measurement
0.5
0
-0.5
-1
-1.5
-1.5
-1
-0.5
0
0.5
t2 from 2nd Measurement
t2 from 1st Measurement

Figure 7

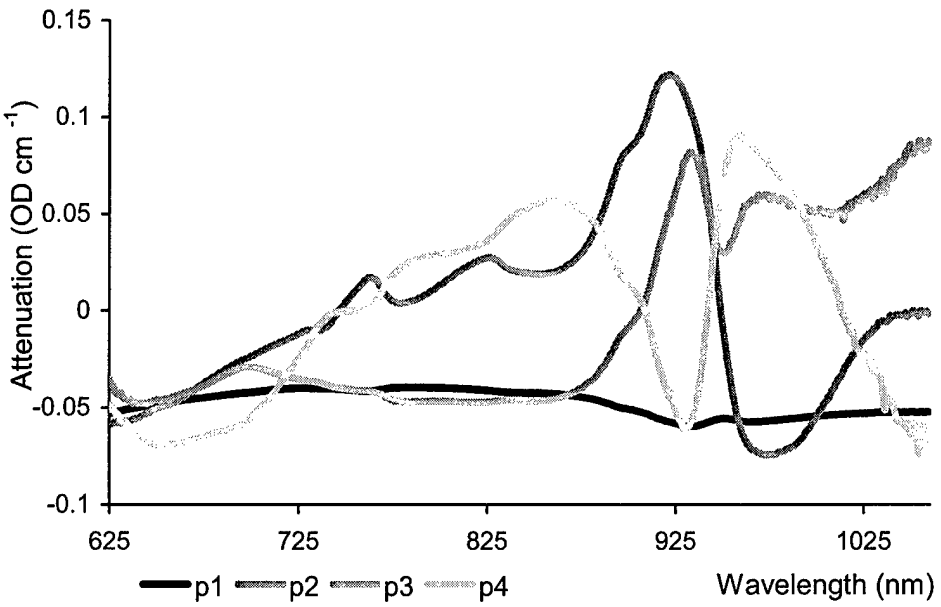
0.15
0.1
0.05
0
-0.05
-0.1
Attenuation (OD cm -1)
625
725
825
925
1025
Wavelength (nm)
p1
p2
p3
p4

Figure 8

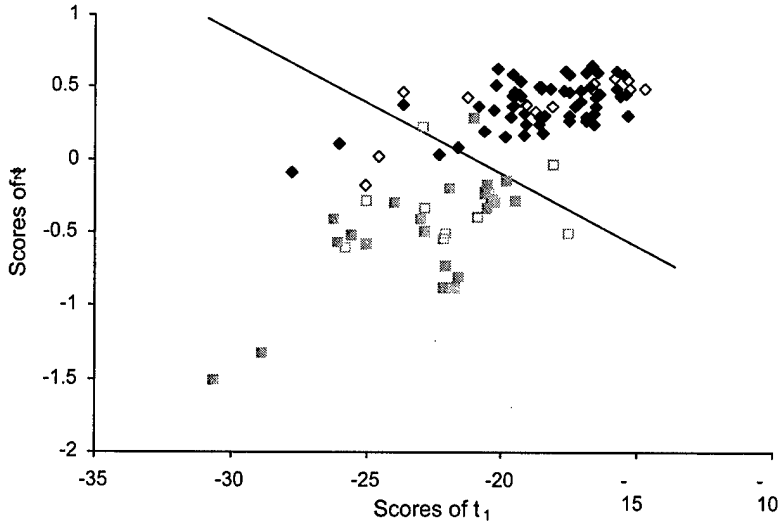

Figure 9

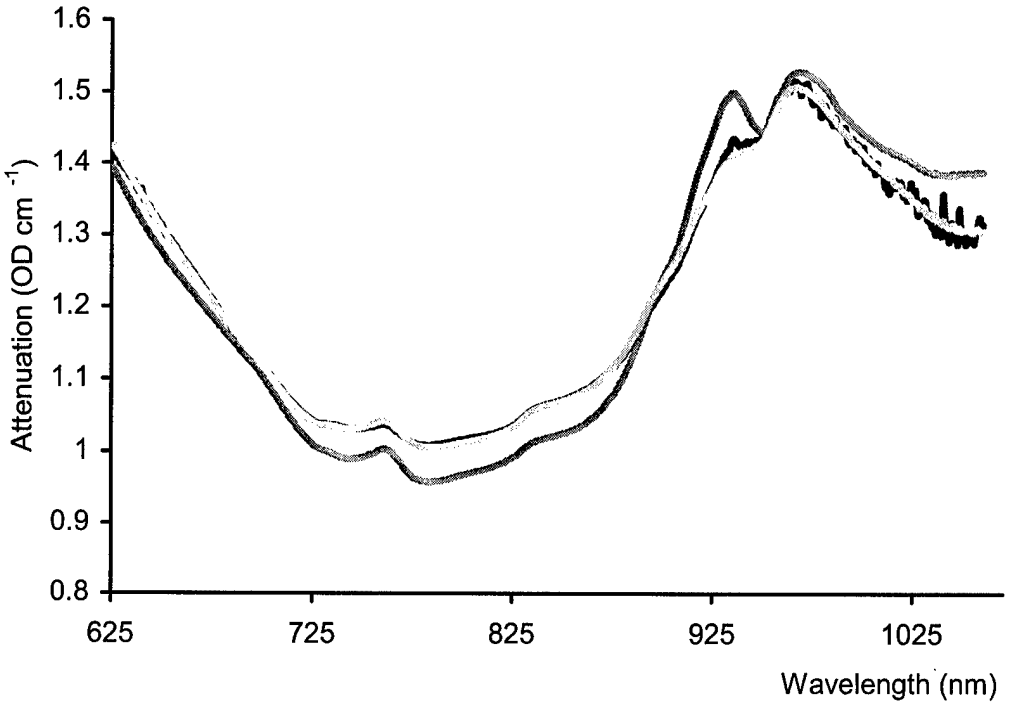
1.6
1.5
1.4
1.3
1.2
1.1
1
0.9
0.8
Attenuation (OD cm -1)
625
725
825
925
1025
Wavelength (nm)

Figure 10

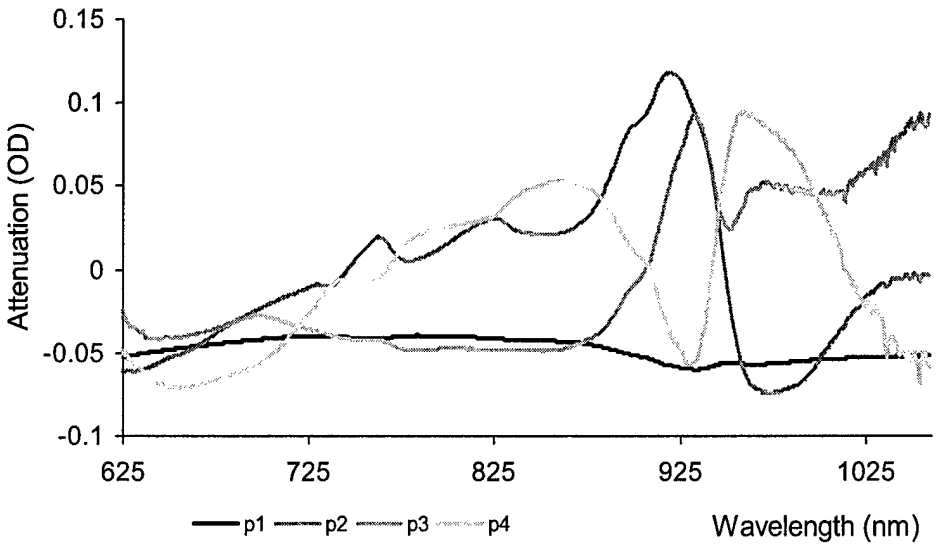
0.15
0.1
0.05
0
-0.05
-0.1
Attenuation (OD)
625
725
825
925
1025
p1
p2
p3
p4
Wavelength (nm)

Figure 11

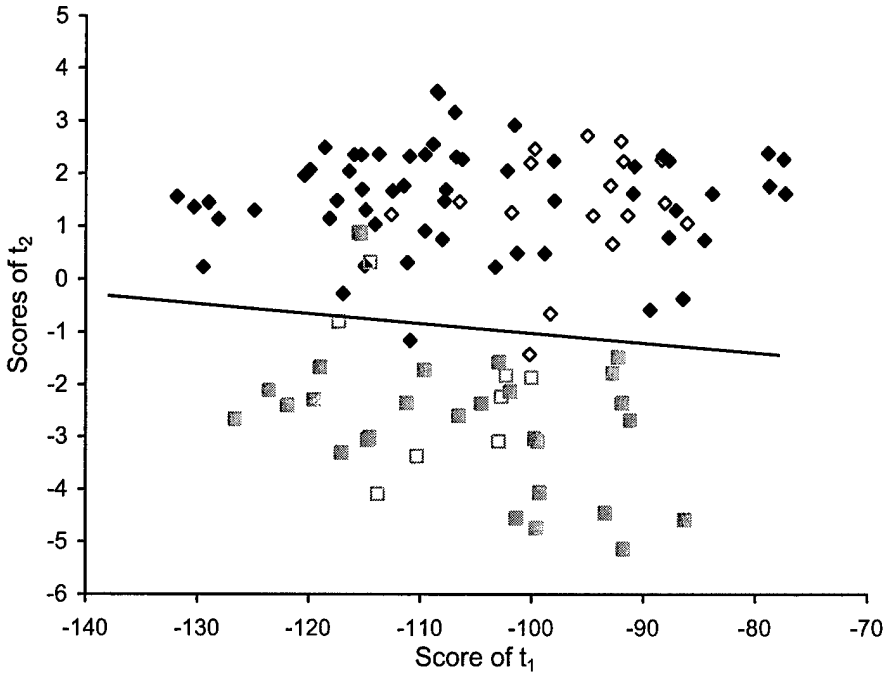
5
4
3
2
1
0
-1
-2
-3
-4
-5
-6
Scores of t_2
-140
-130
-120
-110
-100
-90
-80
-70
Score of t_1

Figure 12

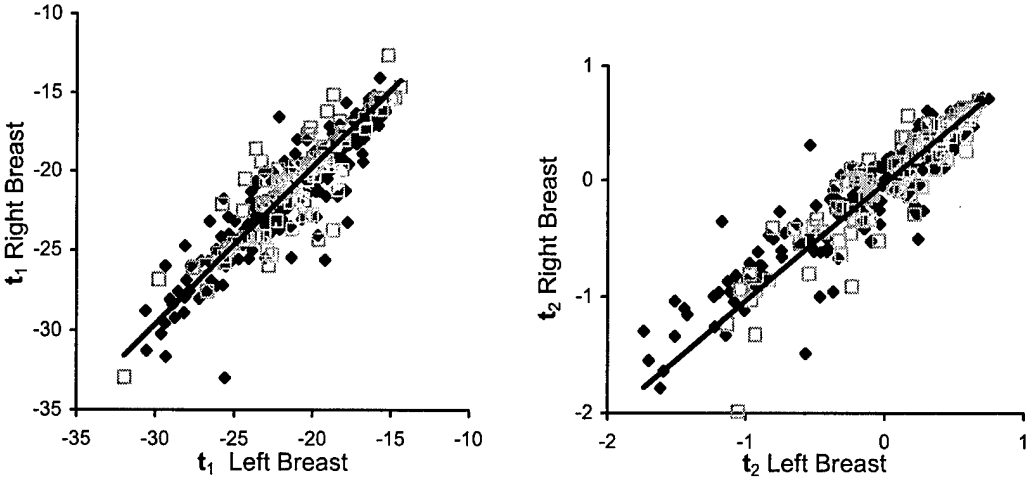
-10
-15
-20
-25
-30
-35
t_1 Right Breast
-35
-30
-25
-20
-15
-10
t_1 Left Breast
1
0
-1
-2
t_2 Right Breast
-2
-1
0
1
t_2 Left Breast

Figure 13

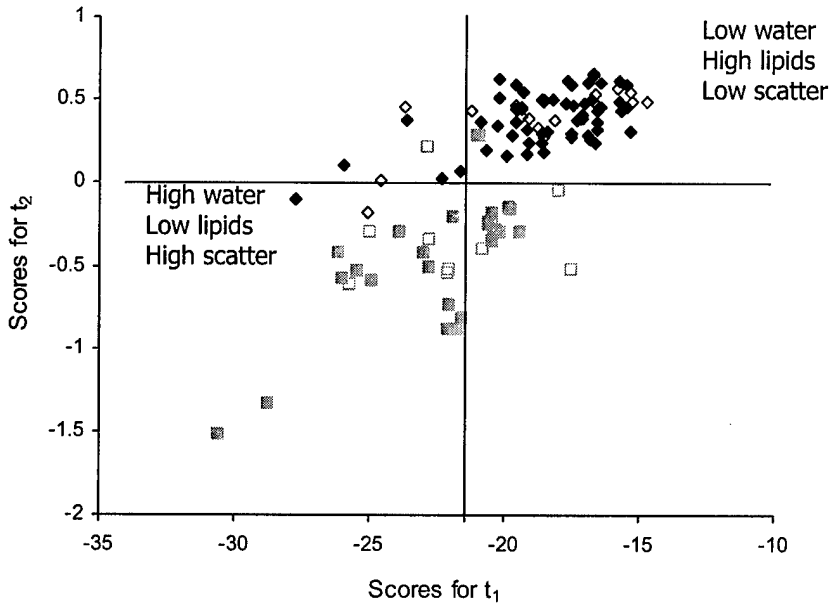
Low water
High lipids
Low scatter
High water
Low lipids
High scatter
Scores for t_2
Scores for t_1
1
0.5
0
-0.5
-1
-1.5
-2
-35
-30
-25
-20
-15
-10

Figure 14

Appendix 2

Optical Transillumination Spectroscopy of Breast Tissue for Cancer Risk Assessment.

Lothar Lilge[1,2], Kristina Blyschak[1], Michelle Simick[3], Roberta Jong[4],

[1]Ontario Cancer Institute, University Health Network, Toronto, Ontario, Canada M5G 2M9;
[2]Department of Medical Biophysics, University of Toronto, Toronto, Ontario Canada M5G 2M9
[3]Toronto-Sunnybrook Regional Cancer Centre, Toronto, Ontario, Canada M4N 3M5;
[4]Sunnybrook and Women's College Health Science Centre, Toronto, Ontario, Canada M4N 3M5;

ABSTRACT

Breast cancer is the most commonly occurring cancer in women. The lifetime risk of being diagnosed with breast cancer is approximately 1 in 10 thereby the highest out of all cancers. Breast cancer screening programs have been shown to decrease the mortality rates of women between ages 50-69, since cancers are detected at an earlier, more favourable stage. It is apparent that the development of breast cancer is a slow process following initial transformation of the breast tissue. Hence, there has been a strong effort within the research community to understand risk factors for the disease. Risk factors are defined as those characteristics that are more common in people with the disease when compared to the normal population. Quantification of an individual's breast cancer risk may lead that individual to modify her lifestyle and/or diet. Lifestyle changes could lead to a reduction in the incidence of breast cancer.
Anatomically, the presence of increased amounts of fibroglandular tissue raises the estimated risk by up to 6 fold (corrected for age), hence representing one of the strongest known risk factor pertaining to the entire female population. In this study the relative area of mammographic densities within a mammogram will be used as a global risk assessment tool. It has been shown previously that quantification of water, lipids, haemoglobin and other tissue chromophores of the optically interrogated breast tissue which give also give rise to the mammographic densities, is feasible through near-infrared spectroscopy. Thus, the hypothesis for this study is that optical transillumination spectroscopy provides consistent and/or complementary information to conventional mammography in quantifying breast density.

Keywords: optical transillumination spectroscopy, breast tissue density, breast cancer risk, principle component analysis.

1. INTRODUCTION

Preventive oncology involves two tasks, first identification of the population at risk and second the implementation and efficacy monitoring of intervention strategies. The first task requires methods and techniques based on physical measurements that identify individuals at high risk and who would benefit most from the interventions. These risk quantification techniques must be applicable to the entire population and allow for identification of individuals at high risk for developing cancer with high sensitivity and specificity. The latter is important for several reasons: to identify all individuals at risk, to decrease the number of individuals undergoing unnecessary treatment (i.e. those who are low or medium risk), and to empower individuals to make informed decisions regarding their health and the potential benefits of risk reduction strategies. While some genetic predisposition towards a certain cancer is known, they often target only a small subpopulation such as women with BRCA1 and BRCA2 genetic mutations [1] and hence are not suitable for population wide risk screening.

Breast cancer is the most commonly occurring cancer in women. The lifetime risk for developing breast cancer is 1 in 5-10, depending on the reporting agency [2]. While, these statistics are rather poor one needs to consider that the tissue transformation preceding breast cancer can occur 20 years prior to the development of the disease [3] thereby providing a "window of opportunity" to employ risk reduction interventions such as modification in lifestyle, diet, chemopreventive treatments (i.e. Tamoxifen, Raloxifene) [4] or in severe cases, such as women with BRCA1 and BRCA2 genetic mutations or similar risk prophylactic mastectomy [5]. All of these interventions are designed to prevent cancer and inadvertently they will influence

the quality of a woman's life, particularly by those rather aggressive interventions designed to achieve a risk reduction in only a few month or years. Thus, considering that identification of the women at risk at an earlier age may result in an adequate reduction in breast cancer risk by only a relatively small lifestyle changes, such as exercise or diet but acting over a longer period of time. Thus, a risk assessment technique should be inherently, compatible with screening of a women at an earlier age.

Current methods of establishing the breast cancer risk include the Gail Risk Model [ref] and parenchymal density patterns derived from standard x-ray mammography. The former is mostly based on demographic information while the latter represents a physical property of tissue. Parenchymal density patterns reflect the ratio of glandular and connective tissue to adipose tissue within the breast. Women with mammographically dense tissue occurring in more than 70% of the breast are 4 to 6 times more likely to develop breast cancer than those with low tissue density (< 25%) [6]. Because of the inherent risks of x-rays, mammography is not recommended as an annual diagnostic for women younger than 40 in most countries [7], thereby limiting the time available for risk reduction interventions to assert their influence. Similarly, the demographic information required for the Gail Risk Model is often not available for women until they have reached thier late 30ties or 40ties. Strictly speaking the Gail Risk Model is only valid for women over 30.

Near-infrared optical transillumination spectroscopy (OTS) has been shown to give information about breast tissue composition [8]. Specifically, OTS results in unique optical spectra, governed by hemoglobin, water and lipid absorption in the tissue and the average scattering power [9]. The differences in chromophore contributions in the tissue have also been shown to mirror the x-ray dense and x-ray lucent areas of the mammogram [10]. In contrast to mammography, which is based on ionizing radiation probing the nuclear composition of tissue, OTS uses non-ionising radiation with quantum energies that interact with the electronic and vibrational levels of the molecules, representing more the anatomic, metabolic status of the breast. Consequently, OTS can be used more frequently and on younger women and should be able to detect differences in tissue composition between high and low risk groups, based on molecular composition.

To establish the feasibility of OTS as a Breast Cancer Risk assessment technique, correlations between the spectra and the Parenchymal density pattern were established. These correlations were initially established using Principle Component Analysis (PCA), using tissue density classifications by a radiologist as. Multivariate analysis techniques are used to determine if stratification of the spectral data by eiher measurement position on the breast in cranial-caudal projection (center, medial, distal, or lateral) or physical parameters, such as the volunteer's age and body mass index (BMI), is beneficial in increasing the tissue density prediction by OTS.

2. MATERIALS AND METHODS

2.1 Patient recruitment

The data set used in this study includes a collection of mammograms and OT spectra gathered from 156 volunteers recruited through the Marvelle Koffler Breast Centre at Mount Sinai Hospital, Toronto, Ontario. All women had a film screening mammogram within the last 12 months of being recruited, which was negative for cancer lesions, and did not show a large bilateral variation in tissue density. All women also had no previous surgery to the breast tissue, including reduction, implants or tattoos.

Film mammograms were classified on a nominal scale by a radiologist (Dr. Roberta Jong) into either low (< 25 %), medium (25% to 75%) or high (> 75% dense tissue area) density categories. Sixty-one women were classified by the radiologist as having low, 68 as having medium, and 27 as having high tissue density. The population contributions of the tissue density categories in this study closely reflect the population proportions seen in the Canadian National Breast Screening Study [12] (Table 1). The age of the volunteers ranged from 36 to 72 years.

2.2 Visible near-infrared transmission

A 12W halogen lamp served as broadband light source, ultra-violet, part of the visible spectrum and mid-infrared radiation were eliminated using a cut-on filter and a heat rejection filter, respectively, and the remaining light was coupled into a 5 mm diameter liquid light guide in contact with the skin on top of the breast tissue. A total power of 0.25W, covering the 550 to 1300 nm bandwidth, was delivered to the skin. Transmitted light was collected via a 7 mm diameter optical fiber bundle (P&P Optica, Kitchener, Waterloo,

140 fibres, 200μm, N.A. 0.36) and wavelength dependent detection in the visible and near-infrared was achieved using a Kaiser spectrophotometer with holographic transillumination grating (15.7rules/mm blazed at 850nm) and a 2D cryogenically cooled silicon CCD (Photometrics, New Jersey, USA) at a spectral resolution of better than 3 nm between 625 and 1060 nm. Spectral resolution was achieved by positioning a 0.5 mm slit between the distal end of the collection fibre and the spectral grating. The peak quantum efficiency of the back thin CCD is at 780 nm with a quantum efficiency of 0.2 remaining at 1060 nm. By imaging the entrance slit of the spectrograph onto the 2D CCD, 50 rows of pixels were exposed to detected light thereby increasing the dynamic range of the electronic detection by a factor of > 30. Cryogenic cooling was used to minimize background noise. Further signal to noise improvement was accomplished by using exposure times of 3 to 5 seconds, and averaging 5 scans for all spectra. Figure 1 shows a block diagram of the setup

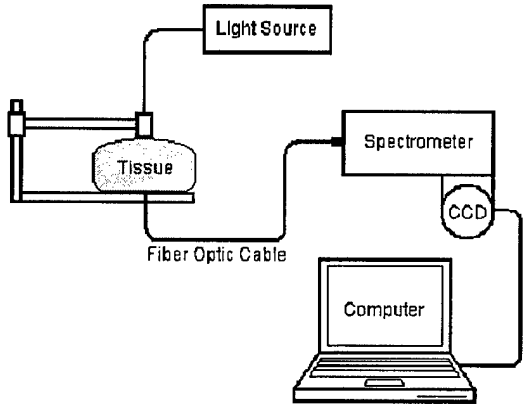

Figure 1. Schematic of OTS setup.

All spectra were corrected for daily variations in the wavelength dependent signal transfer function of the optical system and the thickness of the interrogated tissue. To correct for the signal transfer function, spectra were referenced to a transmission standard made of 1 cm thick ultra high density polyurethane (Gigahertz Optics, Munich, Germany). Consequently, all volunteer spectra are expressed in units of optical density per centimeter [OD/cm], given by the negative log of the raw data spectrum divided by the reference spectrum of the polyurethane block plus the optical attenuation of the polyurethane block divided by the interoptode distance. The scattering and absorption properties of the standard were measured in a separate experiment using an integrating sphere diffuse reflectance set-up [13] (OD ~ 1.8 – 2.3 over the wavelength range of interest).

All volunteer measurements were taken in the dark, with the volunteer seated comfortably in an upright position and the breast resting on a horizontal platform. A total of eight measurements in cranial-caudal projection were taken, four per breast (center, medial, distal, and lateral). Typical data acquisition for all 8 measurements averaged 160 to 200 seconds. The source and detector fibers (optodes) were held coaxially, pointing towards each other, by a caliper attached to the resting platform providing the interoptode distance. The source fibre was placed against the skin on the top surface of the breast with minimal compression. Considering typical tissue optical properties [14] and a tissue thickness of 5 cm, an ovoid shape volume estimated at 30 cm^3 is interrogated.

Table 1. Breakdown of study volunteers: including study and population proportions and total number of spectra analysed (numbers in parentheses).

Density Category	*Training Set*	*Validation Set*	*Proportion*	
			Study	*Population*
Low	46(368)	15(120)	39.0%	37.0%
Medium	51(408)	17(136)	43.6%	49.0%
High	20(160)	7(56)	17.3%	14.0%
Totals	117(936)	39(312)		

2.3 Data Analysis

Principle Component Analysis (PCA) was used to establish a correlation between the obtained optical transillumination spectra and mammographic density. PCA is an analytic mathematical method optimized for comparison of vectors (i.e. spectra) with nominal data (i.e. tissue density) [11, 15]. PCA determines the amount of variance within the population of spectra and iteratively reduces the data to a few representative spectra called components (p_i). Scores (t_i) are then assigned to each individual's spectra to show how much of each component is present in the original data spectrum. The scores of two or more components can also be plotted against one another to identify clusters of spectra that are closely related and that exhibit common traits. Clusters are assigned an outcome, here low versus high tissue density, and lines or planes separating clusters are determined analytically. Scores that enable differentiation between tissue densities identify useful component spectra and hence

chromophore contributions to density and thus indirectly risk.

In this study, PCA was executed on 75% of all spectra (n = 936, 117 volunteers x 8 measurements) randomly selected from each of the defined tissue density categories comprising the training set. In this manner, the relative contribution of each tissue density category in the data sets was retained during the analysis. The remaining 25% of the spectra (n = 312, 39 volunteers x 8 measurements) were placed in a validation set (Table 1). The principle components (p_i) derived from the training set spectra were then used to determine the scores (t_i) on the validation set spectra, thereby testing the predictive ability of the model. The PCA data sets were not stratified by menopausal status (i.e. pre versus post-menopausal) since a previous study by our group [11] demonstrated no influence of the menstrual cycle on the spectral measurements.

To determine the predictive value of the PCA model and hence OTS, two measures comparable to sensitivity and specificity, a high density measure (HDM) and a low density measure (LDM), were determined for both the training and validation sets, where HDM are the correctly predicted women with high tissue density over all women with high density, and LDM respectively are all correctly predicted women with low tissue density over all women with low density.

HDM and LDM were determining using a separation plane that differentiated the high and low tissue density clusters resulting from spectra of the training sets in R^3. Analysis was executed on cluster plots using either component scores (t_i) (n = 528) resulting from all individual spectra or their means per individual ($\bar{t}_i$) (n = 66, Table 1). For this each cluster was represented by a linear regression analysis to calculate the plane of best fit for both tissue density clusters, respectively, defined by:

$$t_z = b + a_x t_x + a_y t_y \qquad (2.1)$$

Where t_z represents one component randomly chosen as dependent variable, t_x and t_y are the independent component scores using either t_i or $\bar{t}_i$, a_x and a_y are the resulting slopes, and b is the z-intercept.

The equation of the plane (t_i) separating the high and low tissue density training sets was calculated as the plane halfway between the low and high tissue density planes defined by equation (2.1):

$$t_i = \frac{1}{2}\left[\left(b_{low} + a_{xlow}t_{xlow} + a_{ylow}t_{ylow}\right) + \left(b_{high} + a_{xhigh}t_{xhigh} + a_{yhigh}t_{yhigh}\right)\right] \qquad (2.2)$$

Where a_{xlow}, a_{ylow} and a_{xhigh}, a_{yhigh} are the slopes for the low tissue density cluster and the high tissue density cluster, respectively, b_{low} and b_{high} are the respective z-intercepts, and t_{xlow}, t_{ylow}, t_{xhigh}, t_{yhigh} are the respective component scores again using either t_i or $\bar{t}_i$.

Differences between component scores t_1 to t_4 by measurement position (center, medial, distal and lateral) were tested by non-parametric methods using a Kruskal-Wallis rank test. When testing for differences between measurement positions, only measurements from the left breast were used since we showed [11] no significant difference between component scores from the left and right breast.

PCA derived component scores t_1 to t_4 for the low and high tissue density categories as a function of a volunteer's age and body mass index (BMI) were examined using Spearman's r correlation analysis. Linear regression analysis was also executed for component scores t_1 to t_4 as a function of age or BMI. For correlation and linear regression analyses, either all scores (n = 1248) or scores averaged per individual (n = 156) were used.

For all analyses, p-values ≤ 0.05 were considered to be statistically significant.

3. RESULTS

3.1 PCA of density categories

Figure 1a and b shows examples of the raw data collected for women with high and low tissue density, respectively. Figure 1c shows the resulting first four principle components (p_i) from the PCA for non-stratified spectra thus using n = 936 spectra. These first four components contain 99.87%, 0.06%, 0.05% and 0.01% of the variance in the total data set, respectively, yielding a combined total of 99.99%. In principle, the data can be represented in R^4.

A R^3 cluster plot of component scores t_1, t_2 and t_3 from the training spectra for only high and low tissue densities (n = 528) is presented in Figure 2a. A corresponding plot using mean component scores $\bar{t}_i$,

$\bar{t}_2$ and $\bar{t}_3$ per individual for the high and low tissue densities for the training and validation sets (n = 88) is shown in Figure 2b, demonstrating improved cluster separation. Thus, spectra related to breast tissue classified by the radiologist as either or low density show differences in their spectral compositions, resulting in reasonably tight clusters.

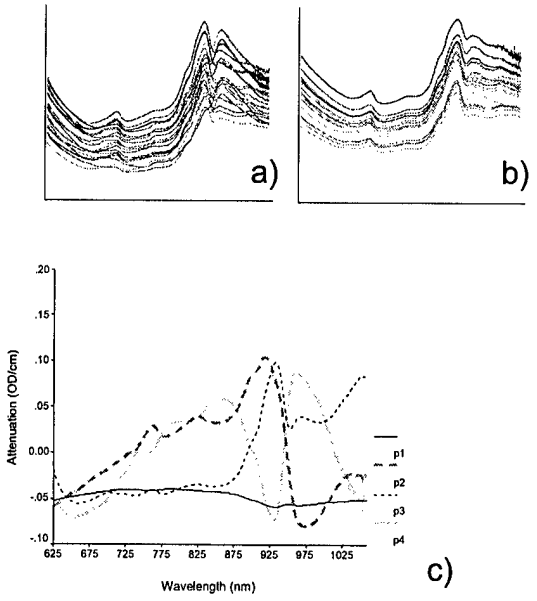

Figure 1. Examples for transillumination spectrum from women with a) high tissue density, b) low tissue density and c) the resulting principle components p_1 to p_4 of thickness and transfer function corrected spectra, all given as a function of wavelength.

3.2 PCA of density categories by measurement position

For the low tissue density of the training set, a Kruskal-Wallis rank test demonstrated a significant difference in component scores $\bar{t}_1$ to $\bar{t}_4$ between each measurement position (all at $p < 0.01$). For the high tissue density training set, only component score $\bar{t}_2$ resulted in a significant difference between each measurement position. As a result, PCA was repeated separately for each measurement position (center, medial, distal and lateral). Spectra from both the left and right breasts were used for training, e.g. 234 spectra from 117

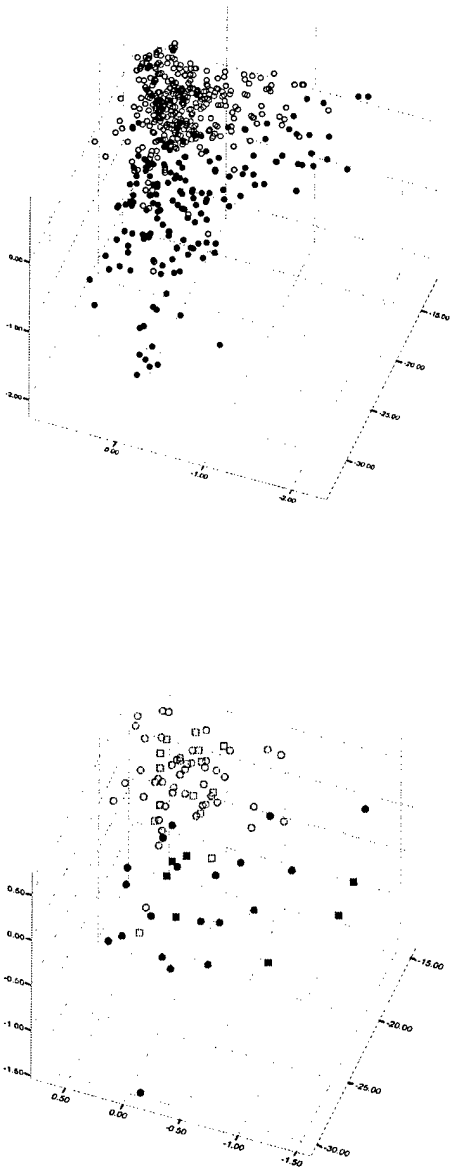

Figure 2. Three-dimensional cluster plots of t_1, t_2 and t_3 for all component scores (a) and mean scores per individual (b) resulting from thickness and transfer corrected spectra of high and low tissue density. Open symbols, scores from tissue classified as low density; closed symbols, scores from tissue classified as high density.

volunteers and 78 spectra from 39 volunteers for validation.

Figure 3 shows the first four principle components (p_i) for the center and distal positions after stratified for measurement position. Of the variance in the total data set, the first component p_1 contains between 99.85% and 99.91%, p_2 between 0.05% and 0.08%, p_3 between 0.03% and 0.05%, and p_4 contains 0.01%. Three-dimensional cluster plots of component scores t_1, t_3 and t_4 at the center position and scores t_1, t_2 and t_4 at the distal position are shown in Figure 4, respectively, for high and low tissue density combined data sets (n = 176).

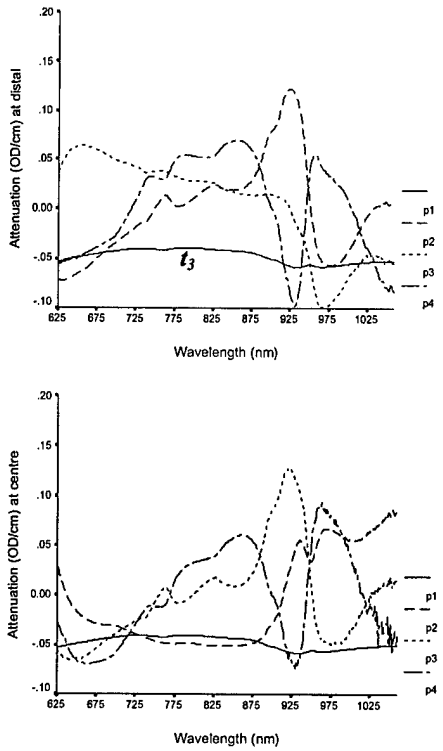

Figure 3. Plots of principle components p_1 to p_4 for the center (a) and distal (b) measurement positions.

3.3 HDM and LDM

Table 2 shows the resulting HDM and LDM calculated using scores t_1, t_2 and t_3 for the training and validation sets using either all component scores (training = 528, validation = 176) or the mean component score per individual (training = 66, validation = 22). In the majority of cases, HDM and LDM increase when the mean component score $\bar{t}_i$ per individual is used.

Table 3 provides the best HDM and LDM results for the training and validation sets for each measurement position. The center and distal positions show the best HDM and LDM for the training and validation sets.

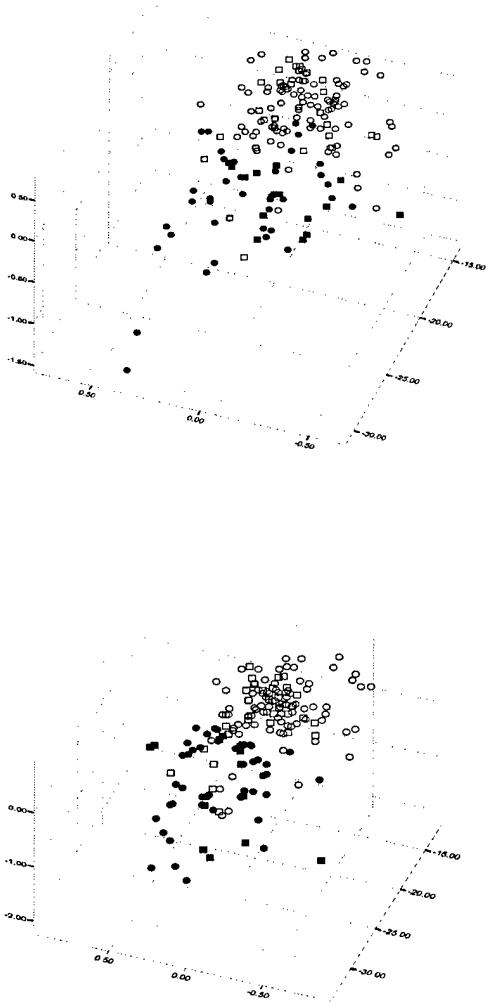

Figure 4. Three-dimensional cluster plot of t_1, t_3 and t_4 and t_1, t_2 and t_4 resulting from thickness and transfer corrected spectra from high and low density tissue for the center (a) and distal (b) positions. Open symbols are low tissue density; closed symbols are high tissue density. Circles refer to training set and squares to validation set.

Table 2. HDM and LDM for test and validation sets using all component scores and mean scores per individual.

	Scores Used	Training Set [%]		Validation Set [%]	
		HDM	LDM	HDM	LDM
All scores	$t_2 f(t_1, t_3)$	76.9	88.3	75.0	96.7
Mean score	$\overline{t_2} f(\overline{t_1}, \overline{t_3})$	85.0	89.1	85.7	100.0

Table 3. HDM and LDM for test and validation sets for each measurement position

Position	Scores Used	Training Set [%]		Validation Set [%]	
		HDM	LDM	HDM	LDM
Center	$t_3 f(t_1, t_4)$	95.0	87.0	92.9	90.0
Distal	$t_2 f(t_1, t_4)$	90.0	91.3	100.0	100.0
Medial	$t_3 f(t_1, t_4)$	77.5	71.7	85.7	86.7
Lateral	$t_2 f(t_1, t_3)$	80.0	95.7	71.4	100.0

3.4 Number of Measurement Positions

Figure 5 shows histograms indicating the frequency of true high and low tissue density predictions from OTS for each individual. If scores t_i from 3 or more of four spectra indicate high tissue density, the best HDM and LDM are obtained using spectra from the center and distal measurement positions (compare Fig. 5a to 5b). When including medium tissue density for the centre and distal position 33% would be classified as false positive, see figure 6. While this appears to result in an overall higher false positive rate, specifically when considering that the medium density comprises half the population, one also needs to consider that plane of separation was determined only based on the total difference between high and low clusters.

3.5 PCA and Physical Parameters (Age and BMI)

Linear regression analysis demonstrated a significant correlation between the component scores t_i and age or BMI. However, further analysis showed that the age dependent slopes of the different tissue densities are in effect parallel and hence without a priori knowledge of the tissue density, no age or BMI correction can be introduced.

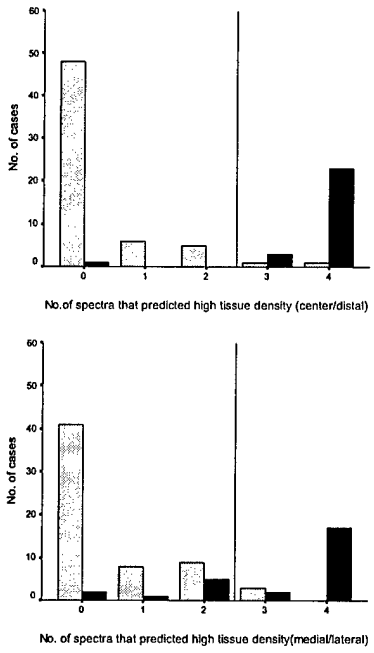

Figure 5. The number of spectra from (a) the center and distal positions to predict global tissue density with a resulting LDM =96.7% and HDM 96.3% and (b) the medial and lateral positions with a resulting LDM =95.1% and HDM 70.4% (b) that correctly predicted high tissue density. High tissue density shown in black, low tissue density shown in grey.

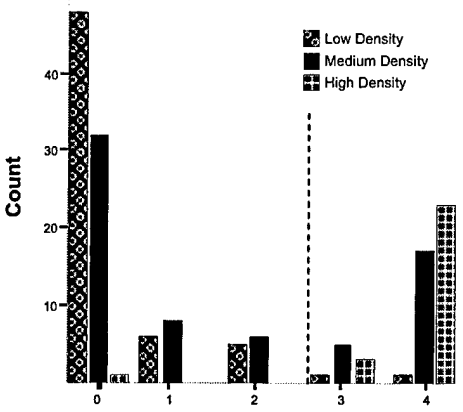

Figure 6. The number of spectra from the center and distal positions to predict global tissue density, with a resulting LDM =67.6% and HDM 96.3%

Scatter plots of mean component scores $\overline{t_1}$ and $\overline{t_2}$ per individual as a function of the volunteer's age and body mass index for the high and low tissue densities are shown in Figure 7 and 8 respecitvely. The results of linear regression analysis between age or BMI and the first two component scores are also indicated. According to Spearman's r, a significant but weak correlation exists between both component scores $\overline{t_1}$ and $\overline{t_2}$ and age or BMI. Similar results were obtained for component scores t_3 and t_4 (data not shown).

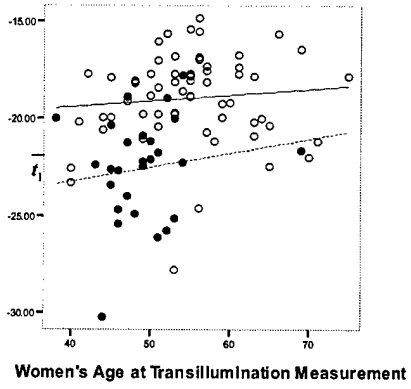

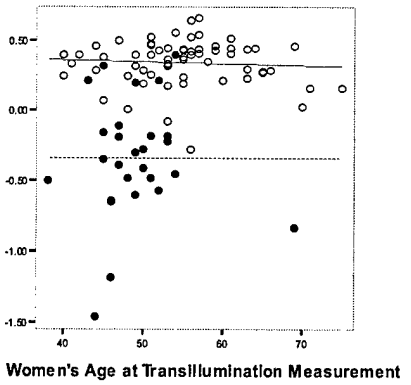

Figure 7. Scatter plots of averaged component scores $\overline{t_1}$ (top) and $\overline{t_2}$ (bottom) per individual as a function of age for high (closed symbols and dashed line) and low (open circles and solid regression line) tissue density categories.

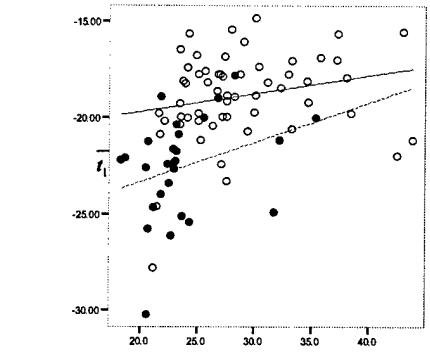

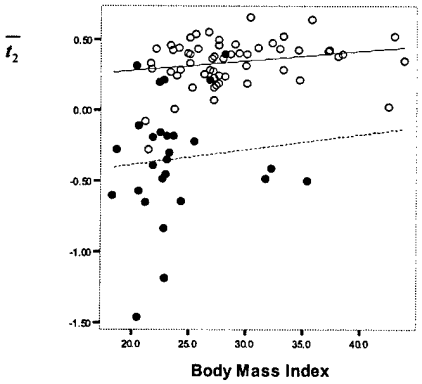

Figure 8. Scatter plots of averaged component scores $\overline{t_1}$ (top) and $\overline{t_2}$ (bottom) per individual as a function of BMI for high (closed symbols and dashed line) and low (open circles and solid regression line) tissue density categories.

4. DISCUSSION

4.1 Principle Component Analysis (all measurement positions)

Input parameters such as known tissue chromophore spectra were not implemented in the training of our PCA model. Despite this fact, each derived principle component, p_i, includes a combination of spectral signatures comprising light scattering and chromophore absorptions (water, lipid and hemoglobins), which vary with breast tissue density.

Scores associated with principle component p_1 contain information on wavelength independent absorption due

to differential optical path length, and light losses at the breast boundary and have negative values in the PCA model (Fig. 1). Light scattering is tissue dependent and its wavelength dependence can be described by $u_s' = a\lambda^{-b}$ [16]. Light losses due to scattering occur because of an increase in photon path length and thus a lower probability of traversing tissue. The polyurethane standard, also a Mie scatterer, with an albedo > 0.999 was used to calibrate the spectral transfer function of the optical system daily and thus, the wavelength dependence of the scattering in the breast tissue is minimized or lost [11]. Hence, p_1 carries wavelength independent optical path length information and via the change in optical path length between tissue types it can contributes to determine tissue density. For example, low density tissue has reduced scattering when compared to high density tissue [17], resulting in higher values of t_1 (i.e. less negative), indicating less attenuation or loss of light and a shorter optical path length.

Light losses at the breast boundary are also captured in p_1. We have shown previously that measurements taken at the medial position are different from the centre measurement and similar to measurements made closer to the edge of the breast [11]. This further suggests that stratification by position is beneficial.

The most important spectral features in the spectrum of p_2 are the lipid peak at 925 nm and the inverse water peak at 975 nm (Fig. 1). Low density tissue is characterized by adipose tissue resulting in positive scores t_2 (Fig. 2) when the lipid peak is the dominant spectral feature. Smaller contributions in the low tissue density spectrum are also evident at 770 nm (deoxy hemoglobin) and 825 nm, a minor lipid absorption peak. Conversely, high density tissue has a higher water content [18] and the scores t_2 are predominantly negative, when the water peak is the dominant spectral feature (Figs. 1, 2). Contributions from deoxy hemoglobin are also evident in the high tissue density spectrum of p_2 between 625 and 750 nm, where the negative slope of the deoxy hemoglobin curve is visible (Fig. 1).

The spectrum of p_3 is relatively flat between 625 nm and 875 nm, which can be attributed to contributions from the oxy hemoglobin curve (Fig. 1). Another notable feature is that the lipid and water peaks are positive compared to the spectra of p_2 and p_4 (see below). Component scores t_3 for low density tissue are positive when the lipid peak is the dominant spectral feature (Figs. 1, 2). Component scores t_3 for high density tissue are negative, suggesting a shift from an oxy hemoglobin curve to a deoxy hemoglobin curve (as seen in the spectrum of p_2). Since decreases in oxygen are associated with increased cellular metabolism [19], oxygen saturation is smaller in high density tissue when compared to low density tissue.

The spectrum of p_4 is similar to that of p_2 (Fig. 1), however, for low density tissue, component scores t_4 are negative and for high density tissue, they are positive (Fig. 2).

Cluster plots in three dimensional space defined by t_1, t_2 and t_3 result in a good separation between high and low tissue densities, either when all component scores are used (t_i) or when the mean score per individual is used ($\bar{t}_i$) (Figs. 2a and b). The improvement in HDM and LDM for the mean component scores is given by the fact based on the definition of high and low density only 3 of 4 quadrants scores need to be with in the cluster based on the mammographic global classification. Averaging the scores reduces the effect of measuring possible a local volume not expressing the globally assessed density.

4.2 Principle Component Analysis by measurement position

Positional analysis suggests that the PCA model should be trained independently on each measurement position (center, medial, distal, and lateral). The results of the PCA for each individual position and the subsequent analysis of cluster plots in three dimensional spaces show that only two positions need to be interrogated: the center and the distal. In general, the component spectra p_i for these two positions are comparable with the exception that component spectrum p_2 for the center position is similar to component spectrum p_3 for the distal position and vice versa (Fig. 3). Both component spectra (p_2 at center and p_3 at distal) are spectrally flat over a large wavelength region with poor differentiation of the lipid and water peaks. Consequently, cluster plots in a three dimensional space defined by t_1, t_3 and t_4 result in a good separation between high and low tissue densities for the center position and cluster plots in a three dimensional space defined by t_1, t_2 and t_4 result in a good separation between high and low tissue densities for the distal position (Fig. 4). The exchange of the significance between t_2 and t_3 for the center and distal positions is most likely limited by the small amount of variance captured by them in association with the limited number of observations available to date.

4.3 HDM and LDM

Because radiological assigned parenchymal density is a global analysis, calculating HDM and LDM using all eight spectra derived component scores induces obvious additional variability as the density is not distributed homogeneously throughout the tissue. Using the mean score per individual reduces the variability in the OTS predicted density within an individual's breast tissue (Fig. 2b; Table 2).

The best estimation of a global classification is pooling spectra from different positions (n = 2). The highest HDM and LDM is achieved using spectra from the center and distal positions. (Fig. 5a). The HDM and LDM based on these two positions might be a slight overestimate of the predictive power of the test given that women who demonstrated variation in the bilateral organ were excluded from analysis. However, it also suggests that improved PCA training is possible if the regional tissue density associated with each optically interrogated volume is known.

The medial position provides acceptable HDM and LDM for our validation set (Table 3). The lateral position provides LDM comparable to the distal position, but the lowest HDM among positions for our validation set (Table 3). This difference in the predictive value of the different quadrants is a direct reflection of the spatial prevalence of parenchymal density pattern within the breast [21].

4.4 Component scores and physical parameters (Age and BMI)

As the population ages one would expect an increase in component scores t_1 and t_2 since atrophy of the tissue, still ongoing past menopause, would result in less light scatter and an increase in lipid content [20]. However, from Figures 6a and b, it is evident that there is a small increase in component scores t_1 with age for both low and high density tissue, and little to no increase in t_2 with age for the low and high tissue density categories. So as a predictive tool the odds ratio or relative risk should be independent of age. Similarly, with an increase in BMI we anticipate component scores t_1 and t_2 to increase. A small but significant association exists with BMI and component scores t_1 and t_2 for the low tissue density group (Figs. 6c, d). A cluster of scores t_1 and t_2 related to the high density tissue is seen for low BMI, which results in an apparent large slope for this group; however, the correlation coefficients are weak.

While some statistically significant correlations can be established between age and BMI and the component scores t_1 and t_2, these associations are also dependent on a woman's density classification. Consequently, no correction for age or BMI is possible since the density of a woman coming in for OTS measurements is not known a priori. This further suggests that the physiological changes in breast tissue density due to age and BMI are already contained in the component spectra and hence captured by the derived component scores.

5. CONCLUSION

OTS is a physical assessment technique applicable to the population at risk that only requires information on the inter-optode distance and the location of the measurements on the breast in cranial caudal projection (center, medial, distal, and lateral). Consequently the spectra are independent of the instrument and interrogated tissue thickness, and are hence portable between instruments. Furthermore, only two positions need to be interrogated, the center and the distal, to produce sensitivity and specificity values above 96%.

ACKNOWLEDGEMENTS

This work was funded by CDMRP (Congress Directed Medical Research Plan) under DAMD 17-00-1-0393. The authors wish to thank Dr. Robert Weersink for his assistance in the development of the analytic mathematical models used and Mrs. Samantha Dick for her help with the recruitment of study volunteers.

REFERENCES

[1] G.S. Dite, M.A. Jenkins, M.C. Southey, J.S. Hocking, G.G. Giles, M.R. McCredie, D.J.Venter, J.L Hopper, "Familial risks, early-onset breast cancer, and BRCA1 and BRCA2 germline mutations," J Natl Cancer Inst, 95(6), 448-57 (2003).

[2] National Cancer Institute of Canada. Canadian Cancer Statistics 2001, Toronto, Canada, (2001).

[3] L.E. Janocko, K.A. Brown, C.A. Smith, L.P. Gu, A.A. Pollice, S.G. Singh, T. Julian, N. Wolmark, L. Sweeney, J.F. Silverman, and S.S. Shackney, "Distinctive patterns of Her-2/Neu, c-myc and Cyclin D1 gene amplification by fluorescence in situ hybridization in primary human breast cancers," Cytometry (Communications in Clinical Cytometry), 46, 136-149 (2001).

[4] G. Rollins, "Tamoxifen and raloxifene may benefit women at high risk for breast cancer," Rep Med Guide Outcomes Res, 13(14), 1-2 (2002).

[5] E. Remmel, F. Harder, "Prophylactic mastectomy--evaluation and treatment of high risk patients," Swiss Surg 8(2), 45-52 (2002).
[6] N.F. Boyd, G.A. Lockwood, J. Byng, D.L. Tritchler, and M.Yaffe, "Mammographic Densities and Breast Cancer Risk," Cancer Epidemiology, Biomarkers and Prevention, 7, 1133-1144 (1998).
[7]] E. Paci , S. Duffy, M. Rosseli di Truco, The Oxford Textbook of Oncology, Mammographic screening: from the scientific evidence to practice, Oxford; New York: Oxford University Press, (2000).
[8] H. Heusmann, J. Kolzer, J. Otto, R. Plus, T. Friedrich, S. Heywang-Kobrunner, and W. Zinth, "Spectral transillumination of female breasts and breast-like material," SPIE 2326, 370-382 (2001).
[9] V. Quaresima, S. J. Matcher and M. Ferrari, "Identification and quantification of intrinsic optical contrast for near-infrared mammography," Photochem Photobiol, 67, 4-14 (1998).
[10] R.L. Egan and P.D. Dolan, "Optical spectroscopy. Pre-mammography marker," Acta Radiologica, 29, 497-503 (1988).
[11] M. Simick, "Near Infrared Transillumination Spectroscopy of Breast Tissue for Correlation with Mammographic Density," Masters Thesis, Department of Medical Biophysics, University of Toronto (2002).
[12] N.F. Boyd, J.W. Byng, R.A. Jong, E.K. Fishell, L.E. Little, A.B. Miller, G.A. Lockwood, D.L. Tritchler, and M.J. Yaffe, "Quantitative Classification of Mammographic Densities and Breast Cancer Risk: Results from the Canadian National Breast Screening Study," J Natl Cancer Inst, 87(9), 670-5 (1995).
[13] R.A. Weersink, L.D. Marret, and L. Lilge. "Validation of self-reported skin colour via Principal Component Analysis of Diffuse Reflectance Spectra of the Skin," Proc. Soc. Photo-Opt. Instr. Eng., 3917, 232-237 (2000).
[14] V.G. Peters, D.R. Wyman, M.S. Patterson, and G.L. Frank, "Optical properties of normal and diseased human breast tissues in the visible and near infrared," Phys Med Biol, 35, 1317-1334 (1990).
[15] B.M. Wise, PLS Toolbox Tutorial: Matlab Version 6, Eigenvector Research Inc. (2000).
[16] A.J. Welch and M.J.C van Gemert (Editors) Optical-Thermal Response of Laser-Irradiated Tissue, Plenum Press New York, USA (1995).
[17] N. Shah, A. Cerussi, C. Eker, J. Espinoza, J Butler, J. Fishkin, R. Hornung and B. Tromberg, "Noninvasive functional optical spectroscopy of human breast tissue," Proc Natl Acad Sci U S A, 98(8), 4420-4425 (2001).
[18] S.J. Graham, M.J. Bronskill, J.W. Byng, M.J. Yaffe, and N.F. Boyd, "Quantitative correlation of breast tissue parameters using magnetic resonance and X-ray mammography," Br J Cancer, 73(2), 162-8 (1996).
[19] A.E. Cerussi, A.J. Berger, F. Bevilacqua, N. Shah, D. Jakubowski, J. Butler, R.F. Holocombe, and B. Tromberg, "Sources of absorption and scattering contrast for near-infrared optical tomography," Acad Radiol, 8, 211-218 (2001).
[20] C. Stromper, J. D'Souza, A. DiNitto, and A. Arrendo, "Analysis of parenchymal density on mammograms in 1353 women 25 – 79 years old," American Roentgen Ray Society, 167, 1261-1265 (1996).
[21] Wolfe JN "Breast Patterns as an Index of Risk for Developing Breast Cancer". Am J Roentgenol, 126:1130-37, 1976.

Appendix 3

Classification of breast tissue density by Optical Transillumination Spectroscopy: optical and physiological effects governing predictive value.

Kristina Blyschak[1], Michelle Simick[2], Roberta Jong[3], Lothar Lilge[1,4,*]

[1]Ontario Cancer Institute, University Health Network, Toronto, Ontario, Canada M5G 2M9
[2]Toronto-Sunnybrook Regional Cancer Centre, Toronto, Ontario, Canada M4N 3M5
[3]Sunnybrook and Women's College Health Science Centre, Toronto, Ontario, Canada M4N 3M5
[4]Department of Medical Biophysics, University of Toronto, Toronto, Ontario, Canada M5G 2M9

*Correspondence: 610 University Avenue, Room 7-416, Toronto, Ontario M5G 2M9; 416-946-4501, ext. 5743; email: llilge@uhnres.utoronto.ca

Running title: Breast density by transillumination spectroscopy

Keywords: optical transillumination spectroscopy, breast tissue density, breast cancer risk, preventive oncology, principle component analysis.

Abstract

Preventive oncology is in need of a risk assessment technique that can identify individuals at high risk for breast cancer and that has the ability to monitor the efficacy of a risk reducing intervention. Optical transillumination spectroscopy (OTS) gives information about breast tissue composition and tissue density. OTS is non-invasive and in contrast to mammography, uses non-ionising radiation. It is safe and can be used frequently on younger women, potentially permitting early risk detection and thus increasing the time available for risk reduction interventions to assert their influence. Before OTS can be used as a risk assessment and/or monitoring technique, its predictive ability needs to be demonstrated and maximized through the construction of various mathematical models relating OTS and an established breast cancer risk factor. Here we selected parenchymal density pattern as risk predicting standard.

To establish a correlation between OTS and parenchymal density pattern Principle Components Analysis (PCA), using risk classifications, is executed. The PCA scores from 156 volunteers are presented in three-dimensional cluster plots and a plane of differentiation that separates the high and low tissue densities is used to calculate the predictive value. Stratification of PCA for measurement position on the breast in cranial-caudal projection is introduced. Analysis of PCA scores as a function of the volunteer's age and body mass index (BMI) is examined, as options for further subject stratification.

A small but significant correlation between the component scores and age or BMI is noted but the correlation is dependent on the tissue density category examined. Correction of the component scores for age and BMI is not recommended, since a priori knowledge of a women's breast tissue density is required. Stratification for the center and distal measurement positions provide a predictive value for OTS above 96%.

Introduction

Preventive oncology involves identification of the population at risk and the implementation and monitoring of intervention strategies. The first task requires methods and techniques based on physical measurements or demographic information that identify individuals at high risk who would benefit most from the interventions. These risk quantification techniques must be applicable to the entire population and permit identification of individuals at high risk for developing cancer with high sensitivity and specificity. The technique should exploid a risk identifier providing a high relative risk or high odds ratio so all individuals at risk are identified while decrease the number of individuals undergoing unnecessary treatment (i.e. those who are low risk). Thus, individuals are provided with the information required to empowering them to make informed decisions regarding their health and the potential benefits of risk reduction strategies. While genetic predisposition towards certain cancers is known, only a small percentage of the population is affected, such as women with BRCA1 and BRCA2 genetic mutations[1] who comprise only a fraction of one percent of the general population and hence this information is not suitable for population-wide screening.

Breast cancer is the most commonly occurring cancer in women. The lifetime risk for developing breast cancer is 1 in 5-10, depending on the reporting agency[2]. The tissue transformation preceding breast cancer can occur 20 years prior to the development of the disease[3] thereby providing a "window of opportunity" to employ risk reduction interventions such as modification in lifestyle, diet, chemopreventive treatments (i.e. Tamoxifen, Raloxifene) [4] or in severe cases, prophylactic mastectomy[5]. While all of these interventions are designed to prevent cancer, they will inadvertently influence the quality of a woman's life, specifically those

interventions designed to achieve a reduction in risk in only a few months or years. Conversely, identifying women at risk at an earlier age may only require relatively small lifestyle changes, which, acting over a longer period of time, may also achieve an adequate reduction in risk. To achieve this goal, a technique capable of detecting women at high risk for breast cancer at an earlier age is required. Employing a physical method of assessing the breast cancer risk may also prove useful in monitoring the efficacy of risk reducing interventions, as the intervention may change the physical properties, whereas the demographic information about an individual is not altered due to the intervention.

Current methods of establishing breast cancer risk include the Gail Model[6] and parenchymal density patterns derived from standard x-ray mammography. The former method is primarily based on demographic information while the latter represents a physical property of tissue. Parenchymal density patterns reflect the ratio of glandular and connective tissue to adipose tissue within the breast. Women with mammographically dense tissue occurring in more than 70% of the breast are 4 to 6 times more likely to develop breast cancer than those with density showing in less than 25% of the area[7]. Because of the inherent risks of x-rays, mammography is not recommended as an annual diagnostic for women younger than 50 in some countries and younger than 40 in others[8], thereby limiting the time available for risk reduction interventions to assert their influence. Similarly, the demographic information required for inclusion in the Gail Model is often not available until women have reached their late thirties or forties. Furthermore, the Gail Model is only valid for women older than 30 again forgoing useful intervention years.

Near-infrared optical transillumination spectroscopy (OTS) has been shown to give information about breast tissue composition[9]. Specifically, OTS results in unique optical spectra,

governed by hemoglobins, water and lipid absorption within the tissue and the average light scattering power[10]. The differences in chromophore contributions in the tissue have also been shown to mirror the x-ray dense and x-ray lucent areas of the mammogram[11]. In contrast to mammography, which is based on ionizing radiation probing predominantly the atomic composition of the tissue, OTS uses non-ionising radiation with quantum energies that interact with the electronic and vibrational levels of the molecules, representing more the anatomic, metabolic status of the breast. Consequently, OTS can be used more frequently and on younger women and has the capability of detecting differences in tissue composition between high and low risk groups, based on molecular composition.

In an ongoing feasibility study using mammographic breast density classified on a nominal scale as an interim indicator of risk, our group has shown that OTS can identify women with high breast tissue density with a predictive value above 85%. However, before OTS can be implemented as a tool for risk estimation and/or as a monitoring technique during risk reducing interventions, it is necessary to optimize the predictive ability or the relative risk provided by OTS, thus minimizing the number of patients given an incorrect risk assessment. By establishing a relative risk for OTS similar to that of mammography through the use of non-ionizing radiation a gain two decades for risk reduction interventions to exert their benefit is possible.

The present investigation is an extension of earlier studies performed by our group[12] with the main purpose to improve the predictive power of OTS by identifying required stratifications on a larger number of volunteers, prior to employing our analysis techniques. Principle Components Analysis (PCA) using risk classification by a radiologist as the 'gold standard' is employed to establish a correlation between OTS and mammographic density pattern. Multivariate analysis techniques are used to determine if stratification of the spectral data by

measurement position on the breast in cranial-caudal projection (center, medial, distal, or lateral) or physical parameters such as the volunteer's age and body mass index (BMI) is beneficial in increasing the tissue density prediction by OTS.

Materials and Methods

Patient recruitment

The data set used in this study includes a collection of mammograms and spectral information gathered from 156 volunteers. All volunteers were recruited through the Marvelle Koffler Breast Centre at Mount Sinai Hospital, Toronto, Ontario. All women had a film screening mammogram within the last 12 months of being recruited, which was negative for radiological suspicious lesions. All women also had no previous surgery to the breast tissue, including reduction or implants. Volunteer recruitment for this study was approved by the IRBs of the University of Toronto and the University Health Network. Informed consent was received from all volunteers prior to OTS.

Film mammograms were classified on a nominal scale by a radiologist (Dr. Roberta Jong, Women's College and Sunnybrook Health Science Centre, Toronto, Ontario) into either low (< 25 %), medium (25% to 75%) or high (> 75% dense tissue area) density categories. Women who displayed bilateral variations on their mammograms were not included in this analysis. Sixty-one women were classified by the radiologist as having low, 68 as having medium, and 27 as having high tissue density. The population contributions of the tissue density categories in this study closely reflect the population proportions seen in the Canadian National Breast Screening Study[13] (Table 1). The age of the volunteers ranged from 36 to 72 years.

Table 1 before next section

Visible near-infrared transmission

The instrumentation used to gather transillumination spectra was described previously in detail[12]. Briefly, a 12W halogen lamp served as broadband light source, ultra-violet and part of the visible spectrum and mid-infrared radiation were eliminated using a cut-on filter (λ>550 nm) and a heat rejection filter, respectively. The remaining light was coupled into a 5 mm diameter liquid light guide [Fiberguide Industries, Bridgewater, NJ] placed in contact with the skin on top of the breast tissue. A total power of 0.25W, covering the 550 to 1300 nm bandwidth, was delivered to the skin. Transmitted light was collected via a 7 mm diameter optical fiber bundle [P & P Optica, Kitchener, Waterloo, 140 fibres, 200 μm, N.A. 0.36]. Wavelength dependent detection in the visible and near-infrared was achieved using a spectro photometer (Kaiser, California, USA) equipped with holographic transillumination grating (15.7rules/mm blazed at 850nm) and a 2D cryogenically cooled silicon CCD (Photometrics, New Jersey, USA) at a spectral resolution of better than 3 nm between 625 and 1060 nm. Spectral resolution was achieved by positioning a 0.5 mm slit between the distal end of the collection fibre and the spectral grating. The peak quantum efficiency of the back thin CCD is at 780 nm with a quantum efficiency of 0.2 remaining at 1060 nm. By imaging the entrance slit of the spectrograph onto a 2D CCD, 50 rows of pixels were exposed to detected light thereby increasing the dynamic range of the electronic detection by a factor of > 30. Cryogenic cooling was used to minimize background noise. Further signal to noise improvement was accomplished by using exposure times of 3 to 5 seconds, and averaging 5 scans for all spectra. Hospital Grade Canada Standards Association (CSA) certification was obtained for use of the instrumentation on volunteers. Health Canada regulation (IEV 825 equivalent)[14] for the maximum permissible exposure for radiation sources at non-therapeutic doses was not exceeded.

All volunteer measurements were taken in the dark, with the volunteer seated comfortably in an upright position and the breast resting on a horizontal platform. A total of eight measurements in cranial-caudal projection were taken, four per breast (center, medial, distal, and lateral, see Fig. 1, they are rotated by about 45^0 relative to standard radiological quadrants). A computer allowed for system control and data display. Typical data acquisition for all 8 measurements averaged 160 to 200 seconds, each. The source and detector fibers (optodes) were held coaxially, pointing towards each other, by a caliper attached to the resting platform providing the interoptode distance. The source fibre was placed against the skin on the top surface of the breast with minimal compression. Considering typical tissue optical properties[15] and a tissue thickness of 5 cm, an ovoid shape volume estimated at 30 cm^3 is interrogated. In this study tissue thickness ranged from 2.5 to 8 cm, equivalent to 12 or 54 cm^3.

Figure 1 before next paragraph

All spectra were corrected for daily variations in the wavelength dependent signal transfer function of the optical system and the thickness of the interrogated tissue, such that all spectra are independent of the instrument and the interoptode distance. This is achieved by referencing all spectra to a transmission standard made of 1 cm thick ultra high density polyurethane (Gigahertz Optics, Munich, Germany). Consequently, all volunteer spectra used in this study are expressed in units of optical density per centimeter [OD cm^{-1}], given by the negative log of the raw data spectrum divided by the reference spectrum of the polyurethane block plus the optical attenuation of the polyurethane block and divided by the interoptode distance. The scattering and absorption properties of the standard were measured in a separate experiment using an integrating sphere diffuse reflectance set-up[16] (OD ~ 1.8 to 2.3 over the wavelength range of interest).

Data Analysis

Principle Components Analysis (PCA) was used to establish a correlation between the obtained optical transillumination spectra and mammographic density[17]. PCA is an analytic mathematical method optimized for comparison of vectors (i.e. optical spectra) with nominal data (i.e. tissue density). PCA relies upon an eigenvector decomposition of the covariance or correlation matrix of the data matrix ($m \times n$) comprised of a training data set of spectra ($m = 936$) and the monitored spectral range ($n = 436$ wavelengths). PCA decomposes this data matrix as the sum of the outer product of vectors $\boldsymbol{t_i}$ and $\boldsymbol{p_i}$ plus a residual matrix. The elements of the $\boldsymbol{t_i}$ vectors, called scores (i.e. scalar coefficients), contain information on how the samples (i.e. spectra) relate to each other; the $\boldsymbol{p_i}$ vectors, or components, are the eigenvectors of the covariance matrix and show how the selected variables (i.e. wavelengths) relate to each other. It is noteworthy that the component vectors $\boldsymbol{p_i}$ are orthogonal to one another.

Every individual spectrum can be approximated as a linear combination of the principle component spectra ($\boldsymbol{p_i}$) where each component is weighted by the scalar coefficient or score ($\boldsymbol{t_i}$) for that individual spectrum. It is generally found that the data can be described in fewer components than original variables (n) and still capture > 99.9% of the total variance. The first component tends to capture the greatest amount of variation in the data; each subsequent component captures the greatest possible variance remaining. The scores of two or more components can also be plotted against one another as they are based on orthogonal vectors. To identify spectra that are closely related and that exhibit common traits, clusters within those 2 or higher dimensional plots are analyzed. Clusters are assigned an outcome, here low versus high tissue density, and lines or planes separating the clusters are determined analytically. Scores that enable differentiation between tissue densities identify useful component spectra and hence

specific chromophore contributions to various tissue density and thus indirectly to risk. For a more detailed description of PCA and the mathematical models employed, the reader is referred to Simick (2001)[12] and Wise (2000)[17].

In this study, PCA was executed on 75% of all spectra (n = 936, 117 volunteers x 8 measurements) randomly selected from each of the defined tissue density categories comprising the training set. In this manner, the relative contribution of each tissue density category in the data sets was retained during the analysis. The remaining 25% of the spectra (n = 312, 39 volunteers x 8 measurements) were placed in a validation set (Table 1). The principle components $\boldsymbol{p_i}$ derived from the training set spectra were then used to predict the scores ($\boldsymbol{t_i}$) on the validation set spectra, thereby testing the predictive ability of the model. As previously described, the data was only corrected for the spectral transfer function of the optical system and the thickness of the interrogated tissue. The data sets were not stratified by menopausal status (i.e. pre versus post-menopausal) since a previous study by our group[12] demonstrated no influence of the menstrual cycle on the spectral measurements.

Furthermore, as optical transillumination spectroscopy (OTS) is proposed as a physical method for risk assessment applicable to the entire population, this analysis focuses only on variables associated with physical parameters, more specifically measurement position, volunteer's age, and volunteer's body mass index (BMI), although information on other risk factors, such as family history of breast cancer, parity and ethnicity, was collected for each volunteer. All statistical analyses were carried out using SPSS 11.0 (Statistical Package for the Social Sciences, SPSS Inc., USA).

To determine the predictive value of the PCA model and hence OTS, two measures, comparable to sensitivity and specificity were determined: high density measure (HDM) and low

density measure (LDM). HDM and LDM were determined for both the training and validation sets using the following equations:

$$HDM = \frac{TP}{TP + FN} \qquad LDM = \frac{TN}{TN + FP}$$

Where true positive (TP) is the number of spectra representing high tissue density located below the separation plane in a three-dimensional cluster plot, defined below, and false negative (FN) is the number of spectra representing high tissue density situated above the separation plane. Conversely, true negative (TN), is the number of spectra representing low tissue density located above the separation plane and false positive (FP) is the number of spectra representing low tissue density situated below the separation plane.

HDM and LDM were estimated by determining the separation plane that differentiated the high and low tissue density clusters resulting from the training set scores in three-dimensional plots using either all component scores (t_i) (n = 528, all 8 measurements per volunteer) or mean scores per individual ($\overline{t_i}$) (n = 66, Table 1). Linear regression analysis was used to first calculate the plane of best fit for both the high and low tissue density clusters, respectively, defined both by:

$$t_z = b + a_x t_x + a_y t_y \quad (2.1)$$

selecting the scores of one component randomly as the dependent variable z, and where b is the z-intercept, a_x and a_y are the slopes for the two independent component scores, t_x and t_y using either all or the mean scores (t_i or $\overline{t_i}$),.

The equation (t_{icrit}) of the plane separating the high and low tissue density training sets was calculated as the plane halfway between the two low and high tissue density planes:

$$t_{icrit} = \frac{1}{2}\left[\left(b_{low} + a_{xlow}t_{xlow} + a_{ylow}t_{ylow}\right) + \left(b_{high} + a_{xhigh}t_{xhigh} + a_{yhigh}t_{yhigh}\right)\right] \quad (2.2)$$

Where a_{xlow}, a_{ylow} and a_{xhigh}, a_{yhigh} are the slopes for the low tissue density cluster and the high tissue density cluster, respectively, b_{low} and b_{high} are the respective z-intercepts, and t_{xlow}, t_{ylow}, t_{xhigh}, t_{yhigh} are the respective component scores used (t_i or $\overline{t_i}$).

Differences between component scores t_1 to t_4 by density classification and by measurement position (center, medial, distal and lateral) were tested by non- parametric methods using either the Mann-Whitney U test or a Kruskal-Wallis rank test. Non-parametric testing was warranted since the component scores for the majority of cases are not normally distributed. When testing for differences between measurement positions only, measurements from the left breast were used since we showed previously[12] no significant difference between component scores from the left and right breast when excluding women showing variability in the tissue density.

PCA derived component scores t_1 to t_4 for the low and high tissue density categories as a function of a volunteer's age and body mass index (BMI) were examined using Spearman's r correlation analysis. Linear regression analysis was also executed for component scores t_1 to t_4 as a function of age or BMI. For correlation and linear regression analyses, either all scores (n = 1248) or scores averaged per individual (n = 156) were used.

For all analyses, p-values ≤ 0.05 were considered to be statistically significant.

Results

PCA of density categories all measurement positions

Figure 2 shows the resulting first four principle components (p_i) from the PCA not stratified for measurement position and thus based on n = 936 spectra. These first four

Figure 2 after first paragraph

components contain 99.87%, 0.06%, 0.05% and 0.01% of the variance in the total data set, respectively, yielding a combined total of 99.99%.

Box and whisker plots of the first four component scores (t_i) for each density category for the training and validation sets are presented in Figure 3. A Kruskal-Wallis rank test demonstrated that the scores for the first four components t_1 to t_4 are each significantly different between the low, medium and high tissue densities for both the training and validation data sets (all at $p < 0.01$). The Mann-Whitney U test demonstrated that the scores for the first four components t_1 to t_4 for the training set differed significantly between all permutations of density classification at $p < 0.01$. However, for the validation set, only three scores per permutation showed significance at $p < 0.01$: t_1, t_2 and t_4 between low and medium tissue density, t_1, t_2 and t_3 between low and high tissue density, and t_2, t_3 and t_4 between medium and high tissue density.

Figure 3 before paragraph

An example of a three-dimensional cluster plot of component scores t_1, t_2 and t_3 from the training spectra using only information from woment with either high or low tissue densities (n = 528) is presented in Figure 4. Discrimination of the high and low tissue densities is achieved across a three-dimensional plane of separation (not shown) analytically derived from linear regression analysis. A similar 3D plot using mean component scores $\overline{t_1}$, $\overline{t_2}$ and $\overline{t_3}$ per individual for those with either high or low tissue densities for the training and validation sets (n = 88) is shown in Figure 5, demonstrating improved cluster separation.

Figures 4 and 5 after paragraph

PCA of density categories by measurement position

Figure 6 displays mean component scores $\overline{t_1}$ to $\overline{t_3}$ in the training set for each of the four left measurement positions for the high and low tissue densities resulting from the position independent PCA. For the low tissue density group in the training set, a Kruskal-Wallis rank test

demonstrated a significant difference in component scores $\overline{t_1}$ to $\overline{t_3}$ between each measurement position (all at $p < 0.01$). For the high tissue density group, only component score $\overline{t_2}$ resulted in a significant difference between each measurement position. There is no difference in component score $\overline{t_1}$ between positions ($p = 0.055$) at a power > 0.6. For component scores $\overline{t_3}$, there is no difference between measurement positions ($p = 0.095$) at a power > 0.9.

Because of the significant differences observed PCA was repeated separately for each measurement position (center, medial, distal and lateral). Spectra from both the left and right breasts were used for training. For each position, 234 spectra from 117 volunteers were used to train the models, and 78 spectra from 39 volunteers were used to validate them. Box plots, three-dimensional cluster plots and results of non-parametric tests are presented for the center and distal measurement positions only, since these positions provided the best HDM and LDM (see below).

Figure 7 shows the first four principle components (p_i) resulting from PCA stratified for measurement position. Of the variance in the total data set, the first component p_1 contains between 99.85% and 99.91%, p_2 between 0.05% and 0.08%, p_3 between 0.03% and 0.05%, and p_4 contains 0.01% .

Figure 7 after paragraph

Box and whisker plots of the first four component scores (t_i) for each density category for the center and distal positions for the training and validation sets are presented in Figures 8 and 9. For the center position, a Mann-Whitney U test demonstrated a significant difference between the low and high tissue density for both training and validation sets in component scores t_1 and t_3 ($p < 0.01$). For component scores t_2 and t_4 in the validation set, there is no difference between high and low tissue densities ($p = 0.579$ and $p = 0.338$, respectively) at a power > 0.6 and 0.9,

Figures 8

respectively. For the distal position, a Mann-Whitney U test demonstrated a significant difference in component scores t_1, t_2 and t_4 between the low and high tissue density for both training and validation sets (all at $p < 0.01$). For component score t_3 in the validation set, there is no difference between high and low tissue densities ($p = 0.860$) at a power > 0.6.

Three-dimensional cluster plots of component scores t_1, t_3 and t_4 at the center position and scores t_1, t_2 and t_4 at the distal position are shown in Figure 10 and 11 respectively for high and low tissue density combined datasets ($n = 176$).

Figures 10 and 11 after paragraph

HDM and LDM

Table 2 shows the resulting HDM and LDM calculated for the training and validation sets using either all component scores (training = 528, validation = 176) or the mean component score per individual (training = 66, validation = 22) without stratification for measurement position. The best HDM and LDM values for both data sets are obtained separating the two tissue density classes when t_2 is a function of t_1 and t_3. In the majority of cases, the HDM and LDM increase when the mean component score $\overline{t_i}$ per individual is used.

Table 3 provides the best HDM and LDM results for the training and validation sets for each measurement position using either t_2 or t_3 as the dependent variable. The center and distal positions show the best HDM and LDM for the training and validation sets.

Tables 2 and 3 after paragraph

Number of Measurement Positions

Figure 12 shows histograms indicating the frequency of true high or low tissue density predictions through OTS for each individual. From these figures it is apparent that if scores t_i from 3 or more of four spectra indicate high tissue density, the best HDM and LDM are obtained using spectra from the center and distal measurement positions only (Fig.12a). Spectra from the medial and lateral positions conversely result in the lowest HDM and LDM values (Fig.12b).

Figure 12 after paragraph

PCA and Physical Parameters (Age and BMI)

Linear regression analysis demonstrated a significant correlation between the component scores t_i and age or BMI. However, further analysis showed that the age dependent slopes of the different tissue densities are in effect parallel and hence without a priori knowledge of the tissue density, no age or BMI correction can be introduced.

A scatter plot of mean component scores $\overline{t_1}$ and $\overline{t_2}$ per individual as a function of the volunteer's age for the high and low tissue densities is shown in Figure 13. Figure 14 is a similar scatter plot of the mean component scores $\overline{t_1}$ and $\overline{t_2}$ for each individual versus their BMI. The results of linear regression analysis between age or BMI and the first two component scores are also indicated. According to Spearman's r, a significant but weak correlation exists between both component scores $\overline{t_1}$ and $\overline{t_2}$ and age or BMI. Similar results were obtained for component scores t_3 and t_4 (data not shown).

Figures 13 and 14 after paragraph

Discussion

Principle Component Analysis (all measurement positions)

The fact that significant differences between component scores (t_i) for different permutations of density classification were found for the training set but not for the validation set, specifically for scores t_1 between medium and high tissue densities, t_3 between low and medium tissue densities, and t_4 between low and high tissue densities (Fig. 3), suggests possible overtraining of our PCA model. The fact that t_4 showed no significant difference between the low and high tissue densities for the validation set indicates that the residual variance of ~ 0.01% is not capable of differentiating between these two extreme density categories.

Input parameters, such as known tissue chromophore spectra, were not implemented in the training of our PCA model. Despite this fact, each derived principle component (p_i) includes

a combination of spectral signatures related to light scattering and chromophore absorptions (water, lipid and hemoglobins), which vary with age [ref], menopausal status [ref], pathology [ref] and breast tissue density [ref].

Scores associated with principle component p_1 can be interpreted as contain information on wavelength independent light loss, due to increased absorption based on the differential optical path length, and light losses at the breast boundary. The scores have negative values in the PCA model (Fig. 2). Light scattering and hence, the differential optical path length is tissue and wavelength dependent and can be described by $u_s' = a\lambda^{-b}$ [18]. Light losses due to scattering occur because of an increase in photon path length and thus a lower probability of traversing tissue. A polyurethane standard, with scattering properties similar to tissue and an albedo > 0.999, was used to calibrate the spectral transfer function of the optical system daily and by obtaining the ratio of the tissue transillumination spectra and the standard spectrum the wavelength dependence of light scattering in the breast tissue is minimized or lost[12]. Hence, p_1 carries wavelength independent optical path length information but contributes information to determine tissue density. For example, low density tissue has reduced scattering when compared to high density tissue[19], resulting in higher values of t_1 (i.e. less negative), indicating less attenuation or loss of light resulting from a shorter optical path length (Fig. 3). The relationship between tissue density and light scattering has been observed previously by other groups[15,19,20,21] where pre menopausal tissue (mostly high density) has a higher scattering coefficient than post menopausal tissue (mostly low density).

Light losses at the breast boundary are also captured in p_1. The difference in component scores t_1 observed between positions (Fig. 6) can be explained by light losses where the breast boundary is parallel to the optical axis between optodes (medial, lateral, and distal positions). We

have shown previously that measurements taken at the medial position are different from the centre measurement and similar to measurements made closer to the edge of the breast[12]. The larger t_1 values at the center position indicate minimal light losses due to boundary conditions. Light losses are highest at the distal position, where the shift towards smaller scores suggests more transmission attenuation due to light losses. These observations suggest that stratification as a function of position is beneficial.

The most important spectral features in the spectrum of p_2 are the lipid peak around 925 nm and the inverse water peak around 975 nm (Fig. 2). Low density tissue is characterized by adipose tissue and positive scores t_2 resulting in lipid peak being the dominant spectral feature (Fig. 3). Smaller contributions in the low tissue density spectrum are also evident at 770 nm (deoxy hemoglobin) and 825 nm, a minor lipid absorption peak. Conversely, high density tissue has a large water content[22] and the scores t_2 are predominantly negative, resulting in the water peak being the dominant spectral feature (Fig.3). Contributions from deoxy hemoglobin are also evident in the high tissue density spectrum of p_2 between 625 and 750 nm, where the negative slope of the deoxy hemoglobin curve is visible.

The spectrum of p_3 is relatively flat between 625 nm and 875 nm, which can be attributed to contributions from the oxy hemoglobin curve (Fig. 2). Another notable feature is that lipid and water are positive, compared to the spectra of p_2 and p_4 (see below). Component scores t_3 for low density tissue are positive when the lipid peak is the dominant spectral feature (Fig. 3). Component scores t_3 for high density tissue are negative, suggesting a shift from an oxy hemoglobin curve to a deoxy hemoglobin curve (as seen in the spectrum of p_2). Since decreases in oxygen are associated with increased cellular metabolism[21], oxygen saturation is anticipated to be smaller in high density tissue when compared to low density tissue.

The spectrum of p_4 is similar to that of p_2 (Fig. 2), however, for low density tissue, component scores t_4 are negative and for high density tissue they are positive (Fig. 3). The lipid peak at 925 nm and the water peak at 975 nm are the dominant spectral features for the low and high density tissue, respectively. Smaller contributions from presumably the hemoglobin saturation between 775 nm and 875 nm are also noticeable.

Cluster plots in three dimensional space defined by t_1, t_2 and t_3 result in a good separation between high and low tissue densities, either when all component scores are used (t_i) or when the mean score per individual is used ($\overline{t_i}$) (Figs. 4 and 5). In both cluster plots, scores for low density tissue are tightly clustered above a plane of separation, whereas scores for the high density tissue are more spread out and are situated below a plane of separation. The low density cluster is tight despite the fact that low density breasts are more common in the general and in our study population (Table 1).

The results of positional analysis (Fig. 6) suggest that the PCA model should be trained independently on each measurement position (center, medial, distal, and lateral). For instance, analysis of component scores t_2 and t_3 by measurement position demonstrates differences in wavelength dependent attenuation within various regions of the breast. The smaller values for component scores t_2 at the distal and lateral positions indicate greater attenuation by water at these positions, compared to the center and medial positions for both density groups. This water associated increase in attenuation can be explained by the location of the ducts and mammary glands, respectively. Component scores t_3 suggest a decrease in attenuation due to oxy hemoglobin and a concomitant increase due to deoxy hemoglobin at the distal and lateral regions of the breast. Hence, the spatial prominence of various tissues within the breast is well reflected in the scores.

Principle Component Analysis by measurement position

The results of the PCA for each individual position and the subsequent analysis of cluster plots in three dimensional spaces suggest that only two positions need to be interrogated: the center and the distal. The high predictive value of the center position is explained by the fact that parenchymal densities are rarely observed in this area of the breast in women with low and medium tissue densities. Conversely, the high predictive value of the distal position results from the location of the lactic ducts.

In general, the component spectra p_i for these two positions are comparable with the exception that component spectrum p_2 for the center position is similar to component spectrum p_3 for the distal position and vice versa (Fig. 7). Both component spectra (p_2 at center and p_3 at distal) are spectrally flat over a large wavelength region with poor differentiation of the lipid and water peaks. Consequently, cluster plots in a three dimensional space defined by t_1, t_3 and t_4 result in a good separation between high and low tissue densities for the center position (Fig. 10) and cluster plots in a three dimensional space defined by t_1, t_2 and t_4 result in a good separation between high and low tissue densities for the distal position (Fig. 11). The results of Mann-Whitney U tests also demonstrated no significant difference in component scores t_2 between low and high tissue densities (validation set) for the center position and in component scores t_3 between low and high tissue densities (validation set) for the distal position (Figs. 8 and 9). This exchange of the significance between p_2 and p_3 for the center and distal positions is most likely limited by the small amount of variance captured by them in association with the limited number of observations available to date. The p_i for the medial and lateral positions show similar shapes with the lateral being more similar to the distal and the medial more similar to the center.

HDM and LDM

Because radiological assigned parenchymal density is a global analysis, calculating HDM and LDM from all eight spectra derived component scores induces obvious additional variability as the density is not distributed homogeneously throughout the tissue. Using the mean score per individual reduces the variability in the OTS predicted density within an individual's breast tissue (Fig. 5). This results in improved HDM and LDM for our validation set when mean scores ($\overline{t_i}$) defined by t_1, t_2 and t_3 or t_1, t_2 and t_4 are plotted in three dimensional space (Table 2). However, when the mean scores ($\overline{t_i}$) defined by t_1, t_3 and t_4 or t_2, t_3 and t_4 are plotted in three dimensional space, the LDM increases but the HDM decreases. This latter observation suggests that the lipid to water ratio captured in component p_2 is better at differentiating high tissue density than is the oxy to deoxy hemoglobin ratio captured by component p_3.

The best estimation of a global classification is pooling spectra from different positions (n = 2), since the patchy nature of the parenchyma is best reflected. The highest HDM and LDM are achieved using spectra from the center and distal positions, such that if three or more of four spectra indicate high tissue density, resulting in both density measured being above 96% (Figure 12a). The HDM and LDM based on these two positions might be a slight overestimate of the predictive power of the test given that women who demonstrated variation in the bilateral organ were excluded from analysis. However, it also suggests that improved PCA training is possible if the regional tissue density associated with each optically interrogated volume is known.

The medial position provides acceptable HDM and LDM for our validation set. The lateral position provides LDM comparable to the distal position, but the lowest HDM among positions for our validation set. The difference in the predictive value of the different quadrants is a direct reflection of the spatial prevalence of the parenchymal density pattern within the breast [23].

The HDM and LDM values obtained in our analysis are limited by two facts. First, only one radiologist (R. Jong) was involved in the reading and classification of film mammograms. Second and more important, we have approximated our three dimensional clusters by a linear function. With regard to this point, future analysis will focus on improved density cluster analysis of our component scores in three dimensional space, where the HDM and LDM are likely to improve.

The HDM and LDM achieved by OTS are comparable to both mammography and other spectroscopic techniques. A meta-analysis of published literature showed that the accuracy for mammography alone, for all ages combined, varied from 83% to 95% in sensitivity[24]. Other spectroscopy studies (i.e. optical and elastic scattering spectroscopy) examining the accuracy of these techniques to diagnose breast cancer have achieved sensitivities between 58% and 91% and specificities between 74% and 93% [11, 25].

Component scores and physical parameters (Age and BMI)

As the population ages one would expect an increase in component scores t_1 and t_2 since atrophy of the tissue (i.e. mammary glands), still ongoing past menopause, would result in less light scatter and an increase in lipid content [26].From Figure 13 it is evident that there is but a small increase in component scores t_1 with age for both low and high density tissue, and little to no increase in t_2 with age for the low and high tissue density categories. This suggests that using OTS as a predictive tool for breast cancer risk, its odds ratio or relative risk should be independent of age. Similarly, with an increase in BMI one anticipates component scores t_1 and t_2 to increase and a small, but significant, association exists between BMI and component scores t_1 and t_2 for the low tissue density group (Fig. 14). A cluster of scores t_1 and t_2 related to the high

density tissue is seen for low BMI, which results in an apparent large slope for this group; however, the correlation coefficients are weak.

While some statistically significant correlations can be established between age or BMI and the component scores t_1 or t_2, these associations are also dependent on a woman's density classification. Consequently, no correction for age or BMI is possible since the density of a woman undergoing OTS measurements is not known a priori. This suggests that the physiological changes in breast tissue density due to age and BMI are already contained in the component spectra and hence captured by the derived component scores.

Conclusion

OTS is a physical assessment technique applicable to the entire population that only requires information on the inter-optode distance and the measurements position on the breast in cranial caudal projection (center, medial, distal, and lateral). Thus the spectra are independent of the instrument and interrogated tissue thickness, and are hence portable between instruments. Furthermore, only two positions need to be interrogated, the center and the distal, to produce HDM and LDM values above 96%. Future, work should focus on establishing a direct correlation with risk as not to become dependent on the limited odds ratio given by the currently chosen intermediate standard, breast tissue density.

Acknowledgements

This work was funded by CDMRP (Congress Directed Medical Research Plan) under DAMD 17-00-1-0393. The authors wish to thank Dr. Robert Weersink for his assistance in the development of the analytic mathematical models used, Dr. Brain Wilson for helpful discussions in the preparation of the manuscript, and Mrs. Samantha Dick for her help with the recruitment of study volunteers.

References

[1] Dite, G.S., Jenkins, M.A., Southey, M.C., Hocking, J.S., Giles, G.G., McCredie, M.R., Venter, D.J., and Hopper, J.L. Familial risks, early-onset breast cancer, and BRCA1 and BRCA2 germline mutations. J Natl Cancer Inst, 95(6): 448-57, 2003.

[2] National Cancer Institute of Canada. Canadian Cancer Statistics 2001, Toronto, Canada, 2001.

[3] Janocko, L.E., Brown, K.A., Smith, C.A., Gu, L.P., Pollice, A.A., Singh, S.G., Julian, T., Wolmark, N., Sweeney, L., Silverman, J.F., and Shackney, S.S. Distinctive patterns of Her-2/Neu, c-myc and Cyclin D1 gene amplification by fluorescence in situ hybridization in primary human breast cancers. Cytometry (Communications in Clinical Cytometry), 46: 136-149, 2001.

[4] Rollins, G. Tamoxifen and raloxifene may benefit women at high risk for breast cancer. Rep Med Guide Outcomes Res, 13(14): 1-2, 2002.

[5] Remmel, E. and Harder, F. Prophylactic mastectomy--evaluation and treatment of high risk patients. Swiss Surg 8(2): 45-52, 2002.

[6] Rockhill, B., Spiegelman, D., Byrne, C., Hunter, D.J., and Colditz, G.A. Validation of the Gail Model of Breast Cancer Risk Prediction and Implications for Chemoprevention. J Natl Cancer Inst, 93(5): 358-366, 2001.

[7] Boyd, N.F., Lockwood, G.A., Byng, J., Tritchler, D.L., and Yaffe, M. Mammographic Densities and Breast Cancer Risk. Cancer Epidemiology, Biomarkers and Prevention, 7: 1133-1144, 1998.

[8] Paci, E., Duffy, S., and Rosseli di Truco, M. Mammographic screening: from the scientific evidence to practice. *In*: The Oxford Textbook of Oncology, Oxford, New York: Oxford University Press, 2000.

[9] Heusmann, H., Kolzer, J., Otto, J., Plus, R., Friedrich, T., Heywang-Kobrunner, S. and Zinth, W. Spectral transillumination of female breasts and breast-like material. Proc. Soc Elect Opt Syst Eng, 2326: 370-382, 2001.

[10] Quaresima, V., Matcher, S.J., and Ferrari, M. Identification and quantification of intrinsic optical contrast for near-infrared mammography. Photochem Photobiol. 67: 4-14, 1998.

[11] Egan, R.L. and Dolan, P.D. Optical spectroscopy: Pre-mammography marker. Acta Radiologica, 29: 497-503, 1988.

[12] Simick, M. Near Infrared Transillumination Spectroscopy of Breast Tissue for Correlation with Mammographic Density. Masters Thesis, Department of Medical Biophysics, University of Toronto, 2002.

[13] Boyd, N.F., Byng, J.W., Jong, R.A., Fishell, E.K., Little, L.E., Miller, A.B., Lockwood, G.A., Tritchler, D.L., and Yaffe, M.J. Quantitative Classification of Mammographic Densities and Breast Cancer Risk: Results from the Canadian National Breast Screening Study. J Natl Cancer Inst, 87(9): 670-5, 1995.

[14] International Electrotechnical Commission, Group Safety of Laser Products Part 1: Equipment classification, requirements and user's guide. IEC, Geneva Switzerland, 1993.

[15] Peters, V.G., Wyman, D.R., Patterson, M.S., and Frank, G.L. Optical properties of normal and diseased human breast tissues in the visible and near infrared. Phys Med Biol, 35: 1317-1334, 1990.

[16] Weersink, R.A., Marret, L.D., and Lilge, L. Validation of self-reported skin colour via Principal Component Analysis of Diffuse Reflectance Spectra of the Skin. Proc. Soc. Photo-Opt. Instr. Eng., 3917: 232-237, 2000.

[17] Wise, B.M. PLS Toolbox Tutorial: Matlab Version 6, Eigenvector Research Inc., 2000.

[18] Welch, A.J. and van Gemert, M.J.C. (Editors) Optical-Thermal Response of Laser-Irradiated Tissue, Plenum Press New York, USA, 1995.

[19] Shah, N., Cerussi, A., Eker, C., Espinoza, J., Butler, J., Fishkin, J., Hornung, R., and Tromberg, B. Noninvasive functional optical spectroscopy of human breast tissue. Proc Natl Acad Sci U S A, 98(8): 4420-4425, 2001.

[20] Troy, T., Page, D.L, and Sevick-Muraca, E.M. Optical Properties of Normal and Diseased Breast Tissues: Prognosis for Optical Mammography. Biomedical Optical Spectroscopy and Diagnostics, 3: 59-66, 1996.

[21] Cerussi, A.E., Berger, A.J., Bevilacqua, F., Shah, N., Jakubowski, D., Butler, J., Holocombe, R.F., and Tromberg, B. Sources of absorption and scattering contrast for near-infrared optical tomography. Acad Radiol, 8: 211-218, 2001.

[22] Graham, S.J., Bronskill, M.J., Byng, J.W., Yaffe, M.J., and Boyd, N.F. Quantitative correlation of breast tissue parameters using magnetic resonance and X-ray mammography. Br J Cancer, 73(2): 162-8, 1996.

[23] Wolfe, J.N. Breast Patterns as an Index of Risk for Developing Breast Cancer. Am J Roentgenol, 126:1130-37, 1976.

[24] Mushlin, A.I., Kouides, R.W., and Shapiro, D.E. Estimating the accuracy of screening mammography: a meta-analysis. American Journal of Preventive Medicine, 14(2): 143-153, 1998.

[25] Bigio, I.J., Brown, S.G., Briggs, G., Kelly, C., Lakhani, S., Pickard, D., Ripley, P.M., Rose, I.G., and Saunders, C. Diagnosis of breast cancer using elastic scattering spectroscopy: preliminary clinical results. Journal of Biomedical Optics, 5(2): 221-228, 2000.

[26] Stromper, C., D'Souza, J., DiNitto, A., and Arrendo, A. Analysis of parenchymal density on mammograms in 1353 women 25 – 79 years old. American Roentgen Ray Society, 167: 1261-1265, 1996.

Tables

Table 1. Breakdown of study volunteers: including study and population proportions and total number of spectra analysed (in parentheses).

Density Category	Training Set	Validation Set	Total	Study Proportion	Population Proportion
Low	46 (368)	15 (120)	61 (488)	39.0%	37.0%
Medium	51 (408)	17 (136)	68 (544)	43.6%	49.0%
High	20 (160)	7 (56)	27 (216)	17.3%	14.0%
Totals	117 (936)	39 (312)	156 (1248)		

Table 2. HDM and LDM for test and validation sets using all component scores and mean scores per individual.

	Equation Used	Training Set		Validation Set	
		HDM	LDM	HDM	LDM
All scores	$t_2 f(t_1, t_3)$	76.9%	88.3%	75.0%	96.7%
	$t_2 f(t_1, t_4)$	69.4%	87.5%	64.3%	92.5%
	$t_3 f(t_1, t_4)$	48.1%	81.0%	58.9%	80.8%
	$t_3 f(t_2, t_4)$	56.9%	84.5%	60.7%	86.7%
Mean scores	$\bar{t}_2 f(\bar{t}_1, \bar{t}_3)$	85.0%	89.1%	85.7%	100.0%
	$\bar{t}_2 f(\bar{t}_1, \bar{t}_4)$	85.0%	82.6%	71.4%	93.3%
	$\bar{t}_3 f(\bar{t}_1, \bar{t}_4)$	50.0%	87.0%	42.9%	86.7%
	$\bar{t}_3 f(\bar{t}_2, \bar{t}_4)$	60.0%	89.1%	57.1%	93.3%

Table 3. HDM and LDM for test and validation sets for each measurement position.

Position	Equation Used	Training Set		Validation Set	
		HDM	LDM	HDM	LDM
Center	$t_3 f(t_1, t_4)$	95.0%	87.0%	92.9%	90.0%
Distal	$t_2 f(t_1, t_4)$	90.0%	91.3%	100.0%	100.0%
Medial	$t_3 f(t_1, t_4)$	77.5%	71.7%	85.7%	86.7%
Lateral	$t_2 f(t_1, t_3)$	80.0%	95.7%	71.4%	100.0%

Figure Captions

Figure 1. Location of the transillumination measurements in the cranial caudal projection on a standardized volunteer. Set up shows center position. Other positions include medial (M), distal (D), and lateral (L).

Figure 2. Plot of principle components p_1 to p_4 of thickness and transfer function corrected spectra. **(Should we include examples of spectra from high and low tissue density?)**

Figure 3. Box plots of component scores t_1, t_2, t_3 and t_4 for low, medium and high tissue density; training spectra are left of the center line, validation spectra are to the right. Circles ($> 2\sigma$) and asterisks ($> 3\sigma$) are outliers.

Figure 4. Three-dimensional cluster plot of t_1, t_2 and t_3 resulting from thickness and transfer corrected spectra of high and low tissue density. Only training data set shown (n = 528). Open circles, spectra from tissue classified as low density; closed circles, spectra from tissue classified as high density.

Figure 5. Three-dimensional cluster plot of mean scores $\overline{t_1}$, $\overline{t_2}$ and $\overline{t_3}$ resulting from thickness and transfer corrected spectra of high and low tissue density (n = 88). Open circles and squares, spectra from tissue classified as low density, training and validation set, respectively; closed circles and squares, spectra from tissue classified as high density, training and validation set, respectively.

Figure 6. Mean component scores, $\overline{t_1}$ (a), $\overline{t_2}$ (b), and $\overline{t_3}$ (c) for the four left measurement positions (centre = LC, medial = LM, distal = LD, lateral = LL) for the low (open circles) and high (closed circles) density tissue. Error bars represent 95% confidence intervals of the mean.

Figure 7. Plots of principle components p_1 to p_4 for each measurement position a. center, b. medial, c. distal, and d. lateral.

Figure 8. Box plots of component scores t_1, t_2, t_3 and t_4 for low, medium and high density tissue for the centre position; training spectra are left of the center line, validation spectra are to the right. Circles (> 2σ) and asterisks (> 3σ) are outliers.

Figure 9. Box plots of component scores t_1, t_2, t_3 and t_4 for low, medium and high density tissue for the distal position; training spectra left of the center line, validation spectra are to the right. Circles (> 2σ) and asterisks (> 3σ) are outliers.

Figure 10. Three-dimensional cluster plot of t_1, t_3 and t_4 resulting from thickness and transfer corrected spectra from high and low density tissue for the center position (n = 176). Open symbols are low tissue density; closed symbols are high tissue density. Circles refer to training set and squares to validation set.

Figure 11. Three-dimensional cluster plot of t_1, t_2 and t_4 resulting from thickness and transfer corrected spectra from high and low density tissue for the distal position (n = 176). Open symbols are low tissue density; closed symbols are high tissue density. Circles refer to training set and squares to validation set.

Figure 12. The number of spectra from the center and distal positions (a) and the medial and lateral positions (b) that correctly predicted high tissue density. High tissue density shown in black, low tissue density shown in grey.

Figure 13. Scatter plots of averaged component scores $\overline{t_1}$ (a) and $\overline{t_2}$ (b) per individual as a function of age for high and low density categories (n = 88). Open circles and solid regression line represent low tissue density, closed circles and dashed line represent high tissue density.

Figure 14. Scatter plots of averaged component scores $\overline{t_1}$ (a) and $\overline{t_2}$ (b) per individual as a function of BMI for high and low density categories (n = 88). Open circles and solid regression line represent low tissue density; closed circles and dashed line represent high tissue density.

Figures

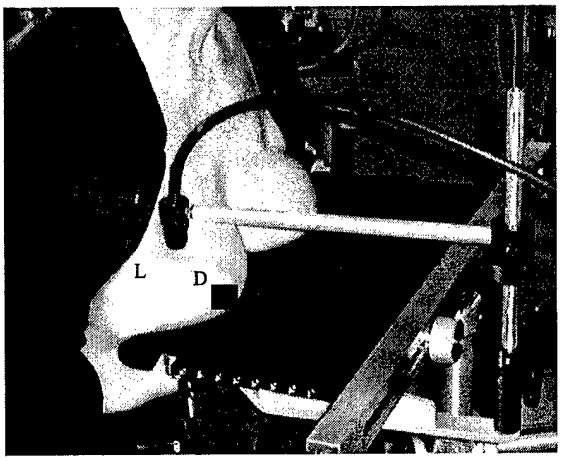

Figure 2.

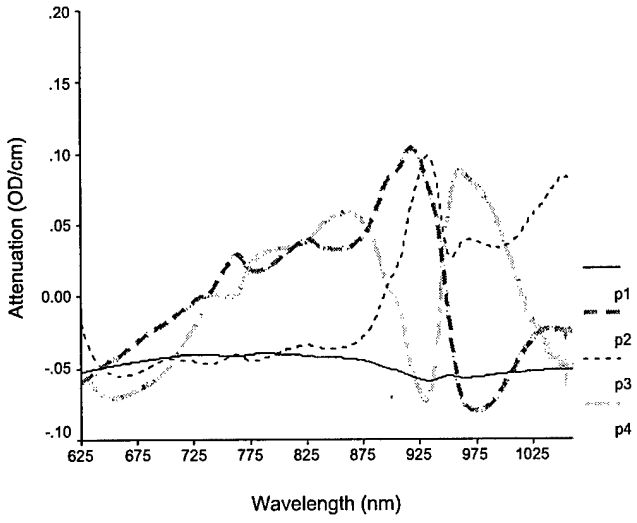

Figure 3.

a.

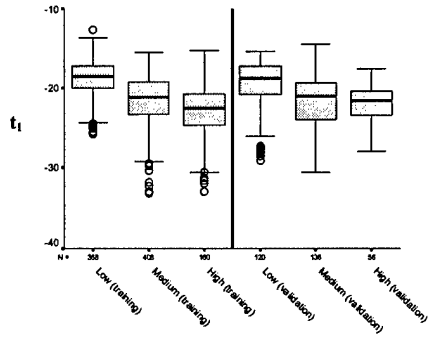

b.

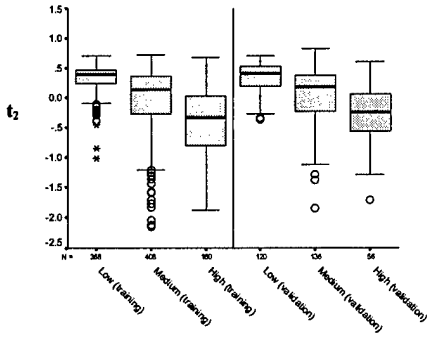

c.

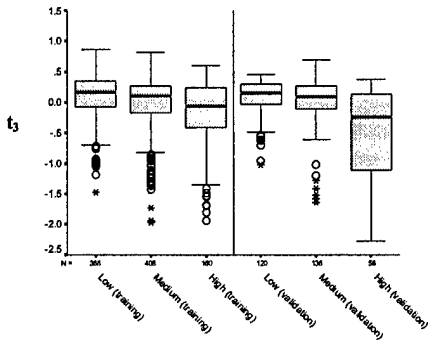

d.

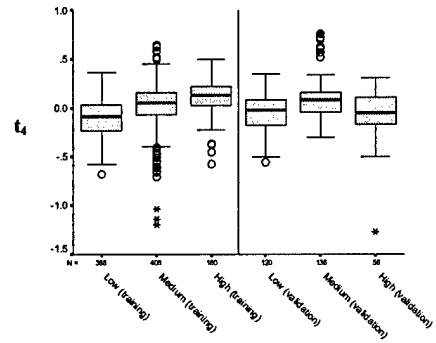

Figure 4.

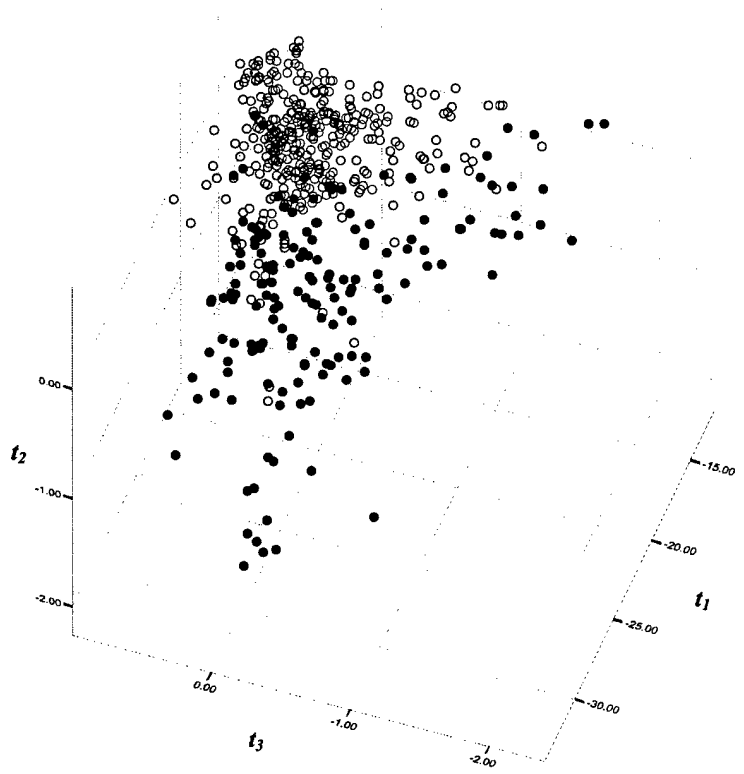

Figure 5.

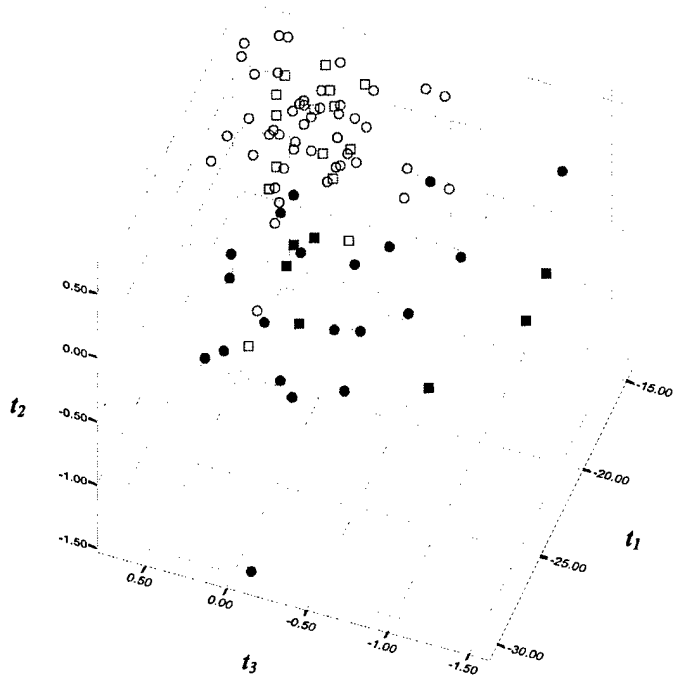
0.50
0.00
-0.50
-1.00
-1.50
t_2
0.50
0.00
-0.50
-1.00
-1.50
t_3
-15.00
-20.00
-25.00
-30.00
t_1

Figure 6.

a.

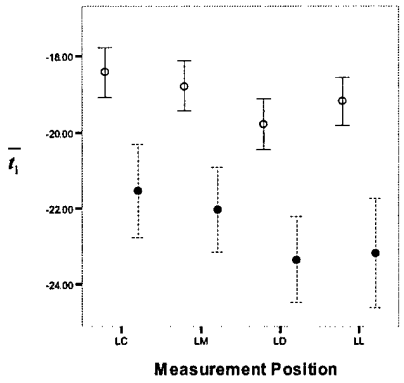
-18.00
-20.00
-22.00
-24.00
LC
LM
LD
LL
Measurement Position

b.

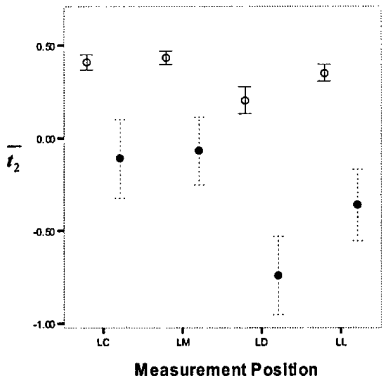
0.50
0.00
-0.50
-1.00
LC
LM
LD
LL
Measurement Position

c.

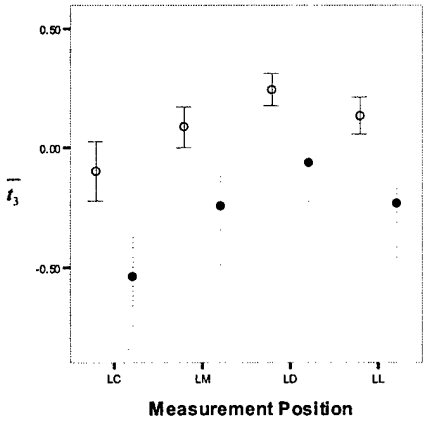
0.50
0.00
-0.50
LC
LM
LD
LL
Measurement Position

Figure 7.

a.

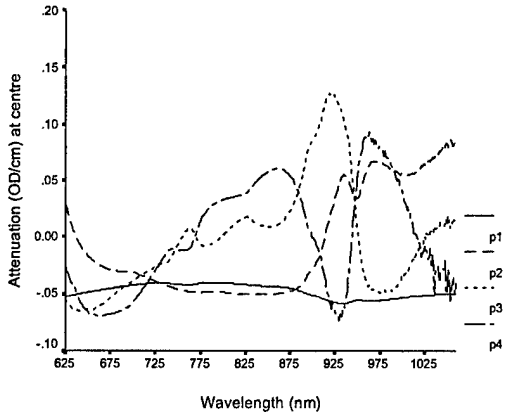

b.

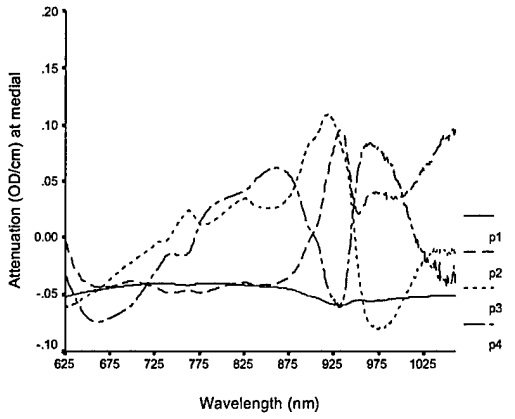

c.

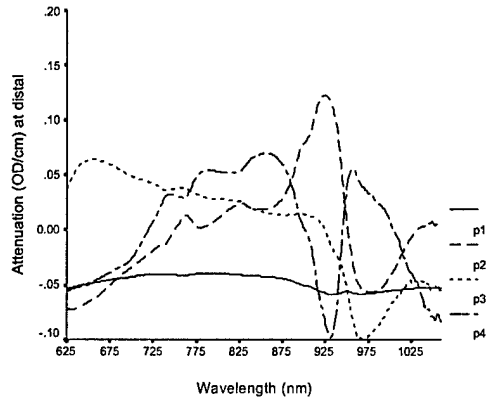

d.

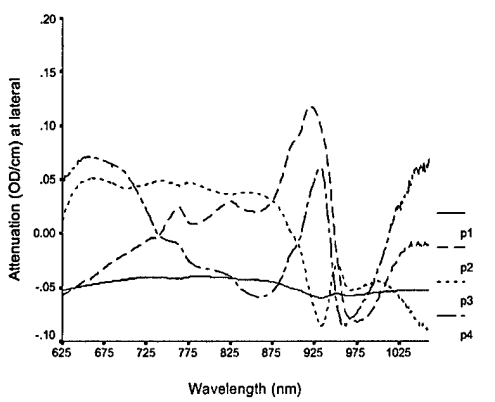

Figure 8.

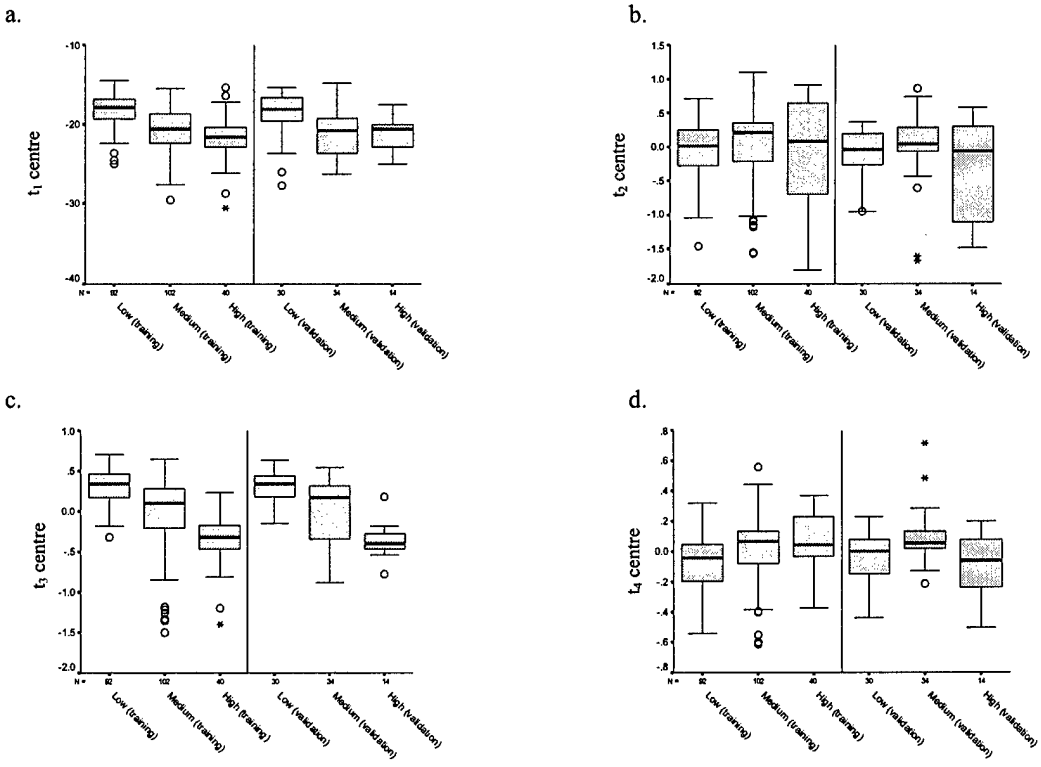
a.
b.
c.
d.
t_1 centre
t_2 centre
t_3 centre
t_4 centre
Low (training)
Medium (training)
High (training)
Low (validation)
Medium (validation)
High (validation)

Figure 9.

a.

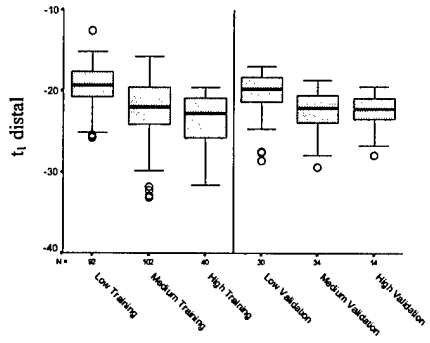

b.

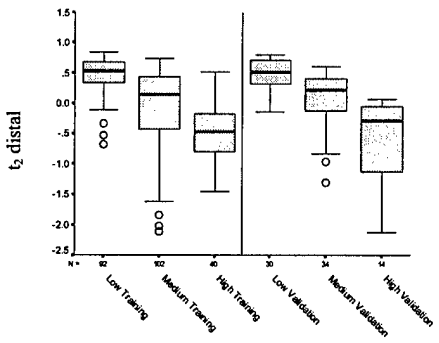

c.

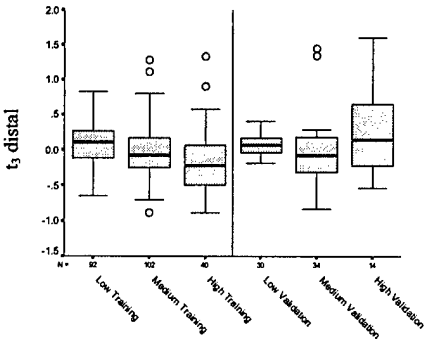

d.

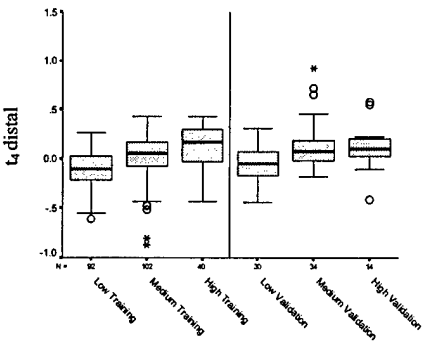

Figure 10.

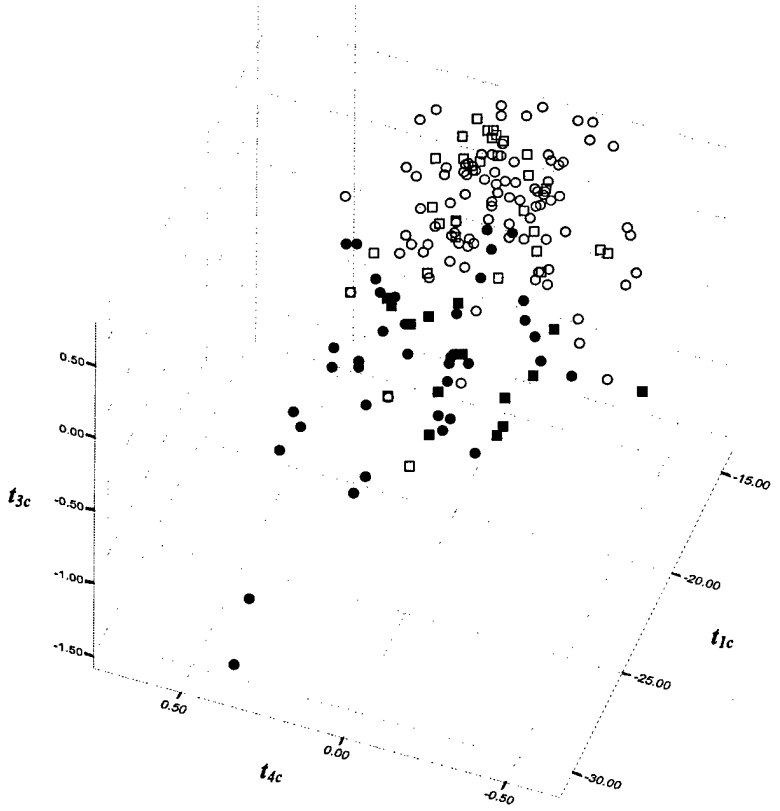

Figure 11.

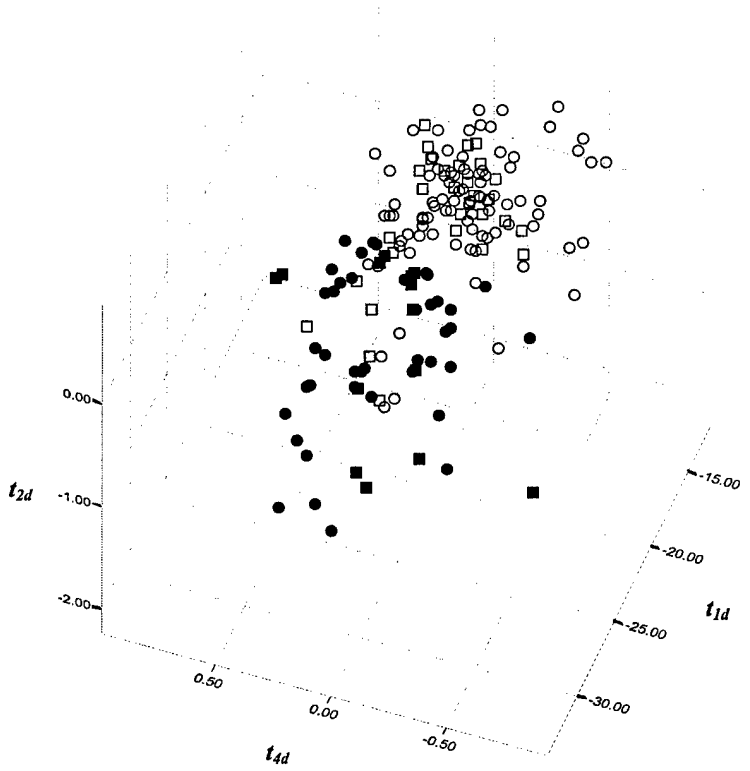

Figure 12.

a.

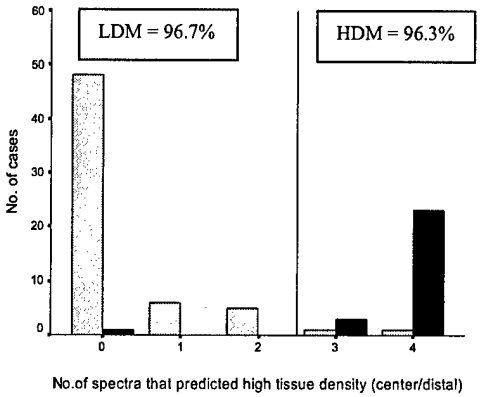

b.

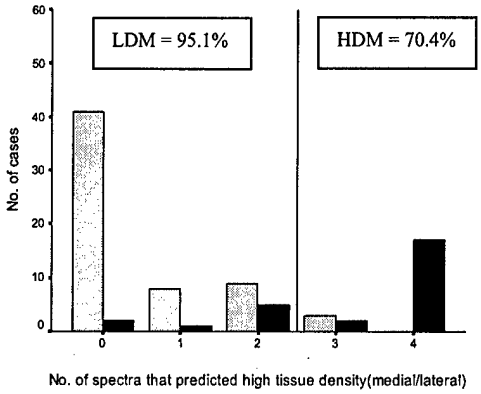

Figure 13.

a.

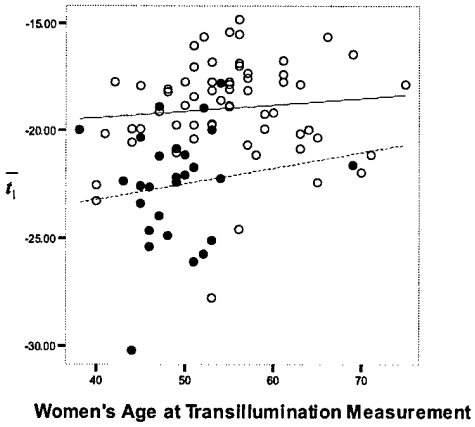

b.

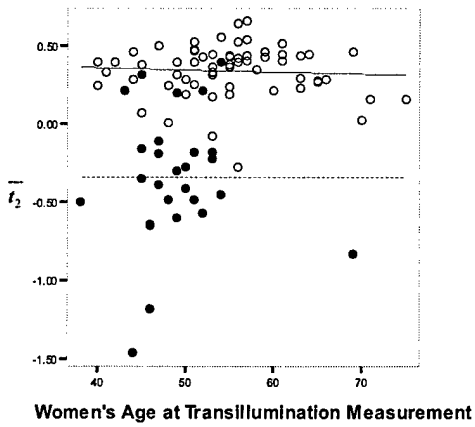

Figure 14.

a.

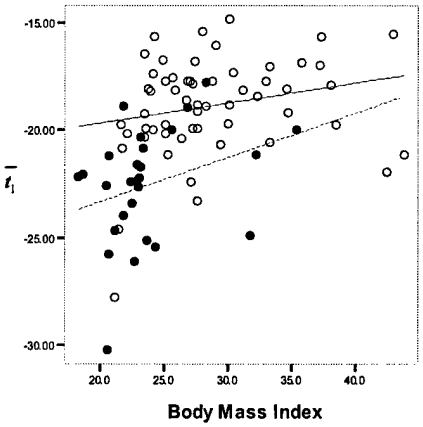
-15.00
-20.00
-25.00
-30.00
$\bar{t}_1$
20.0
25.0
30.0
35.0
40.0
Body Mass Index

b.

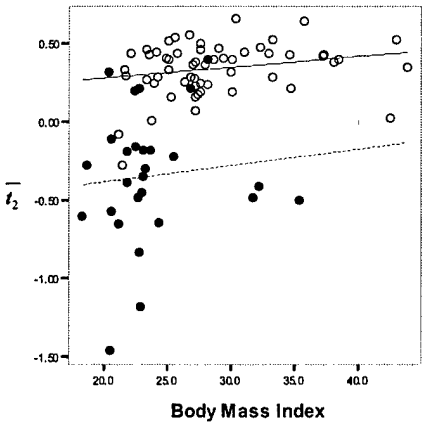
0.50
0.00
-0.50
-1.00
-1.50
$\bar{t}_2$
20.0
25.0
30.0
35.0
40.0
Body Mass Index